SCANNING ELECTRON MICROSCOPY AND PETROGRAPHY OF GLASSY PARTICLES PRODUCED BY LAVA FOUNTAIN ERUPTIONS

Garth H. Ladle

SCANNING ELECTRON MICROSCOPY AND PETROGRAPHY OF GLASSY PARTICLES PRODUCED BY LAVA FOUNTAIN ERUPTIONS

A FINAL REPORT FOR
CONTRACT NAS 9-14499
JOHNSON SPACE CENTER
HOUSTON, TEXAS

LUNAR AND PLANETARY INSTITUTE
CONTRIBUTION NUMBER 325

GARTH H. LADLE
BRIGHAM YOUNG UNIVERSITY
PROVO, UTAH

1978

SCANNING ELECTRON MICROSCOPY AND PETROGRAPHY OF GLASSY PARTICLES PRODUCED BY LAVA FOUNTAIN ERUPTIONS

A Dissertation

Presented to the

Department of Geology

Brigham Young University

In Partial Fulfillment

of the Requirements for the degree

Doctor of Philosophy

---

by

Garth Harrison Ladle

August 1978

This dissertation by Garth H. Ladle is accepted in its present form by the Department of Geology of Brigham Young University as satisfying the dissertation requirement for the degree of Doctor of Philosophy.

Myron G. Best, Committee Chairman

W. Revell Phillips, Committee Member

Morris S. Petersen, Committee Member

Wilford M. Hess, Committee Member

14 Apr 78
Date

Morris S. Petersen, Department Chairman

ABSTRACT

A conceptual model of a lava fountain consists of a vent, spatter ramparts, fountain column, downwind plume and associated pumice deposits. Glassy particles produced by lava fountain eruptions consist primarily of sideromelane glass and minor to moderate amounts of vesicles and crystals. Particles are classified on the basis of morphology as: (1) spherical, (2) elongate, (3) glass-coated mineral grain, (4) shard, (5) reticulite, (6) composite particle, and (7) lithic fragment.

The internal texture and surficial microstratigraphy of a glassy particle indicates its formation history, the capture and accumulation of other particles, the possible loss or removal of material by fracturing or abrasion, and its decomposition or alteration by solution, oxidation or hydration. The formation and modification of glassy particles can be modeled as a process having three stages: (1) initial formation, (2) constructive material accumulation, and (3) destructive removal or alteration of existent surfaces. Factors that affect particles in these three stages are: (1) lava composition and viscosity, (2) vent configuration, (3) flight velocity, (4) flight time duration at temperatures $> 800^{\circ}C.$, (5) surface tension, (6) gas concentration or expansion, (7) particle population within the fountain, and (8) convective cycling. After initial formation, a particle constructively accumulates other solid or liquid materials by accretion or sublimation and condensation or vapor phase crystals, micromounds and condensed liquids. The amount of accreted

material depends upon the duration of particle flight within the fountain column and plume or upon the extent of its cycling within the fountain. Subsequent to but sometimes synchronous with constructive accumulation, particles experience destructive removal of surface materials. Destructive processes modify particles throughout their history but generally have a greater affect on the particle near the completion of its history. Furthermore, particles can be cycled back into any of the previous stages or may by-pass some processes without modification.

Descriptive glass terminology (between the liquid and solid states) is defined based on temperature, viscosity, and physical properties for a basaltic glass as tentatively correlated with synthetic soda-lime-silicate glass. Suggested terms are: (1) rigid (where glass behaves as a solid, viscosity $> 10^{13}$ poise, temperature $\sim 700^{\circ}$C.); (2) semirigid (where glass deforms without fracturing under gradually applied stress but fractures under instantaneous stress and does not wet a host surface, viscosity $\sim 10^{7}$ poise, temperature $\sim 850^{\circ}$C.); (3) semifluid (glass flows, does not retain its shape, deforms under instantaneous stress without fracturing, and wets a host surface, viscosity $\sim 10^{5}$ poise, temperature $\sim 950^{\circ}$C.); (4) fluid (where glass behaves as a liquid, viscosity $< 10^{5}$ poise, temperature $\sim 1250^{\circ}$C.).

Terrestrial and lunar glassy particles have generally similar abundances of particle types, internal texture and surficial features. Notable differences are the dearth of glassy filaments and elongate particles in lunar soils and the paucity

of agglutinates in terrestrial pumice deposits. Two liquid particle forming processes active in the lunar environment are volcanic eruption and meteorite impact. They produce more fluid and semifluid splashes, platelets, and smaller spheres than terrestrial analogs. Destructive processes for lunar particles are primarily meteorite impact with minor disintegration caused by thermal expansion - contraction, solar wind abrasion and internal particle damage due to solar particles. Chemical alteration and solution is generally limited to terrestrial particles. Vapor phase crystallization occurs to a greater extent in lunar pumice deposits, whereas terrestrial analogs accret vapor phase crystals primarily in the fountain column or downwind plume.

TABLE OF CONTENTS

Page

LIST OF TABLES

LIST OF FIGURES

LIST OF PLATES

Plate Page

CHAPTER 1

INTRODUCTION

Purpose

The dark mantle deposits of the moon which contain orange, black and green glassy particles have been interpreted as pyroclastic deposits. Terrestrial glass spheres produced by eruption of low viscosity magma from lava fountains have similar characteristics as spheres collected from the dark mantle deposits of the Apollo 11, 15, and 17 sites.

Although many workers have studied basaltic lava fountains, few have studied the morphology, petrography and chemistry of the volcanic ash. This lack of data constitutes a significant gap in our knowledge of the physical and chemical processes active within the lava fountain and associated deposits. A study has therefore been made of glassy particles from several recent lava fountains to determine particle morphology, surface features and petrography. The data are interpreted in terms of the physical and chemical processes on the earth that created and modified these materials.

Previous Studies

Lava fountains have been studied by many workers (for example: Daly, 1911; Jaggar, 1917; Tyrrell, 1937; Perret, 1950;

Macdonald and Eaton, 1955; Eaton and Murata, 1960; Richter and Murata, 1966; and Swanson and Fabbi, 1973). Until the development of the scanning electron microscope (SEM) in the past decade, descriptive work on volcanic ash was limited to the megascopic and optical microscopic characteristics of shape, size, and general surface features. Wentworth (1938) made the first comprehensive study of volcanic ash including size analyses, morphological descriptions, chemical analyses and general physical parameters such as color, specific gravity and refractive index. Perret (1950) described particle morphology and its relationship to eruptive type. Heiken and Lofgren (1971) made a brief comparative SEM study of lunar glassy particles and terrestrial glassy particles produced by lava fountains and atomic explosions. Muenow (1973) made gas release studies of volcanic glass and found that during heating gases released from bursting vesicles were principally H_2O, CO_2 and CO, whereas gases released by diffusion and in some cases those generated by thermal degradation and reaction with the glass included H_2, O_2, N_2, S_2, H_2S, SO_2, SO_3, COS, HCL, HF, and NH_3. Average mole percent compositions of volatiles relative to the total gas released were 95 percent H_2O, 3.5 percent CO_2 and 1 percent SO_2. Heiken (1974) produced an atlas of volcanic ash in which he described the petrography, surface morphology, and chemistry of ash produced by magmatic and hydrovolcanic (phreatomagmatic) eruptions. In general, surface morphology was characterized by low magnification SEM photographs. Recent improvements in

instrumentation permit study of the more minute surface detail present on glassy particles. Cadle et al., (1968) studied the chemical and physical nature of particles within the fume of Kilauea eruptions. They suggested that droplets of sulfuric acid, hygroscopic particles, and a few acicular particles comprised 95 percent of the particulate material. Duffield et al., (1977) examined Pele's Hair produced by eruption of basaltic lava. They described the range of refractive index for the hair and the sublimate coating which formed on the hair as it fell to the ground. Gas release studies of the hair have suggested that the sublimate consists of carbonates, sulfates, native sulfur and, less commonly, hydrocarbons. Walker (1971) studied the grain size distribution of pyroclastic deposits and noted that pyroclastic-fall deposits can readily be distinguished from pyroclastic-flow materials by comparing median size versus sorting. In a later work Walker and Croasdale (1972) suggested that pyroclastic deposits of strombolian or hawaiian-type basaltic activity were readily distinguished from those of surteseyan type (i.e., the type exemplified by the opening stages of the Surtsey eruption of 1963-64) by being coarser-grained and better sorted.

In recent years several hypotheses have been formulated concerning the origin of the green and orange glassy particles returned by Apollo 15 and 17. McKay et al., (1973) and Heiken et al., (1974) have suggested from brief studies of the surface features of glassy particles produced by terrestrial lava

fountains that similar fountain processes were responsible for surface features found on green and orange glasses of Apollo 15 and 17.

Sample Collection

Samples of volcanic ejecta produced by Hawaiian lava fountains were collected by me and represent five eruptive events: 1959-60 eruption of Kilauea Iki; 1969-73 eruption of Mauna Ulu; July, 1974 eruption of Kilauea; December, 1974 eruption of Kilauea; and July, 1975 eruption of Mauna Loa. The best documented eruptive events were the 1959-60 Kilauea Iki and 1969-73 Mauna Ulu eruptions and therefore a stronger emphasis is placed on the samples collected from those eruptions (Figure 1). Stewart Agrell supplied a sample of ash taken from the early eruptive phases of Mauna Ulu. References to the above eruptions are Richter, et al., (1966); Swanson, et al., (1971); and annual reports of the Hawaiian Volcano Observatory. Documentation of the July and December, 1974 eruptions of Kilauea and July, 1975 eruption of Mauna Loa was obtained by personal visit to the observatory, conversations and later communications with Robert Tilling.

Ejecta samples from lava fountains in other areas of the world were obtained and compared to Hawaiian samples with regard to glassy particle content and morphology. Table 1 lists sample locality, date of eruption, and reference publications for sample areas other than Hawaii.

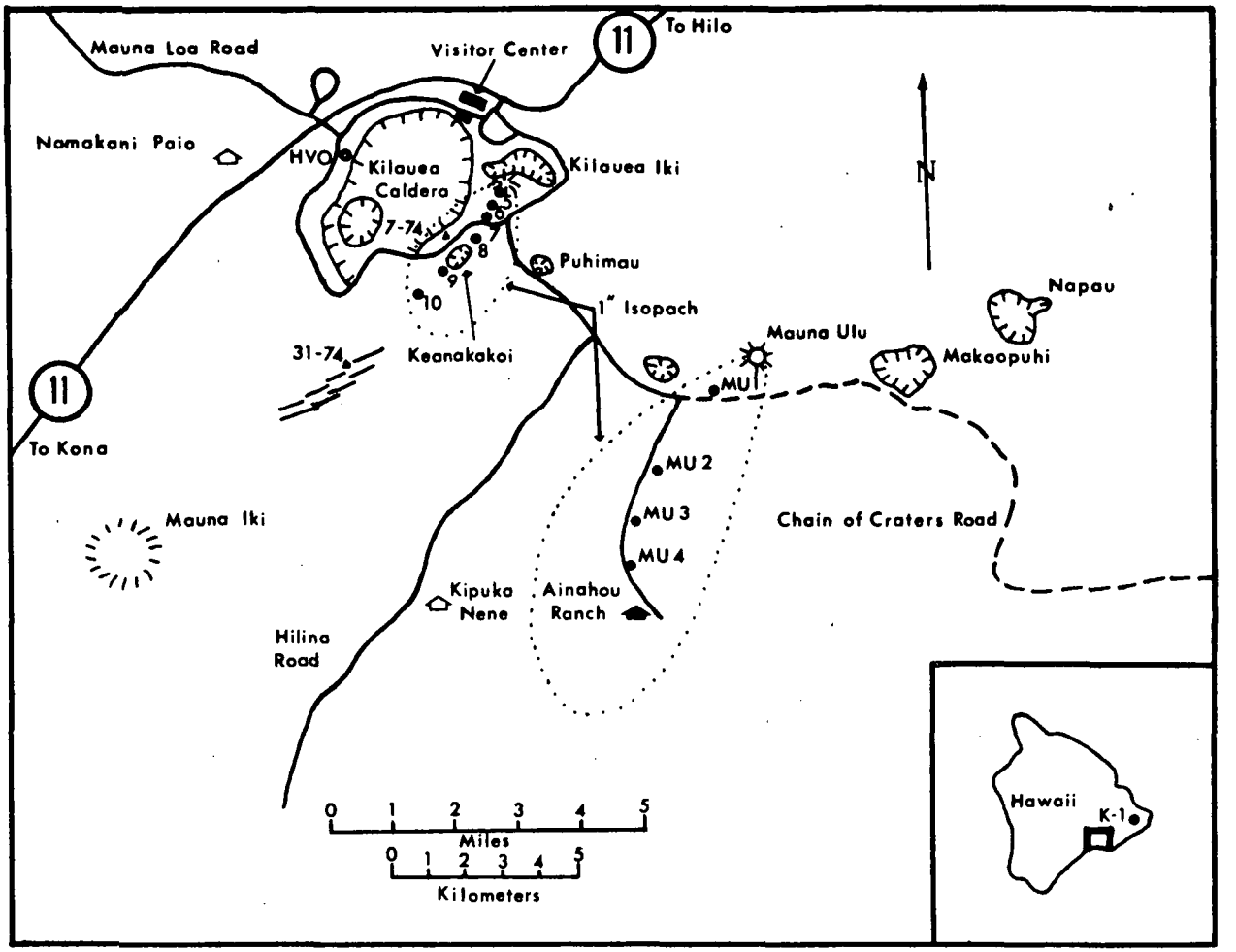

Figure 1. Index map showing sample localities for Kilauea and Mauna Ulu eruptions. Note that sample K-1 (insert to lower right) is off the map but located near the town of Kapoho.

TABLE 1.

SAMPLE LOCALITIES OF NON-HAWAIIAN SAMPLES

(1) Volcano Teneguia
La Palma, Canary Islands
Eruption Date: October 26 to November 20, 1971
Ref: Chaigneau, M and Fūster, J.M., 1972
L'eruption du Teneguia (La Palma, Iles Canaries)
et al. composition des laves et gaz fumeroliens,
C. R. Acad. Sc. Paris, t. 274, pp. 2948-2951.

(2) Volcano Erta' Ale
Ethiopia, Africa
Eruption Date: November, 1968
Ref: Varet, J. and Roubalt, M., 1971
Sur l'activite' re'cente de l'Erta' Ale (Dankalie,
Ethiopie), C. R. Acad. Sc. Paris, t. 272,
pp. 1964-1967.

(3) Volcanoes: Hekla, 1970
Heimay, Feb.-Mar., 1973
Katla, 1755

Iceland

Ref: Thorarinsson, S., Steinthororsson, S.,
Einarsson, Th., Kristmannsdottir, H. and
Oskarsson, N., 1973. The Eruption of Heimay
Iceland, Nature, V. 241, N. 5389, pp. 372-375.

Kilauea Iki ejecta was deposited in a large cinder cone and pumice blanket south-southeast of the vent. Surface samples were collected from a depth of 20-30 centimeters to avoid surficial contamination by animal or botanical debris. A pit was dug near the location of sample 6 (Figure 1) to sample different layers of the blanket in an attempt to correlate physical parameters of each layer with the various phases of the eruption

(Figure 2). Mauna Ulu samples were collected along Ainahou Road and near where Chain of Craters Road is blocked by recent Mauna Ulu flows. Samples collected from the flank eruption of Kilauea in 1960 near the town of Kapoho are indicated on the insert area of Figure 1.

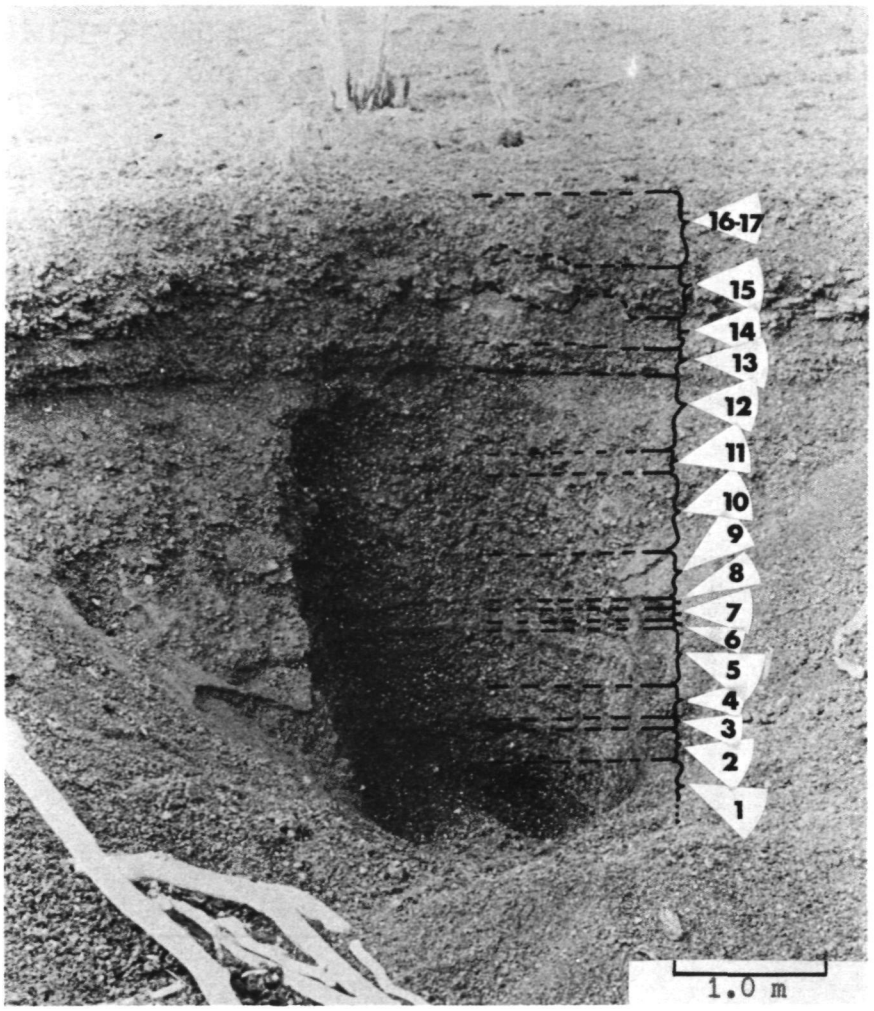

Figure 2. Vertical section through Kilauea Iki ejecta blanket near surface sample #6 (Figure 1). Note sample points of ejecta deposited during each eruptive phase. Correlation of ejecta deposit with eruptive phase is tentative. Total thickness is 4.4 meters.

Acknowledgments

I wish to thank Professor M.G. Best for helpful comment and criticism during the research and manuscript preparation. Thanks are also due to Professors: M.S. Peterson, W.R. Phillips, and W.M. Hess for their careful review of the manuscript and service as my doctoral committee.

This study was made possible by funding from contract NAS 9-14499, NASA, Johnson Space Center. Research facilities and office space were provided during portions of this research while the author was a visiting scientist at the Lunar and Planetary Institute which is operated by the Universities Space Research Association under contract NSR 09-051-001 with the National Aeronautics and Space Administration. Appreciation is also extended to Gulf Research and Development Co., Geological Sciences Dept. Harmarville, Pa., who allowed use of office facilities after work hours. Samples were graciously provided by Messers: S.O. Agrell, U.S. Clanton, A. Hernandez-Pacheco, J. Varet, S. Steinthorsson. Hawaiian sample collection was made possible by permission of the Hawaiian Volcano National Park.

Much helpful discussion of field sample locations and eruption data was provided by R. Tilling of the Hawaiian Volcano Observatory. Fruitful discussions were held with Drs. D. McKay, U. Clanton, and G. Heiken concerning terrestrial fountain processes, glass particle formation and lunar particle analogs.

Finally, this study would not have been possible without the encouragement and assistance of a loving wife, Donna Elaine, and family members: Dawn LaNae, Marcene Ann, Cynthia Lea, April Diane, and Jeremy Garth, many of whom assisted in portions of the typing or illustration preparation.

CHAPTER 2

SEM STUDY OF GLASSY PARTICLES

Introduction

This section of the study characterizes glassy particles produced by basaltic lava fountains. Binocular microscope and SEM were used to determine particle types and respective abundance in the fine-lapilli (< 4 mm) to coarse-ash (> 0.15 mm) size interval. Modal analyses were made of each sample at 1/2Ø intervals from -1.5Ø (coarse ash) to +2.5Ø (fine lapilli) size fractions. Detailed SEM study was made of selected particles from each size fraction to document the presence, morphology and relationship of surface features with the various types of glassy particles.

A JEOLCO JSM-U3 scanning electron microscope with attached energy dispersive x-ray analyzer (EDAX) was used during this work. Particles were mounted on carbon planchets and coated with 75 to 100 Å of carbon or gold (Clanton and Ladle, 1975; Ladle and McKay, 1973). A review of SEM and EDAX methods and techniques is given by Kimoto and Russ (1969) and Wells (1976).

Particle Types

Ejecta produced by recent Hawaiian lava fountains consist predominantly of sideromelane glass with minor amounts of

phenocrysts or microlites and crystalline rock fragments. On the basis of morphology, glassy particles may be classified as: (1) reticulite, (2) shard, (3) spherical and (4) elongate. Other particles include (5) glass coated mineral grains or fragments, (6) composites of (1), (2), (3) and (4), and (7) lithic fragments. Any of these particles may suffer change in shape as a result of breakage or fracture due to collision with other particles or surface impact. Table 2 lists proportions of each category of particles.

TABLE 2

COMPOSITE MODAL ANALYSIS OF PARTICLES PRODUCED BY RECENT HAWAIIAN LAVA FOUNTAINS COLLECTED FOR THIS STUDY (-1.5Ø to +2.5Ø SIZE INTERVAL)

Particle Type		Percent
Reticulite		42.9
Shard		14.7
Spherical or Elongate		
Sphere		23.2
Elongate		11.1
Glassy Filament		1.3
	sub-total	35.6
Coated Mineral Grain or Fragment		
Olivine		4.8
Clinopyroxene		0.2
Orthopyroxene		Tr
Plagioclase		Tr
Spinel		Tr
	sub-total	5.0

TABLE 2 (continued)

COMPOSITE MODAL ANALYSIS OF PARTICLES PRODUCED BY RECENT HAWAIIAN LAVA FOUNTAINS COLLECTED FOR THIS STUDY (-1.5Ø to +2.5Ø SIZE INTERVAL)

Particle Type	Percent
Composite	1.8
Lithic Fragment	Tr
Total	100.0

Reticulite

Reticulite (Pl. 1, fig. 1) consists of delicate lace-like interconnecting strands of glass with triangular cross-sections, three strands joining together at triple-junctions. SEM study of the particles suggests a general paucity of surface features (micromounds, liquid splashes, and welded surface debris) attributed to constructive processes operative within the fountain. Reticulite particles account for 42.9 percent of the material contained in the -1.5Ø (2.83 mm) to +2.0Ø (0.25 mm) size interval (Table 3).

TABLE 3

GRAIN SIZE DISTRIBUTION OF RETICULITE ASH

	Size Intervals (Ø units)						
	-1.5	-1.0	-0.5	+0.0	+0.5	+1.0	Totals
Number of Particles	894	1243	1790	2370	3118	3767	13182
Percent	6.8	9.4	13.6	18.0	23.7	28.5	100.0

Glass Shards

Glass shards are lenticular to sliver shaped fragments commonly exhibiting conchoidal fracture and are composed of non- to slightly-vesicular sideromelane glass (Pl. 1, fig. 2). Most shards have smooth slightly-curved surfaces.

Spherical and Elongate Particles

Spheres. Many ejecta particles produced by lava fountains have spherical or oblate spheroidal shapes (Pl. 1, figs. 3,4). Included in this category are broken spheres fractured by inter-particle collision or surface impact. Spherical particles are subdivided on the basis of morphology, particularly on the presence or lack of surficial debris, and type of debris. Complete or broken spherical particles account for 23.2 percent of the material in the -2.0Ø to +2.5Ø size interval (Table 2). A debris-free sphere (Pl. 1, fig. 5) exhibits numerous small irregular to circular openings.

Surface debris collected on spheres within the fountain

plume or later as an alteration product indicate processes active within the fountain or ejecta blanket. The amount and type of surficial debris collected on a particle surface is a function of the length of time spent within the fountain plume and the particular area the particle passed through during its flight history. Debris covered spheres include: (1) spheres with attached individual or groups of smaller spheres (Pl. 2, fig. 1); (2) spheres with partial coatings of glassy filaments (Pele's Hair, Pl. 2, fig. 2) either as solid fibers or splash material; (3) individual crystals or aggregates of crystals (Pl. 2, fig. 3); (4) complete to partial coatings of fine-grained crystal mats (Pl. 2, fig. 4); (5) composite coatings of the above plus irregular shaped shards and other debris (Pl. 2, fig. 5); and (6) complete coatings of surficial materials, sublimates or alteration products (Pl. 2, fig. 6). Radial and concentric fractures (Pl. 1, fig. 6) are common on spheres and control the localization of spalled regions. Table 4. gives the size distribution of spheres or broken spheres in the -1.5Ø to +2.5Ø size interval. The mode occurs at the -0.5Ø (2.0 to 2.8 mm) size interval.

Elongate Particles. Elongate particles or streamers account for 11.1 percent of the fine-grained lapilli to coarse-ash sized material. Elongate glassy particles have a length to cross-sectional diameter of 2:1. Particle shape is determined by processes active during eruption which disrupt the magma by pulling apart the molten material into elongate strands,

stretched clots or spindles (Pl. 3, figs. 1,2,3); or by aerodynamic streamlining of molten particles during flight (Pl. 3, fig. 4). Some elongate particles contain single or double glass filament tails (Pl. 3, fig. 5); others have surface ripples or waves (Pl. 3, fig. 5,6).

TABLE 4.

GRAIN SIZE DISTRIBUTION OF SPHERES
OR ROUNDED PARTICLES

	Size Intervals (Ø units)									
	-1.5	-1.0	-0.5	+0.0	+0.5	+1.0	+1.5	+2.0	+2.5	Totals
Number of Particles	301	342	397	348	249	248	144	51	24	2,104
Percent	14.3	16.4	18.9	16.5	11.8	11.8	6.8	2.4	1.1	100.0

Glassy Filaments (Pele's Hair). Glassy filaments are a type of streamer characterized by length to width ratios greater than 10:1 and consist of rounded strands or hairs of sideromelane glass. They often form bobby pin shapes or closed loops where the liquid filaments overlap (Pl. 4, fig. 1); or fibers that contain lumps or spherical masses of glass (Pl. 4, fig. 2). Partial to complete debris coats consisting of sublimates, other finer sized glass filaments and spheres are common. Glassy filaments may be either solid or contain numerous elongate gas

vesicules. Filaments as coarse as 1-2 mm in diameter have been noted.

Mineral Grains or Fragments

Mineral grains or fragments account for 5.0 percent of the particles studied in the 1.5Ø to 2.0Ø size interval. Olivine is the predominant phase (4.8 percent) with clinopyroxene accounting for 0.2 percent and plagioclase, orthopyroxene, and spinel occurring in trace amounts. Olivine grains larger than -2.0Ø (4 mm) were seldom observed with the -1.0Ø to -0.5Ø (2.0 to 1.4 mm) size interval occurring as the major mode (Table 5).

TABLE 5.

GRAIN SIZE DISTRIBUTION OF MINERAL GRAINS

	Size Interval (Ø units)								
	-1.5	-1.0	-0.5	+0.0	+0.5	+1.0	+1.5	+2.0	Total
Number of Particles	56	186	263	235	191	182	83	15	1,205
Percent	4.7	14.9	21.8	19.5	15.9	15.1	6.9	1.2	100.0

Mineral morphology is usually masked by a thin to moderately thick glass coating which covers all but a few protruding edges and corners of the crystal (Pl. 4, fig. 3). Most grains observed were covered with glass which contained numerous vesicles (Pl. 4, fig. 4).

Composite Particles

Composite glassy particles consist of other particles welded or held together by a glassy covering. They account for 1.8 percent of the material in the -1.5 to 2.5Ø size interval and decrease in abundance as size decreases (Table 6).

TABLE 6.

GRAIN SIZE ANALYSIS OF COMPOSITE PARTICLES

	Size Intervals (Ø units)									
	-1.5	-1.0	-0.5	+0.0	+0.5	+1.0	+1.5	+2.0	+2.5	Total
Number of Particles	95	85	66	50	47	41	26	16	10	436
Percent	21.7	19.5	15.1	11.5	10.8	9.4	6.0	3.7	2.3	100.0

Forms commonly noted were combinations of spheres and numerous filaments (Pl. 4, fig. 5) or several spheres combined into one particle with a partial to complete coating of surficial debris (Pl. 4, fig. 6).

Lithic Fragments

Lithic fragments that crystallized prior to or during eruption account for trace amounts (less than 1.0 percent) of the material in the -1.5Ø to 2.5Ø size interval. The largest fragments (4 noted) were less than 300μ in diameter with the smallest being about 90μ. Most fragments consist of an inner crystalline core covered by a glass coat and surficial debris (Pl. 5, fig. 1). Some fractured particles exhibiting crystalline

interiors have interior voids or vesicles (Pl. 5, fig. 2).

Glass Terminology

To avoid confusion or misunderstanding when describing glassy particle features it is necessary to establish terminology that refers to the various physical states and properties that a glass possesses. Many adjectives or modifying terms can be used (hard, soft, fluid, rigid, liquid, etc.,) but the physical condition of the glass in reference to temperature or viscosity is only casually implied. In an attempt to standardize a set of physically meaningful terms which describe glass properties it was found that terminology describing glass between the liquid and solid states is generally confusing or lacking. Glass is defined (ASTM, Std., Pt. 13, p. 145) "as an inorganic product of fusion which cooled to a rigid condition without crystallizing". Morey (1954) uses the following terms to describe the physical state and corresponding viscosity values of soda-lime glasses: (1) melting point (10^3 poise); (2) flow point (10^5 poise); (3) softening point (10^7 poise); and (4) rigid point (10^{13} poise). A compilation and extrapolation of data from several sources (Shaw, 1968, 1972; Richter and Moore, 1966; and Macdonald, 1972) allow a comparison of basaltic glass to that of a soda-lime-silica glass (Kingery, et al., 1976) at corresponding viscosities and temperatures. Care must be exercised in using the following viscosity-temperature values for basaltic glass since they have been extrapolated and should be considered preliminary or tentative.

		Na, Ca, Si Glass	Basaltic Glass
Melt point	10^3 poise	~1200°C	~1250°C
Flow point	10^5 poise	~850°	~950°
Softening point	10^7 poise	~700°	~850°
Rigid point	10^{13} poise	~500°	~700°

Descriptive terminology that relates the above glass points to observed features are:

rigid point: where glass behaves as a solid; viscosity $>10^{13}$ poise. Equivalent term used in this study = rigid.

softening point: where glass deforms and bends without fracturing under gradually applied stress but fractures under instantaneous stress; and does not wet* a host surface upon contact. Equivalent term used in this study = semirigid.

flow point: where glass flows or spreads out and does not retain its shape; deforms under instantaneous stress without fracture; and wets* a host surface upon contact. Equivalent term used in this study = semifluid.

melt point: where glass behaves as a fluid; viscosity $<10^5$ poise. Equivalent term used in this study = fluid.

*wetting occurs when adhesive forces are equal to or greater than cohesive forces (Holland, 1964). Cohesive force (surface tension) is highly dependent upon temperature. For basaltic glass wetting does not occur below a surface tension value of 225 ± 25 dynes/cm and temperatures below ~800°C (data for basalt, McBirney and Murase, 1971).

Surface Features

Surface features on glassy particles may be classed as either constructive, represented by features showing a build-up

or accumulation of materials on the surface, or destructive, represented by features indicating the destruction or removal of material from the original or constructive surface.

Constructive Surface Features

Constructive features build-up the surface by the accretion of secondary materials. These features include (Pl. 5, fig. 3): (1) fluid impacts or spashes, (2) glassy filaments, (3) platelets and smaller spheres, (4) crystalline material, (5) thin liquid films, (6) micromounds, and (7) glass shards and other debris.

Splashes. Fluid particles that splash onto host particles vary in shape from near circular forms (Pl. 5, fig. 4) to fluid streamers or jets (Pl. 5, fig. 5). Fluid streamers or jets are included as splash features because they coat the underlying material with a thin fluid film even though they do not exhibit the customary circular to lobate form characteristic of a splash. Splash thickness varies from a few microns to $\sim$1000 Å. Thick bulbous splashes characterize semifluid materials, whereas thin fluid splashes "wet" the surface and often barely cover underlying features. Some impacts exhibit a semirigid core with the surrounding area covered by a thin fluid splash (Pl. 5, fig. 6).

Glassy Filaments. Glassy filaments do not "wet" the host surface, whereas splashes cover the surface with a fluid film. Surficial accumulations of glassy filaments consist of semirigid to rigid fibers that occur as individual strands or clusters of intertwined filaments (Pl. 6, fig. 1). Some filaments have

hollow cores and uniform wall thickness over considerable distances (Pl. 6, fig. 2), whereas others are solid glass. Filament diameter varies from very small threads (~200Å, central area, Pl. 6, fig. 3) to larger filaments (~300 μ). The physical state (viscosity, temperature, degree of vesiculation, etc.,) of the filament at the time of impact determines the degree of shape modification or deformation. Semirigid filaments deform on impact by flattening and developing a semi-continuous series of surface depressions (Pl. 6, fig. 4a). Rigid filaments retain their shapes but may exhibit brittle fracture formed during impact or flight (Pl. 6, fig. 2).

Platelets and Smaller Spheres. Platelets are particles that have circular outlines and rounded upper surfaces, but may be flattened to plate-like shapes (Pl. 7, fig. 1). Platelets occur individually or in groups (Pl. 7, fig. 2). Platelet diameter varies from ~10 μ (largest observed) to ~500 Å, with a mean of ~1 μ. A close association is noted between platelets and the occurrence of small surficial spheres. No difference in composition was noted between platelet and host particle. However, minor difference may have been masked due to the small cross-sectional volume of the platelets in relation to the larger volume of the underlying particle during x-ray analysis.

Smaller spheres on glassy particle surfaces occur as individual spheres or groups of spheres (Pl. 7, fig. 3). Spheres as small as ~400 Å diameter have been observed. Modal analysis by stereomicroscope showed spheres smaller than

+2.0Ø (250 μ) accounted for only 3.5 percent, whereas SEM study of spheres (250 to 50 μ dia.) documented the presence of numerous smaller spheres welded to larger particles. The sphere in (Pl. 2, fig. 5) contained several hundred smaller spheres with a size distribution of: 7Ø (7.8 to 15.6 μ) = 3.3 percent; (3.9 to 7.8 μ) = 6.7 percent; 9Ø (2.0 to 3.9 μ) = 28.2 percent; 10Ø (0.98 to 2.0 μ) = 50.1 percent; 11Ø (0.49 to 0.98 μ) = 11.7 percent. Small spheres exhibit surface features such as "dimples" (Pl. 7, fig. 4) which consist of a set of larger partially filled, smooth-walled depressions and a second set of smaller, closer-spaced vesicles. Other spheres accumulate a partial to complete coating of sulfur compounds or other sublimates (Pl. 7, fig. 3, to right to point d) before attachment to larger particles.

Surface Crystals. Many glassy particles exhibit surficial crystals that formed in-place or were later accreted to the particle surface. Four minerals were identified based on crystal morphology and composition: (1) elemental surfur, (2) jarosite, (3) gypsum, and (4) marcasite.

Elemental sulfur was noted in several instances and typically exhibits a cluster-like habit (Pl. 8, fig. 1). Usually sulfur clusters are closely associated with other surficial materials which contain extensive sulfate coatings. X-ray analysis (EDAX) of the clusters did not indicate the presence of other elements combined with the sulfur.

Jarosite, $K\ Fe_3\ (SO4)_2 \cdot 6(OH)$, was observed on many particles and commonly exhibited two crystalline habits. Some

jarosite develops as small hexagonal crystals of the ditrigonal pyramidal class (Pl. 8, fig. 2). Commonly, such crystals occur where a splash has previously wetted the surface and in the general proximity to gypsum crystals (Pl. 8, fig. 3). A different crystal habit was observed as a secondary or encrusting phase on gypsum crystals (Pl. 8, fig. 4) or as a mesh of intergrown lenticular to tabular crystals on the upper surfaces of earlier formed hexagonal crystals (Pl. 8, fig. 5). Jarosite also occurs on some spheres as a tabular to bladed crystal mat-like surface (Pl. 8, fig. 6). Some hexagonal shaped crystals were noted on this surface suggesting the possibility that the tabular crystals may represent edge views of hexagonal crystals. Jarosite was distinguished from other sulfates by the presence of potassium, sulfur, and a three fold increase in iron (Figure 10). A small amount of sodium and titanium was noted, probably substituting for potassium and iron respectively.

Gypsum crystals occur on most glassy particles in addition to significant amounts of amorphous calcium sulfate. Tabular crystals are most common (Pl. 9, fig. 1) and often form crystal aggregates with some crystals exhibiting rudimentary swallow-tailed twins along the {100} plane. Single large crystals that lack any evidence of deformation or cracking of the crystal by impact (Pl. 9. fig. 2,3) are a common feature on many surfaces. An exceptionally well developed crystal (Pl. 9, fig. 3) exhibits {110} prisms (upper surfaces), {010} faces (clinopinacoids), and the partial development of {111} pyramids. Local development of

radial crystal clusters was noted (Pl. 9, fig. 4). No discernible substitution was noted in the chemical composition of the gypsum (Figure 9). The presence of small surficial blebs on some crystals were noted but were not chemically distinguishable from the underlying crystals.

The observation of anhedral masses of iron sulfide (Figure 8) was noted on several glassy particles. The iron sulfide differs from jarosite by the absence of potassium, sodium and titanium. It forms multiple sheaths of scale-like crystals (Pl. 9, fig. 5) with some crystals exhibiting serrated or cockscomb structures on the ends of tabular forms (Pl. 9, fig. 6). Identification of the iron sulfide as marcasite is based on composition and crystal habit. Marcasite forms at lower temperatures and more acidic environments than pyrite and pyrrhotite.

Glassy Films. Particle surfaces often have partial to complete thin liquid films (Pl. 10, fig. 1) that gradually accumulate by the build-up of overlapping fluid splashes (Pl. 7, fig. 1, area b). Film thickness can be measured or estimated depending on whether the film covers underlying features of known size (Pl. 10, fig. 4). Some films contain small closely-spaced vesicles (Pl. 10, fig. 1) or dispersed larger vesicles (Pl. 10, fig. 2). Some vesicles have sharp versus smooth rounded rims (Pl. 10, figs. 1,2). Other vesicles occur in clusters and have very noticeable rounding of the outer margins (Pl. 10, fig. 3) with non-vesiculated areas between clusters.

Micromounds. Surficial micromounds occur on most glassy particles in various amounts; some particles have extensive development, whereas others have sparse or patchy accumulations. Multiple stages of micromound growth are illustrated (Pl. 10, fig. 4) where chipping or spalling has removed several surficial layers documenting continued growth after spalling. X-ray analyses of the micromounds indicate basically the same composition as the host glass with the addition of small amounts of sulfur, iron, copper, and zinc. The extremely small size of the micromounds does not allow quantitative analysis since the electron beam excites a volume of the sphere of roughly 10^4 angstroms diameter. Micromounds vary in diameter from less than 500 Å to several thousand angstroms (Pl. 10, fig. 5). Coarser micromounds, connected together as "beaded micromounds" (Pl. 10, fig. 6), were noted on several surfaces and clearly exhibit a different morphology than previously described micromounds. Numerous beads are interconnected with the glass surface between "bead strands" being free of material.

Glass Shards and Other Debris. Glass shards are commonly observed as accumulations on glassy surfaces (Pl. 11, fig. 1). Often the shards exhibit surface features (micromounds etc.,) which developed prior to fracture into irregular fragments (Pl. 11, fig. 2). Irregular masses of debris (spheres, filaments, platelets, and shards) intermixed with alteration products (sulfates and oxides) cover large areas of some glassy particles (Pl. 11, fig. 3).

Destructive Surface Features

Destructive features break apart, remove, and alter accumulated surficial debris or break the particle into fragments. These features include: (1) particle fractures, (2) surficial chips and spalls, (3) decomposed surfaces, (4) oxide films, and (5) crystal encrustation remnants. Included in this section are morphological modifications such as ripples and waves.

Particle Fractures. Fractures of particles vary from partial surficial polygons (Pl. 12, fig. 1) to larger fractures that penetrate into the particle interior. Often particles are broken into halves or several fragments. Smaller surficial fractures occur as: (1) polygonal fractures, (2) minute shallow fractures (Pl. 12, fig. 2, area d), and (3) small local fractures or spalls near particle impacts (Pl. 12, fig. 3). Fractures are locally observed that contain micromounds on fracture walls and exterior surfaces near the fracture (Pl. 12, fig. 2). Fractures are often covered by secondary materials.

Surficial Chips and Spalls. Glassy surfaces commonly exhibit areas of thin concentric fragmental shards (Pl. 12, fig. 3). Locally these shards have been removed from the surface (Pl. 12, fig. 4). Spalls exhibit both conchoidal fractures on near vertical surfaces and underlying cuspate or tensional fractures (Pl. 12, fig. 5). Many spalls have smooth slightly-curved surfaces. Some spall regions exhibit multiple spalls that have chipped or broken off successive layers (Pl. 12, fig. 6).

Decomposed Surfaces. Small elliptical surface depressions that contain several terraced steps (Pl. 13, fig. 1) do not resemble vesicles or spalls. Closely associated with the deeper, multi-layered depressions are semi-circular to irregular shaped, shallow, single-layer depressions (Pl. 13, fig. 1, area c) or small depressions with slightly raised rims but do not have halos (Pl. 13, fig. 2). Other surfaces exhibit abundant angular to circular cavities and also contain numerous small irregular and branching fractures (Pl. 13, fig. 3). Surface area is increased by the large number of cavities and fractures. These depressions and irregular cavities indicate chemically decomposed or altered surfaces.

Oxide Films. Some particle surfaces have abundant scale-like masses, numerous cracks, irregular to circular cavities, and exhibit an encrusted appearance (Pl. 13, fig. 4). Other surfaces contain abundant small globular masses that accumulated or grew into patches (Pl. 13, fig. 5) and locally cover the entire surface (Pl. 13, fig. 6). Both surface types greatly increase the surface area of the particle. EDAX analyses indicate the same composition for the scale-like or globular masses (insofar as elements heavier than 10 [Neon] are concerned) and the underlying host particle. This fact, together with the expanded nature of these surfaces, suggest that they are oxides developed on the underlying host material. Nitride surfaces can be ruled out in that nitrogen is inert at temperatures and pressures observed in lava fountains.

The gradual build-up of an oxide layer can be observed in Pl. 14, figs. 1,2,3,4. A rippled surface on a double-tailed, rounded particle (Pl. 3, fig. 5, lower view) from the 1969-73 Mauna Ulu eruption is shown in Pl. 14, fig. 1. Numerous small fractures can be observed along the base of the ripples or as radiating cracks on the flanges of the burst vesicle. Small spots or clumps of oxidized material can be observed along ripple edges or on the upper surfaces of the ripples. Note the similarity between the ripple pattern in this view and that of the surface pattern (Pl. 14, fig. 2) exhibited by a particle from the 1959-60 eruption of Kilauea Iki. An advanced stage of oxidation has almost covered the surface of the ripples and the flat area around the vesicles. Several small circular openings disrupt both the ripple pattern and oxide coating suggesting a period of vesiculation after oxide formation. A higher magnification view of the coating (Pl. 14, fig. 3) illustrates the presence of a massive coating on the ripple surfaces, whereas the troughs exhibit a blocky deposit. Further magnification (Pl. 14, fig. 4) indicates the presence of scale-like deposits at the upper right and the build-up of expanded areas between cavities in ripple troughs. Note the increase in void space and surface area produced by the oxide coating.

Some particles exhibit both altered and oxidized features (Pl. 14, figs. 5,6) which form composite surfaces. A composite surface (Pl. 14, fig. 5) exhibits polygonal fractures and adjacent ridges. EDAX analysis of the ridge material shows enrichment of

Fe, K and S which suggests a material similar to jarosite in composition. The inter-ridge oxide coating does not contain an increase in Fe or K. A lower magnification view (Pl. 14, fig. 6) illustrates the formation of "dimples" or slight surface depressions where a second oxide coating has covered the initial coating and polygonal ridges.

Crystal Encrustation Remnants. Surficial encrustation remnants formed on previously existent crystals are sometimes sufficiently preserved to allow inferences as to habit. Some outlines resemble prismatic crystals of the monoclinic crystal system (Pl. 15, fig. 1). Other impressions indicate crystal clusters that may have been twinned (Pl. 15, fig. 2, upper center). Sulfate crusts locally contain cavities suggestive of crystalline shapes (Pl. 15, fig. 3) and usually contain potassium and sodium in the material surrounding such cavities. Small elongate, needle-like impressions have been observed on some surfaces but whether they represent crystal or other debris impressions is uncertain (Pl. 15, fig. 4).

Compression Wrinkles. Some glassy particles display a wrinkled surface (Pl. 3, fig. 6; Pl. 15, fig. 5). Regions of intense wrinkling (Pl. 15, fig. 5, area b) can be suggested as being semirigid, whereas non-to-slightly wrinkled regions (fig. 5, area a) may be nearly rigid. Circular surface vesicles (fig. 5, area c) do not exhibit deformation suggesting that the particles interior may have been fluid allowing the vesicle to rise to the surface and burst through the wrinkled skin. Wrinkled surfaces of

this nature may be formed by particle compression.

Surface Ripples. Surface ripples consist of a contorted pattern of ridges and valleys (Pl. 15, fig. 6) that partially to completely cover the particle surface. Ripples are intersected by surface vesicles (fig. 6, area a) which obstruct the flow of the ripples causing them to accumulate or pile-up around vesicles and become stretched and locally broken (fig. 6, area b). Ridge areas are somewhat flattened and contain small alteration patches on their surfaces (Pl. 14, fig. 1, area b). Valleys are generally curved and separated from ridge walls by small linear cracks (fig. 1, area a). Whether this pattern of ridges and valleys forms in response to surface deforming forces (aerodynamic drag) while the surface is still semifluid or is the surface expression of internally deformed laminae which intersect the surface is uncertain.

CHAPTER 3

PETROGRAPHY OF GLASSY PARTICLES

This section documents the physical and internal properties of glassy particles produced by Hawaiian lava fountains previously discussed. SEM studies are limited to examination of particle exteriors or to fractures that partially reveal the internal nature of the particle. These observations indicate the processes and conditions that the exterior of a particle experienced in the lava fountain or ejecta blanket. However, features formed inside a particle cannot be observed or studied by external examination. Therefore it is important to document the internal properties that have taken place within the particle which in some cases may influence or control the formation of surficial features.

General physical properties of fountain ejecta have been studied previously by other workers. Densities of glassy particles range from 2.66 to 2.98 g/cm^3 with local variation in highly vesicular samples to 1.8 g/cm^3. For additional information the reader is referred to studies by Wentworth (1938) and Richter and Moore (1966). Refractive index studies of Hawaiian sideromelane glass show little variation (1.597 to 1.606) for most samples. Additional information is given by Duffield, et al., (1977) and Swanson, et al., (1971).

Several workers have performed chemical analyses on ejecta produced by Kilauea Iki and Mauna Ulu eruptions.

Qualitative analyses in this investigation were made using energy dispersive x-ray techniques. Mineral phases were identified and compositions determined primarily by optical properties.

Grain Size Distribution

Glassy particles produced by basaltic lava fountains range in size from several meters to several thousand angstroms in diameter. The size classification (Fisher, 1961) utilized in this study has the following categories: (1) blocks and bombs >64 mm; (2) lapilli = 64 to 2 mm; (3) coarse ash = 2 to 0.065 mm; and (4) fine ash <0.065 mm. To facilitate graphing and description of the particles, a transform of particle size from millimeters to Ø (phi) units is used (Krumbein and Pettijohn, 1938). Sieve sizes were selected at 1/2Ø intervals from -5Ø (32 mm) to +5Ø (0.032 mm). Each sample was seived for 20 minutes on a vibrator-shaker table. Three statistic measures were computed for each sample (Folk, 1969) and include: (1) median, Md = (50 percentile of cumulative weight probability percent); (2) mean size, $Mz = \frac{16\emptyset + 50\emptyset + 84\emptyset}{3}$; and (3) a measure of sorting or standard deviation, $\sigma_I = \frac{84\emptyset - 16\emptyset}{4} + \frac{95\emptyset - 5\emptyset}{6.6}$.

Samples of ejecta studied during this report were taken from the following eruptions: (1) Kilauea Iki, 1959-60 (9 surface and 13 pit samples; see Figure 2 for depth of pit samples); (2) Mauna Ulu, 1969-73 (4 surface samples); (3) Kilauea, July, 1974 (2 surface samples); and (4) Kilauea, Dec., 1974 (2 surface samples). Grain size parameters, median (Md), mean size (Mz), and sorting (σ_I), were calculated for each sample and are summarized

in Table 7. Figure 1 shows the site of each sample. Mean grain size (Mz) decreases as distance from the vent increases for both Kilauea Iki and Mauna Ulu surface samples. Sorting (σ_I) generally improves with distance. Cumulative probability weight percent curves for Kilauea and Mauna Ulu ejecta (Figures 3 and 4) illustrate that the majority of the particles are coarser than -1Ø (2 mm) and have less than 1 percent coarser than -4Ø (32 mm). Samples obtained farthest from the vent contained a higher percentage of fine-grained particles. All samples exhibit a fine-grained or positive skewed tail that accounts for less than 10 percent of the cumulative weight.

A plot (Figure 5) of mean size versus sorting illustrates good correlation between mean size and sorting for Mauna Ulu samples, whereas Kilauea Iki samples show moderate correlation except for samples 7,8 and 9 which were collected near the eruption site of July, 1974 (eastern edge of Kilauea caldera). Samples of the December, 1974 Kilauea eruption contain some contamination from the underlying finer-grained material of the 1924 phreatomagmatic eruption of Kilauea and therefore plot on Figure 3 as finer-grained samples than typical Hawaiian fountain ejecta. All of the ejecta samples plot in the "fall" category of Walker (1972) in reference to deposits of air fall ash versus ash flows.

Internal Properties

General

The internal properties of glassy particles produced by lava fountains in part control the type of surface features

TABLE 7

GRAIN SIZE STATISTICS OF EJECTA PRODUCED

BY HAWAIIAN LAVA FOUNTAINS

Sample	Eruptive Phase	Median (Md)	Mean Size (Mz)	Sorting (σ_I)
Kil. Iki, Surface 3	-	-2.78Ø	-2.70Ø	1.14Ø
Kil. Iki, Surface 4	-	-2.90Ø	-2.80Ø	1.00Ø
Kil. Iki, Surface 5	-	-2.68Ø	-2.54Ø	0.78Ø
Kil. Iki, Surface 6	-	-2.39Ø	-2.29Ø	0.66Ø
Kil. Iki, Surface 7	-	-2.30Ø	-2.34Ø	1.43Ø
Kil. Iki, Surface 8	-	-2.52Ø	-2.30Ø	1.52Ø
Kil. Iki, Surface 9	-	-1.97Ø	-1.85Ø	1.12Ø
Kil. Iki, Surface 10	-	-1.45Ø	-1.43Ø	0.64Ø
Kil. Iki, Pit # 12	1	-2.90Ø	-2.67Ø	1.32Ø
Kil. Iki, Pit # 11	2	-2.60Ø	-2.51Ø	1.47Ø
Kil. Iki, Pit # 10	2,4,5	-2.42Ø	-2.38Ø	1.05Ø
Kil. Iki, Pit # 9	6	-2.48Ø	-2.22Ø	1.53Ø
Kil. Iki, Pit # 8	7	-2.22Ø	-2.26Ø	1.20Ø
Kil. Iki, Pit # 7	8	-2.25Ø	-1.91Ø	1.99Ø
Kil. Iki, Pit # 13	9,10,11	-2.25Ø	-2.11Ø	1.51Ø
Kil. Iki, Pit # 6	12	-2.40Ø	-2.27Ø	1.17Ø
Kil. Iki, Pit # 5	12	-2.30Ø	-2.38Ø	0.93Ø
Kil. Iki, Pit # 4	13	-2.40Ø	-2.32Ø	1.81Ø
Kil. Iki, Pit # 3	14	-2.68Ø	-2.75Ø	1.01Ø
Kil. Iki, Pit # 2	15	-2.30Ø	-2.06Ø	1.99Ø
Kil. Iki, Pit # 1	16,17	-1.90Ø	-1.67Ø	1.58Ø
Kapoho # 1	-	-1.42Ø	-1.50Ø	1.79Ø
Mauna Ulu, Surface 1	-	-2.52Ø	-2.41Ø	0.98Ø
Mauna Ulu, Surface 2	-	-2.08Ø	-2.03Ø	0.84Ø
Mauna Ulu, Surface 3	-	-1.73Ø	-1.76Ø	0.77Ø
Mauna Ulu, Surface 4	-	-1.53Ø	-1.39Ø	1.07Ø
Kil. July, 1974 #1	-	-2.27Ø	-2.24Ø	0.97Ø
Kil. July, 1974 #2	-	-2.51Ø	-2.58Ø	0.94Ø
Kil. Dec., 1974 #1	-	-1.30Ø	-1.24Ø	1.10Ø

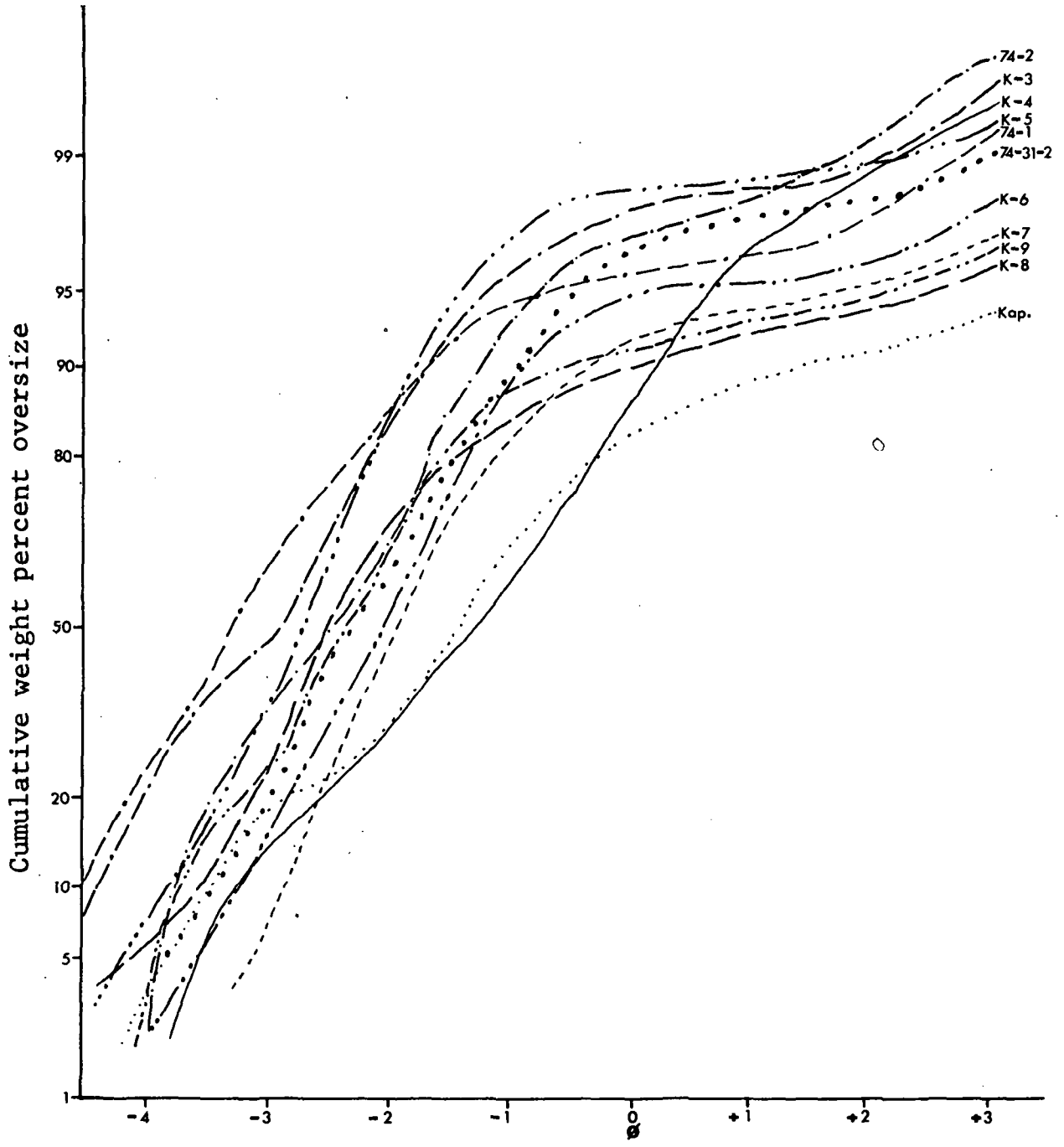

Figure 3. Cumulative probability curves for Kilauea Iki and Kilauea Surface ejecta.

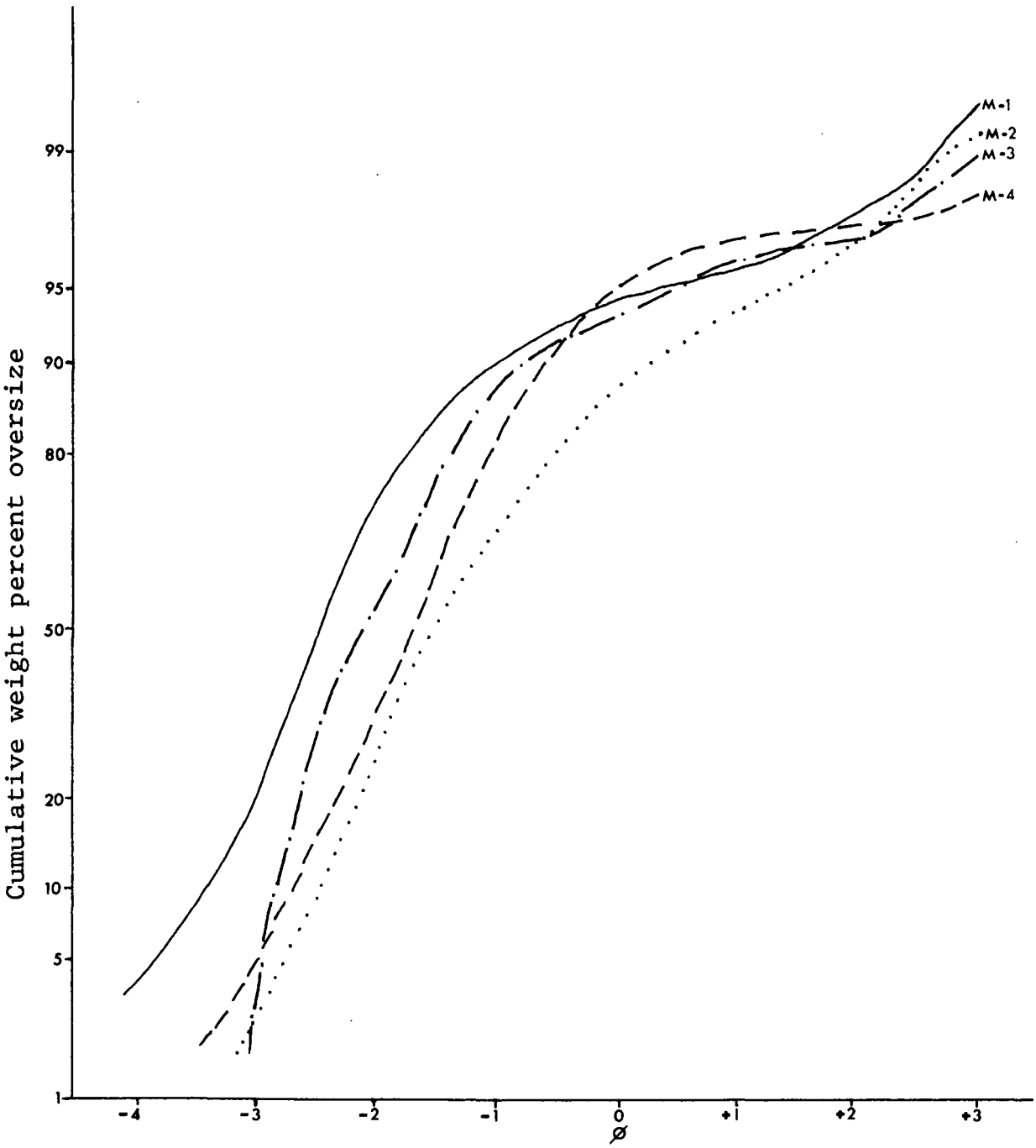

Figure 4. Cumulative probability curves for Mauna Ulu ejecta.

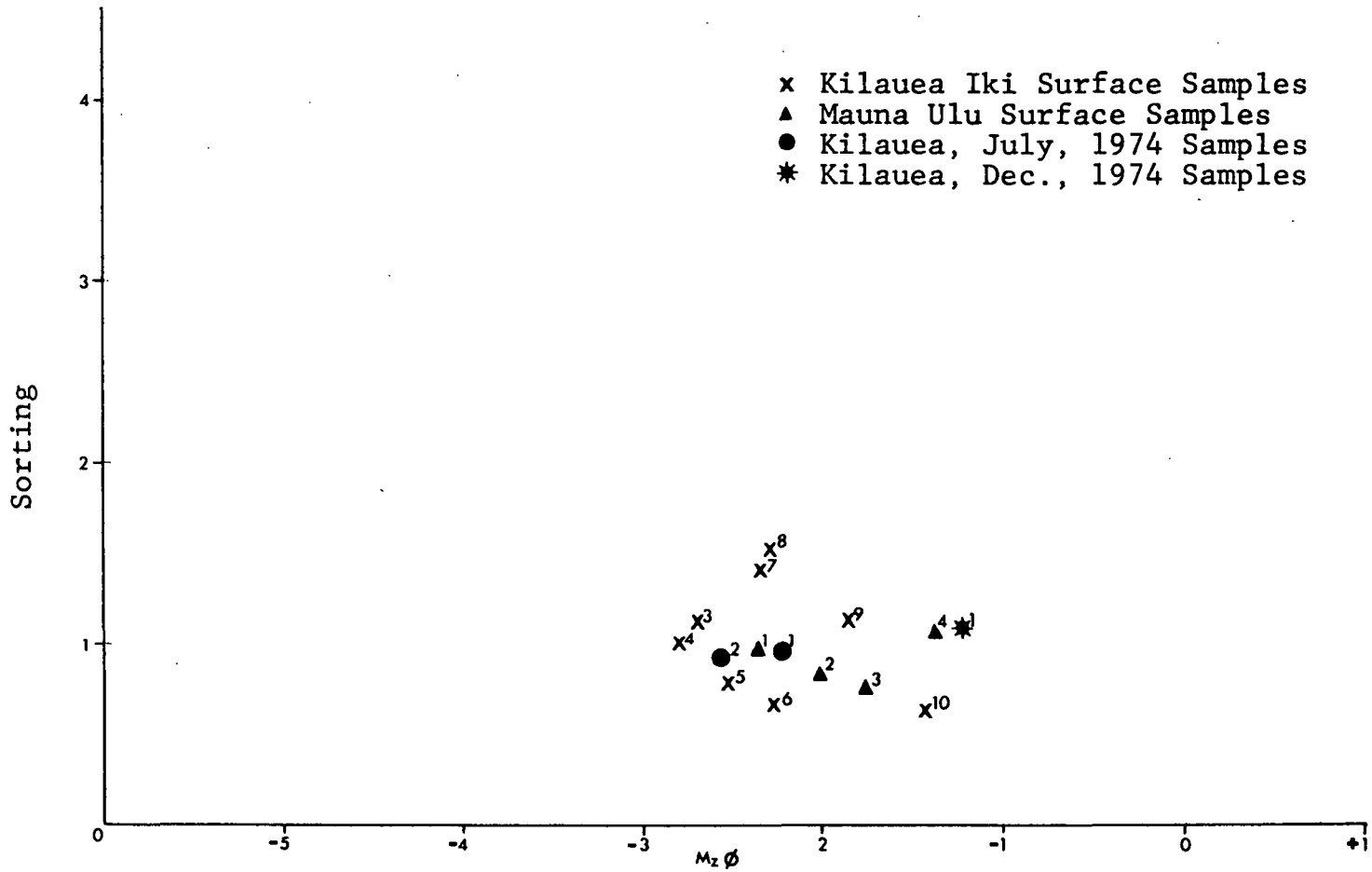

Figure 5. Mean grain size (M_Z) versus sorting (σ_I): Kilauea Iki, 1959-60; Mauna Ulu, 1969-73; Kilauea, July, 1974; Kilauea, Dec., 1974.

observed on particles. The abundance and interrelationship between internal components (vesicles, phenocrysts, fractures, etc.,) determine the development and extent of surface rinds, surface deformation, and fracture patterns. Internal properties indicate the chronological formation of the various components and indicate the effect that earlier formed constituents have on the formation of later features. Glassy particles with similar external morphology may have different internal structures. Petrographic study is thus used to document the internal differences of the particles.

Observations and data gained from the study of internal properties will be used later to interpret the conditions and processes active within the lava fountain and ejecta blanket. Glassy particles have been classified previously on the basis of external morphology using SEM (spheres, filaments, etc.,) which provides a framework for the discussion of internal properties.

Particles having an external spherical morphology exhibit several different types of internal structure. Spheres with mineral grain cores (Pl. 16, fig. 1) are common with the mineral grain exhibiting euhedral to resorbed outlines. Olivine is the predominant mineral noted with minor occurrences of clinopyroxene. The glass coating may be very thin and barely cover the grain, or it may be of considerable thickness with slight to considerable vesiculation. On occasion particles were observed where vesicle coalescence had disrupted the liquid and left only a partial spherical outline around a mineral fragment

core (Pl. 4, fig. 4). Other spheres are composed almost entirely of glass with relatively few vesicles and minor concentric fractures near the edges (Pl. 16, fig. 2). Usually spherical forms contain combinations of phenocrysts, vesicles, and concentric or radial fractures (Pl. 16, fig. 3).

Filaments exhibit two basic types of internal structure: (1) twisted glass strands with elongate vesicles (Pl. 16, fig. 4, upper particle) and (2) straight filaments or Pele's Hair that exhibit numerous stretched vesicles or bundles of vesicle tubes (Pl. 16, fig. 4, lower figure). However, many filaments are composed of solid glass and show little twisting with only slight vesicle development or elongation (Pl. 16, fig. 5).

Composite grains display several types of internal structure depending on the type of particles that combine together. Commonly glassy particles have intertwined filaments (Pl. 16, fig. 6), whereas other combinations of particles consist of glass shards combined with filaments and coated mineral grains.

Texture

Textural relationships indicate the internal processes that take place within a particle during its formation. Glassy particles examined in this study consist primarily of reddish-brown sideromelane glass with numerous crystals and varying amounts of vesicles. Depending upon particle type and internal components, vesicles may be spherical, elongate or confined to areas between mineral grains. Phenocrysts of olivine, clinopyroxene, spinel, orthopyroxene, and plagioclase were observed

as well as microlites (minute birefringent crystals) of olivine and pyroxene. Internal ripples and fractures modify texture.

Two types of texture have been observed: (1) particles consisting nearly or completely of glass (holohyaline texture; Pl. 17, fig. 1); and (2) particles with a glassy groundmass which contain abundant to rare crystals (hypocrystalline texture; Pl. 17, fig. 2). Locally crystals were observed that have aligned orientation (fig. 2, above) due to extension where a glassy particle has been pulled apart or stretched into an elongate form or filament. Over 80 percent of the particles observed were vitrophyric with early formed phenocrysts of partially resorbed olivine and minor amounts of spinel and orthopyroxene. Smaller, later-formed, euhedral crystals of plagioclase, clinopyroxene and olivine were also observed (Pl. 17, fig. 3). Locally the abundance of crystals produces an intersertal fabric (Pl. 17, fig. 5) with a glass to crystal ratio of 3 to 1. Small crystals of olivine and clinopyroxene occur as individuals or in aggregates (Pl. 17, fig. 4).

Vesicles. Vesicles form an important constituent of many glassy particles (Heiken, 1974) and may account for up to 50 percent of the volume of the particle. The abundance, size, shape and surface expression of vesicles have a variable influence on shape, surface morphology and physical properties of the particles. Vesicle shape is usually spherical unless restricted by internal components or modified by external processes which may produce elongate vesicles (Pl. 18, fig. 1).

Extensive stretching of glassy filaments produces stretched vesicles or tubular openings (Pl. 16, fig. 4, lower figure). Vesicle growth may continue until the vesicles impinge on each other and coalesce (Pl. 18, fig. 2) into irregular bubbles encompassing several former individual vesicles. Previously formed crystals locally restrict the area for vesicle growth forcing the vesicle to conform to areas between the crystals (Pl. 18, fig. 3).

The abundance of vesicles in glassy particles varies from few to moderate amounts (Pl. 16, figs. 2,3) to particles that contain abundant vesicles (Pl. 19, fig. 4). Vesicles range in size from small openings of ($< 10\,\mu$) (Pl. 17, fig. 5, lower left) to moderate size ($\sim$0.1 mm) (Pl. 19, fig. 5) or to openings approaching (1-2 mm) diameter (Pl. 19, fig. 6). Vesicles may be uniform in size as noted previously in (Pl. 19, fig. 5) or may have continuous size distribution with no apparent preferred size (Pl. 17, fig. 4).

Fractures. Fractures and cleavage were noted in mineral grains. Mineral grains often exhibit cleavage planes (Pl. 16, fig. 1 and Pl. 19, fig. 3) or basal parting (Pl. 19, fig. 3). Rarely a fracture breaks both the glass and mineral fragment (Pl. 20, fig. 4), otherwise the fracture stops at the grain edge or continues along the glass-mineral boundary.

Glassy particles exhibit several types of fracture: (1) radial, (2) concentric, (3) longitudinal, and (4) polygonal. Radial fractures occur in most glassy particles (Pl. 18, fig. 4), however, they were not observed in spherical particles that have

numerous vesicles (Pl. 19, fig. 4). Radial and longitudinal fractures tend to break along vesicles rather than through glass areas (Pl. 18, fig. 4). Concentric fractures develop near the outer edges of the particle and typically exhibit concave outward cusps (Pl. 18, fig. 5). Usually concentric cracks are accompanied by surface ripples. Where present, concentric cracks usually form the boundary between surface features (such as rinds) and particle interiors. Longitudinal cracks develop in elongate particles, filaments and streamers and parallel the long axis of the particle (Pl. 18, fig. 6). Polygonal fractures were noted in some particles where cracks have developed around vesicles (Pl. 21, fig. 1 and Pl. 18, fig. 6) which contrasts with radial fractures. Triple junctions were commonly observed where fractures join. This type of fracture pattern was observed mainly within particle interiors, however, some fractures continued to the surface. Locally some fractures were noted that were later filled by glass (Pl. 22, fig. 2). Conchoidal fractures were observed that break across thin triangular shaped glass strands of reticulite particles (Pl. 19, fig. 6).

Internal Ripples. Spheres, dumbells, and spheroidal particles with double or single tails often exhibit internal ripples consisting of alternating layers of light and dark glass in contorted swirls from the outer edge to the interior of the particle (Pl. 22, fig. 3). The light and dark layers are bands of optically different material. Whether the banding is due to differences in refractive index between compositionally different

glass layers, or light absorption by minute cracks or inclusions is uncertain. Often a set of light and dark bands can be followed that bend around vesicles (Pl. 22, fig. 4) and either intersect the surface or disappear into the interior of the particle. Where internal ripples intersect the surface they may form the surface ripples observed by SEM (Pl. 15, fig. 6). Internal ripples also tend to be compressed where they pass around vesicles. Fractures usually cut across the ripples without displacement. However, rarely ripples are displaced or concentric fractures develop along the same orientation (Pl. 22, fig. 4, area a). Holohyaline particles that contain few vesicles exhibit ripple patterns throughout the particle (Pl. 22, fig. 3); particles containing phenocrysts and vesicles usually have ripple penetration less than 0.1 mm (Pl. 22, fig. 4). Ripples not only enclose or refract around vesicles as previously noted on the surface (Pl. 15, fig. 6) but also beneath the surface (Pl. 22, fig. 4, central area). Glassy particles that do not develop ripple patterns are: (1) particles with mineral cores (Pl. 16, fig. 1); (2) particles with numerous phenocrysts (Pl. 17, fig. 2); (3) stretched filaments and most elongate particles (Pl. 16, figs. 4,5); and (4) particles with abundant vesicles (Pl. 19, fig. 4).

Surface Features. Surface rinds (Pl. 22, fig. 5) appear on the outer portions of some particles and exhibit numerous concentric fractures and ripples. Usually the rind area is optically darker (greater absorption) as seen in Pl. 22, figs. 1 and 5. Fractures generally break the rind into numerous

fragments (Pl. 18, fig. 5). Particles that contain abundant surficial debris also exhibit surface rinds (Pl. 22, fig. 1). Surface rinds were noted primarily on particles that contained moderate to abundant vesicles and phenocrysts. Rinds seldom exceed a thickness of 0.05 mm and are usually less than 0.02 mm.

Surficial debris is observed on some particles and consists of: (1) irregular shards and fragments (Pl. 22, fig. 1); (2) small hollow or partially crystallized spheres (Pl. 21, fig. 5); and (3) debris patches or clumps (Pl. 16, fig. 3).

Devitrification. Devitrified glassy particles were not observed in this study except for two particles which have features suggestive of devitrification. One sphere has a microcrystalline intergrowth of pyroxene (?) (Pl. 22, fig. 6, lower right). A second possible example is noted in (Pl. 22, fig. 2; Pl. 23, fig. 1) where the upper 1/2 of the particle exhibits crystallites (?) forming within the glass.

Mineralogy

The shape and abundance of each mineral phase depends not only on the eruption but in the case of Kilauea Iki eruption, the location (summit versus flank) and eruptive phase. Modal analyses of 14 particles (Table 8) indicates that: (1) glass ranges from 70 to 90 percent; (2) olivine from 1 to 30 percent; (3) clinopyroxene from 1 to 10 percent; (4) plagioclase from 1 to 4 percent; (5) spinel 1 to 2 percent; and (6) orthopyroxene (hypersthene) less than 1 percent.

Two types of olivine were observed in glassy particles

TABLE 8

MODAL ANALYSES OF GLASS PARTICLES

PRODUCED BY LAVA FOUNTAINS

Sample	Glass	Oliv.	CPX	Plag.	Spinel	OPX
1959-60 Kilauea Iki						
Summit, Surface - 3	85	12	2	-	1	-
Summit, Surface - 4	82	16	2	-	-	-
Summit, Surface - 5	70	24	6	-	-	-
Summit, Surface - 6	90	9	1	-	-	-
Summit, Surface - 7	83	12	5	-	-	-
Summit, Surface - 8	89	11	-	-	-	-
Summit, Surface - 9	86	10	4	-	-	-
Flank, Kapoho - 1	85	5	5	4	-	1
1969-73 Mauna Ulu						
Surface - MU-1	72	18	8	-	2	-
Surface - MU-2	90	3	7	-	-	-
Surface - MU-3	87	8	5	-	-	-
Surface - MU-4	85	10	5	-	-	-
1974 Kilauea, Dec. 31						
Surface - 74-31-1	81	10	8	2	1	-
Surface - 74-31-2	89	8	3	-	-	-

produced by the 1959-60 eruption of Kilauea. The first has a magnesium-rich composition (Fa_{14}), is large ($\sim$ 1-2 mm) and has corroded or resorbed borders (Pl. 20, fig. 1). Liquid inclusions or embayments (Pl. 20, fig. 2) are common. Some partially resorbed olivine crystals have several spinel inclusions arranged in a pattern roughly parallel to the outer edges of the olivine grain (Pl. 17, fig. 6). However, other early formed crystals (Pl. 20, fig. 3), which also contain spinel inclusions, exhibit euhedral forms with excellent development of the {110} faces, and

minor development of {100} or {101} faces. Plate 20, fig. 4 illustrates an olivine grain with an equant shape due to greater development of the {100} and {010} faces. A second type of olivine with a composition of ($\sim Fa_{24}$) has smaller size (< 0.1 mm) and occurs in clumps of equant phenocrysts (Pl. 20, fig. 5). Other euhedral olivine phenocrysts exhibit skeletal forms (Pl. 20, fig. 6) with inclusions or voids parallel to the {110} faces.

The crystallization of an opaque spinel which exhibits well developed cubic faces (Pl. 21, fig. 1) closely follows or is penecontemporaneous with olivine crystallization. Spinel occurs both as crystal aggregates within the glassy groundmass or as enclosed grains within euhedral olivine crystals (Pl. 21, fig. 2).

Clinopyroxene occurs in minor amounts as large phenocrysts (> 0.5 mm) with highly corroded borders (Pl. 21, fig. 3). However, the usual occurrence is either as small tabular individual augite phenocrysts with conspicuous hourglass inclusion structure (Pl. 21, fig. 4) or as radiating clusters (Pl. 21, fig. 5). Skeletal augites are common and exhibit partially developed "H" forms (Pl. 21, fig. 6). Orientation of tabular crystals is generally parallel to the particle surface, whereas radial clusters do not show a preferred direction of growth. At high magnification (> 200X), a study of the glassy groundmass of most vitrophyric particles indicates the ubiquitous presence of small (100 to 500 μ) microlites or crystallites (extremely small, spherical, rod-and hair-like isotropic forms).

Minor amounts of plagioclase and orthopyroxene occur as euhedral phenocrysts. Plagioclase exhibits euhedral, tabular to rhombic-pinacoidal crystals (Pl. 19, figs. 1,2) of negative relief in the higher index glass matrix. Crystals do not exhibit twinning and were sufficiently small that birefringence was not always evident. Trace amounts of orthopyroxene (hypersthene) were noted as large elongate euhedral to subhedral crystals (Pl. 19, fig. 2).

Chemistry

Previous Analyses

Ejecta erupted during the 1959-60 eruption of Kilauea are tholeiitic basalts with a minimum SiO_2 content of 46.7 percent and a maximum of 50.6 percent (Tables 9 and 10).

Energy Dispersive X-ray Analyses (EDAX)

Glass Analyses. Energy dispersive x-ray analyses of glassy particles made in this study are presented in Figures 6 to 10. EDAX spectra display elemental abundance rather than oxide weight percent as given in Tables 9 and 10. A qualitative comparison can be made between the weight percent analyses and the EDAX spectra with the exception that lighter elements (Na, Mg, etc.,) display peaks that are attenuated due to absorbtion. Most Mauna Ulu spheres (Figure 7) have compositions similar to Kilauea spheres except for several spheres (5 noted) that are composed primarily of silicon with minor to trace amounts of other elements (Figure 8, solid line spectrum).

TABLE 9

CHEMICAL ANALYSES OF THE 1959-60 KILAUEA SUMMIT AND FLANK ERUPTION EJECTA

	(1)	(2)	(3)	(4)	(5)	(6)
SiO_2	48.17	48.41	46.74	50.58	48.77	95.20
TiO_2	2.44	2.30	1.92	3.11	2.42	2.40
Al_2O_3	11.65	11.62	9.70	13.88	11.55	1.20
Fe_2O_3	1.87	1.36	1.36	2.18	1.40	0.55
FeO	9.66	10.29	10.44	9.52	10.21	-
MnO	0.22	0.17	0.18	0.18	0.18	0.01
MgO	10.84	13.34	19.25	6.56	13.13	0.20
CaO	10.25	9.77	8.16	10.43	9.29	0.17
Na_2O	3.08	1.94	1.55	2.58	2.08	0.07
K_2O	0.49	0.47	0.41	0.65	0.49	0.05
P_2O_5	0.25	0.23	0.19	0.35	0.26	-
H_2O^+	-	0.04	0.00	0.08	0.09	-
H_2O-	-	-	0.01	0.01	0.02	-
CO_2	-	0.01	0.00	0.02	0.01	-
Cl	-	0.02	0.01	0.02	0.01	-
F	-	0.03	0.02	0.04	0.03	-
S	0.11	-	-	-	-	-
Total	99.03	99.99	99.93	100.19	99.94	100.00

TABLE 9 (continued)

CHEMICAL ANALYSES OF THE 1959-60 KILAUEA SUMMIT

AND FLANK ERUPTION EJECTA

1. Kilauea Iki ejecta, 1959-60; Heiken (1974)
2. Kilauea Iki ejecta, 1959-60; sample S-9; Murata and Richter (1966
3. Kilauea Iki ejecta, 1959-60; sample S-21; Murata and Richter (1966)
4. Kapoho ejecta, 1960; sample F-1; Murata and Richter (1966)
5. Kapoho ejecta, 1960, sample F-17; Murata and Richter (1966)
6. Kilauea Iki altered ejecta, 1959-60; Murata (1966)

TABLE 10

CHEMICAL ANALYSES OF THE 1969-73 MAUNA ULU ERUPTION EJECTA

	(1)	(2)
SiO_2	50.60	50.70
TiO_2	2.30	2.10
Al_2O_3	13.70	13.00
Fe_2O_3	0.60	0.90
FeO	10.00	10.00
MnO	0.18	0.19
MgO	7.60	9.50
CaO	11.30	10.00
Na_2O	2.20	1.90
K_2O	0.51	0.41
P_2O_5	0.30	0.28
H_2O+	0.27	0.37
H_2O-	0.06	0.00
CO_2	0.02	0.01
Total	99.60	99.40

1. Pele's Hair, Mauna Ulu, 1969-73; Duffield, et al., (1977)
2. Glass sphere, Mauna Ulu, 1969-73; Duffield, et al., (1977)

Mineral Analyses. Elemental analysis of gypsum is displayed (Figure 9) where the background spectrum of the underlying glass has been stripped leaving the spectrum of the gypsum crystal with minor amounts of sodium, potassium and chlorine. Figure 10 illustrates the elemental spectrum of jarosite (dotted spectrum) superimposed on the underlying glass analysis (solid lines). Note the increase in iron, potassium and sulfur, whereas a reduction is observed in calcium and silicon in comparison to the glass. An analysis of marcasite is displayed (Figure 8) superimposed over the underlying silicon rich glass spectrum. Spheres with high silicon compositions typically exhibit highly fractured surfaces (Pl. 1, fig. 6).

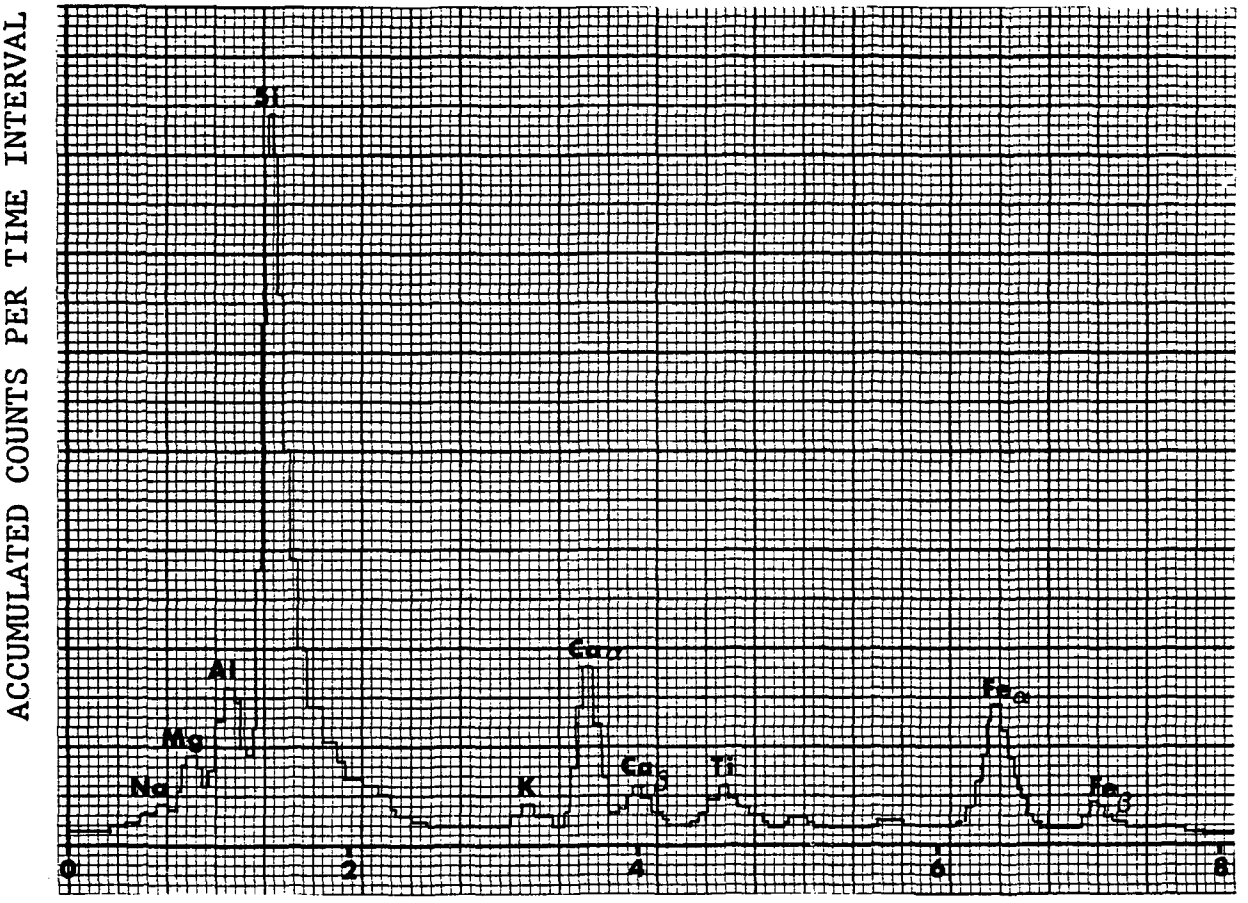

Figure 6. Edax x-ray spectrum of Kilauea sphere.

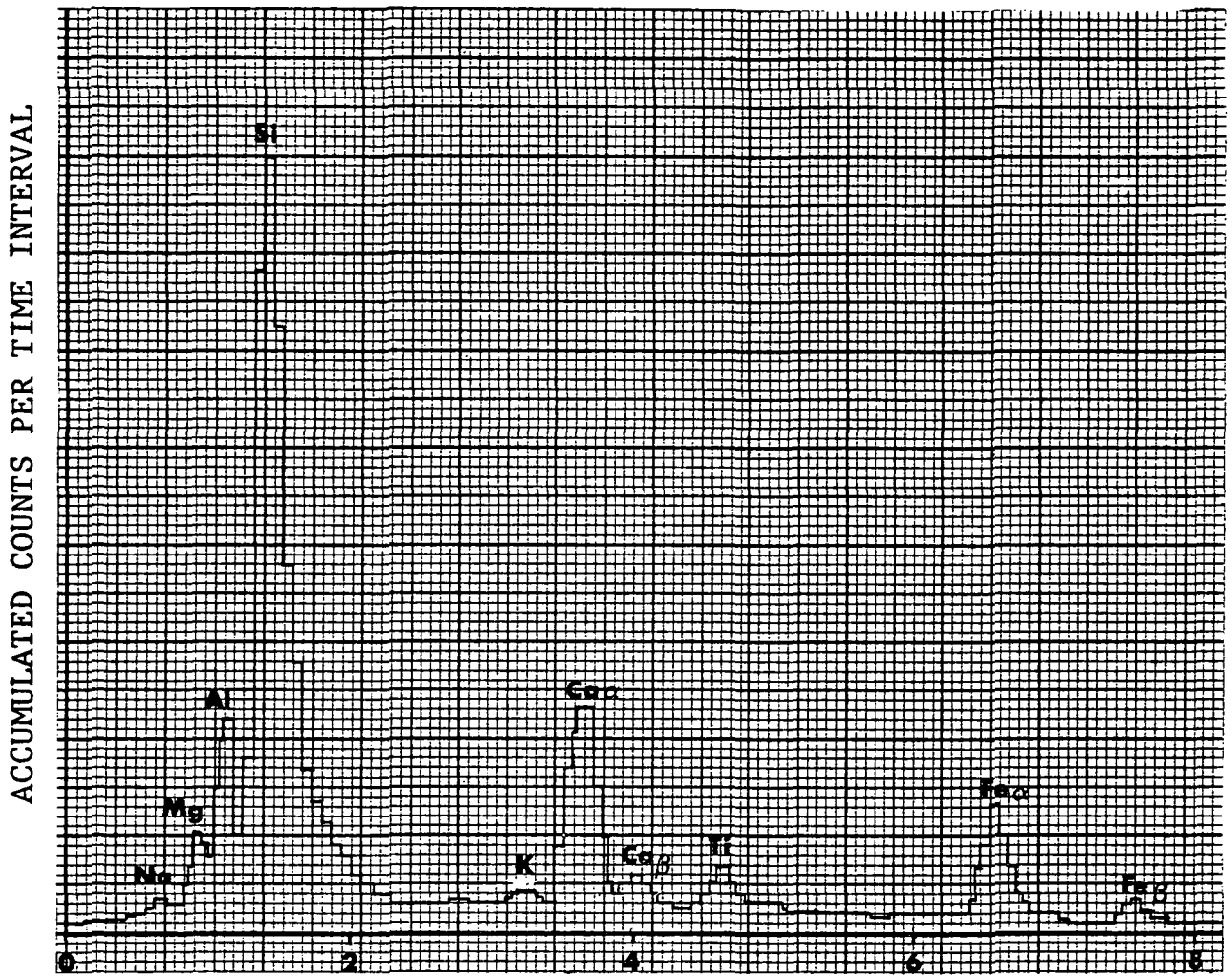

Figure 7. Edax x-ray spectrum of Mauna Ulu Sphere.

Figure 8. EDAX SPECTRUM OF MARCASITE = ...DOTS
MAUNA ULU SPHERE COMPOSITION = —LINES

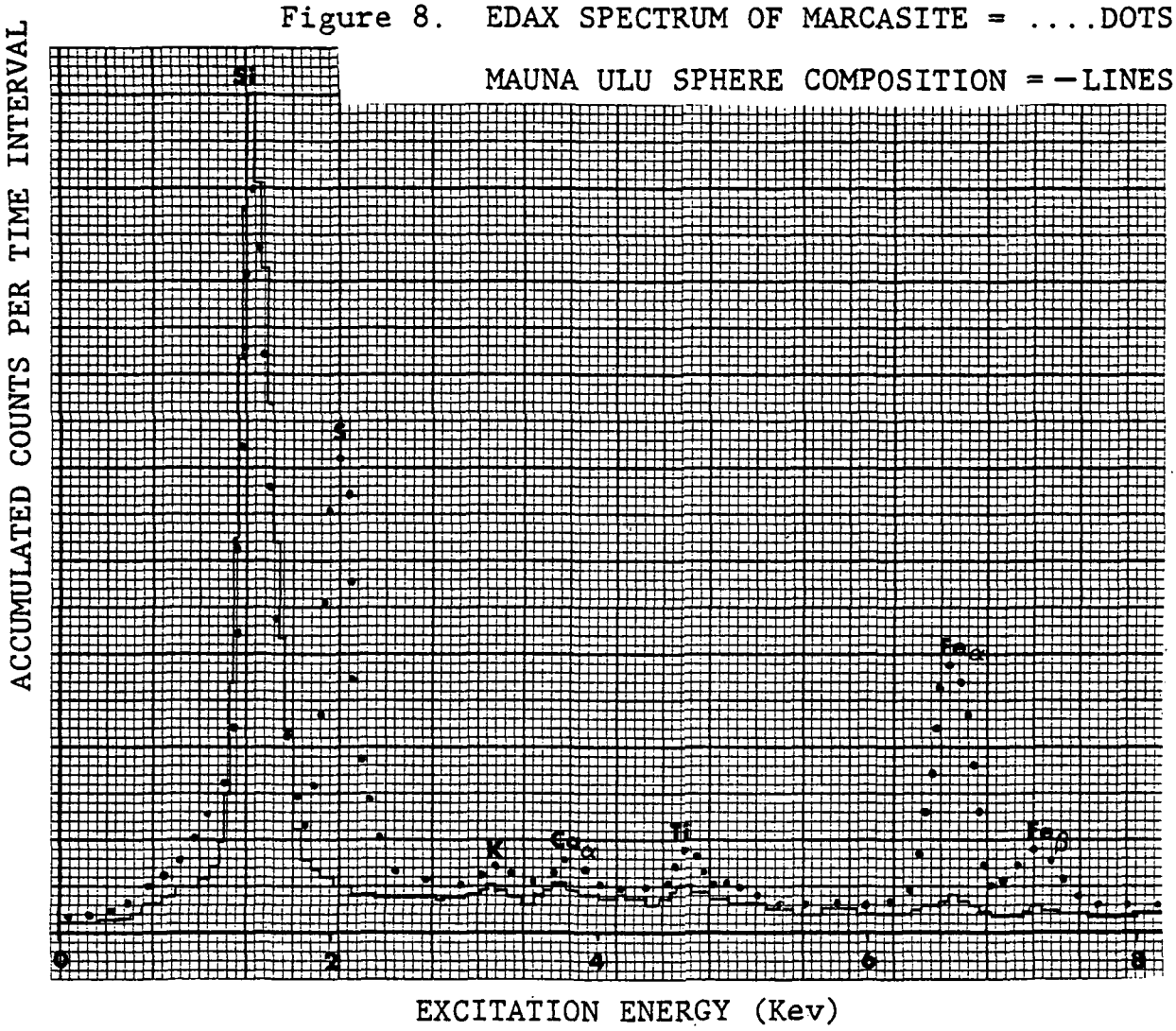

Figure 8. Edax x-ray spectrum of marcasite and Mauna Ulu Sphere.

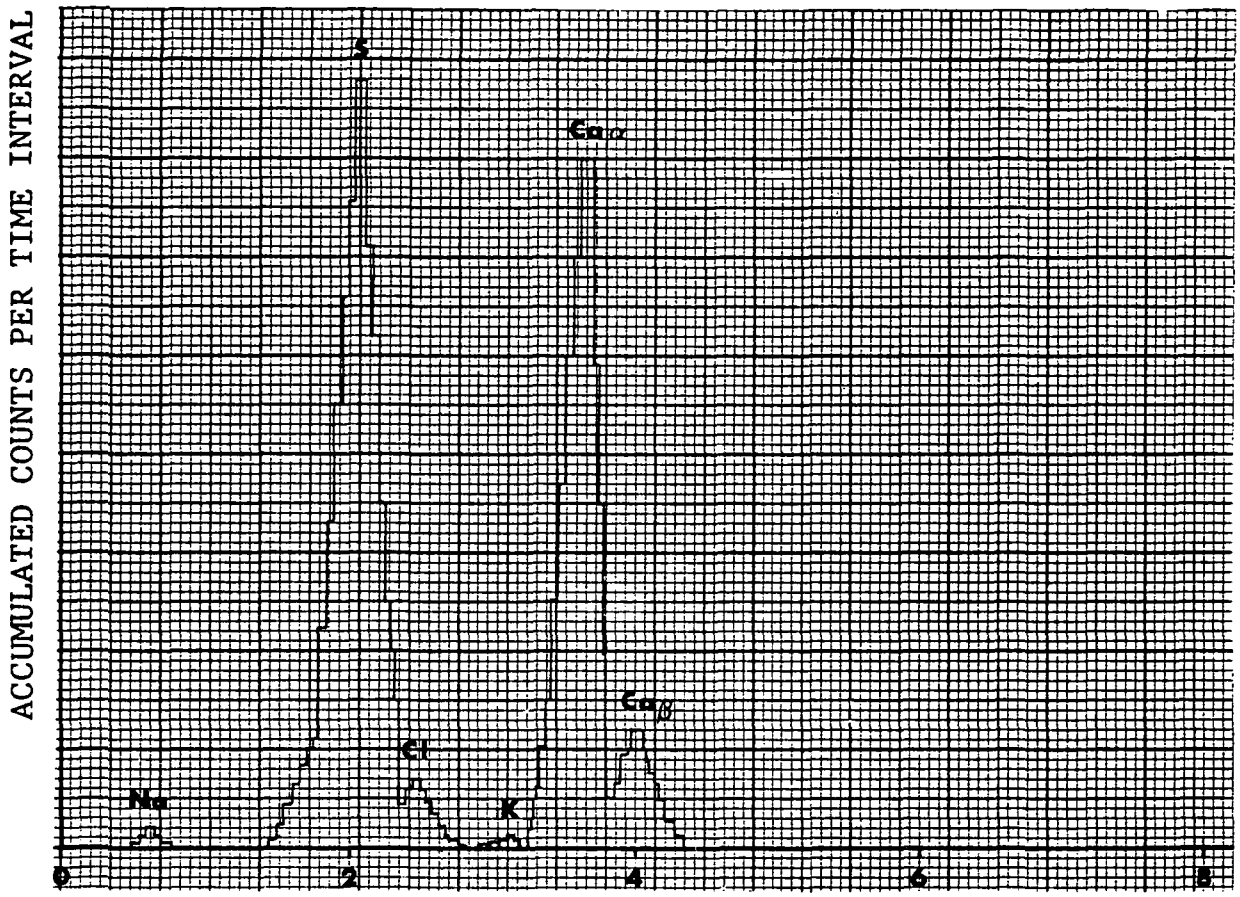

Figure 9. Edax x-ray spectrum of gypsum.

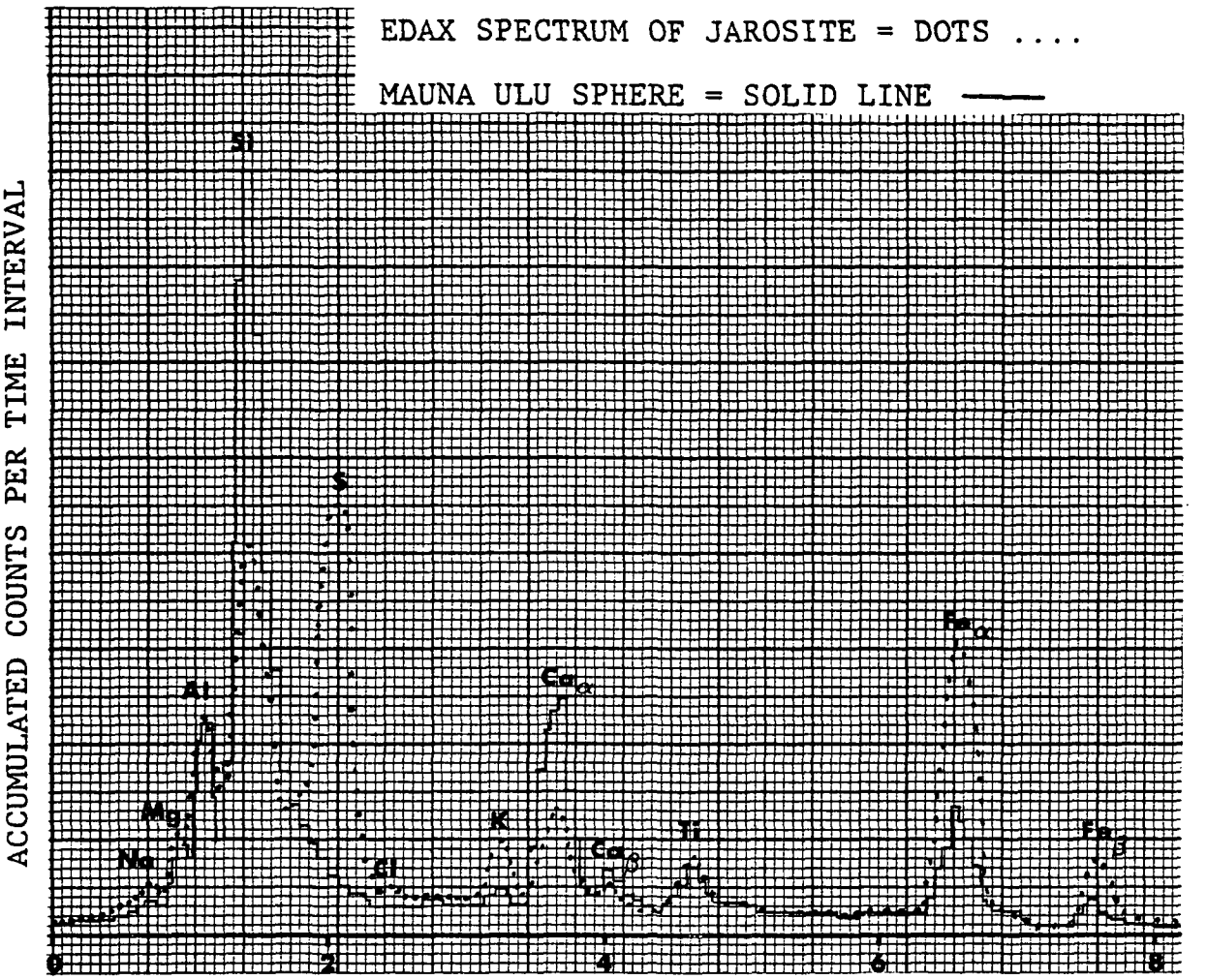

Figure 10. Edax x-ray spectrum of jarosite and Mauna Ulu Sphere.

CHAPTER 4

DISCUSSION AND INTERPRETATION

This chapter discusses the physical and chemical processes active in basaltic lava fountains and associated ejecta blankets that have produced the previously documented glassy particles and their associated external and internal features. Initially, the discussion will present known physical and chemical parameters associated with lava fountains and then follow the format previously established with major sections dealing with the processes of: (1) particle formation, (2) constructional accretion, (3) destructional removal or alteration. One additional section will be discussed: (4) a conceptualized fountain model and model of particle formation and modification. These models will be based on known physical parameters, observations, and data acquired during this study.

Known Physical and Chemical Parameters of Lava Fountains

Physical and chemical characteristics of Hawaiian lava fountains have been documented by several workers and will be summarized here to provide a background for the forthcoming discussion. Temperatures of erupting basaltic lava have been measured by optical pyrometer (Macdonald, 1972) at Kilauea Iki and found to be 1120° to 1190°C with the subsequent flank eruption at Kapoho being slightly cooler (1050° to 1130°C). Temperatures of 1165° to 1170°C were measured during the 1969-71 eruption of Mauna Ulu (Swanson, et al., 1971). These

temperatures are minimal temperatures depending on the atmospheric conditions (haze, smoke, etc.,) present during pyrometer readings. Even more important is that optical methods measure outer rather than inner temperatures of fountains. Even less is known about temperature distribution within the fountain and ejecta plume.

Viscosity is measured by observation of lava flows or from measurements taken from holes drilled into lava lakes. Values obtained are highly dependent upon temperature and amount of crystallization or vesiculation and range for basaltic lava from 500 poise at 1200°C for liquid lava to 8×10^3 poise in a crystal-liquid mixture at 1130°C (Shaw, 1968). Laboratory studies give similar values for remelted lava (Shaw, 1969). Again these values are maximum values since it is not possible to directly measure the viscosity of the liquid within the fountain.

Little data is available on the effects of air current circulation within or around lava fountains. A general conclusion is that strong updrafts will be generated around the outer portions of the vent area with a general tendency of prevailing winds to extend the fountain plume downwind. A distinct possibility exists for particles formed within the fountain and ejected in outward trajectories to be recycled back into the fountain by inward directed convective air currents.

Minimal information is available about chemical conditions within fountains regarding chemical parameters of oxidation, reduction, and partial pressures of various gaseous compounds.

Several workers (Heald, et al., 1963; Nordlie, 1971; and Naughton, et al., 1974) have collected gas samples from erupting fume and performed analyses to determine equilibrium conditions at different temperatures and fugacities. Naughton, et al., (1974) found values for all gas species as real gases in equilibrium with lava at an oxygen fugacity of $\sim 10^{-8}$ atm and at the temperature of eruption, about 1130°C.

Chouet (1973) studied the ballistic nature of ejecta erupted from the volcano Stromboli, Italy, and found that maximum particle velocity was about 72 m/sec, median velocity (50 to 15 m/sec) and a median fragment size of 2-3 cm. Median dispersion of particles from the jet axis was 8° for one eruption and 10° to 45° for a second. Peak gas velocity values were found to be between 112 to 94 m/sec based on several assumed variables.

In summary, lava fountains are produced by vigorous gas driven eruption of basaltic lava at temperatures of $\sim$1200°C and viscosities of $>$ 500 poise. Chemically the lavas are reduced in respect to atmospheric conditions. Low viscosity lava erupted by gas expansion and rapid acceleration through a vent is disrupted into many different particles (clots, blebs, droplets, streamers, filaments or other irregular masses). These particles are further modified by surface tension, aerodynamic streamlining, multiple particle impacts, cooling partially or completely to a rigid state, and possible fragmentation prior to deposition in an ejecta blanket. Particles may be cycled several times between

hot and cold areas within the fountain, further modifying their external and internal characteristics.

Particle Formation

Glassy particles were classified earlier on the basis of morphology as determined by binocular microscope and SEM study and include: (1) spherical, (2) elongate, (3) reticulite, and (4) shard. Other particles noted were (5) glass coated mineral grains or fragments, (6) composites of the above, and (7) lithic fragments. Reticulite and glass shard formation will be discussed later under destructive processes.

Spherical Particles

Spherical glassy particles can be formed by (1) condensation from a gas, (2) heating irregular solid particles above their melting temperature during flight, (3) the break-up of liquid cylinders (jets, streamers, etc.,), and (4) rapid rotation of a liquid mass forming a spray of smaller droplets.

Formation of glassy droplets by condensation from a gaseous phase does not appear to be significant in the production of spheres of basalt composition. Analyses of Kilauean volcanic gases (Macdonald, 1972) indicate that the gases contain very little of the major elements necessary to form basaltic spheres. However, small condensation droplets a few hundred to several thousand angstroms in diameter may form from individual or combined gas phases. Cadle, et al., (1971) observed that gases given off during volcanic eruption consisted largely of dilute sulfuric acid droplets, various dissolved sulfates, and acicular

particles of sulfur. McClain et al., (1968) reported the possible formation of (Si, Ca + Si, Si + Ca + Fe, Ca + S + Cl, and Fe + Ni + Cl) particles by condensation from selective vaporization of basaltic magma erupted from Volcano Syrthlingur, just east of Surtsey, Iceland (1965 eruption).

The remaining three mechanisms seem most likely since liquid lava is disrupted during lava fountain eruption (Naughton, et al., 1974) into many different sizes and shapes. The controlling factors of particle shape depends on the length of flight time, temperature, and viscosity of the particle. The forces acting on the particle are surface tension, angular velocity of rotation, resistance to surface flow, and an outward force of expansion due to vesiculation within the particle. Surface tension is the inward directed forces of cohesion (intermolecular attraction of similar molecules) that tends to modify irregular shapes into forms of minimal potential energy and surface area (Carmichael, et al., 1974). For a liquid that form is a sphere. Levich (1962) found that a liquid cylinder would break-up into spherical droplets (Pl. 2, figs. 1-4) due to surface tension if sufficient time, and high enough temperatures allowed the particle surface to flow. Estimates of the time necessary for the break-up of a basaltic glass cylinder into droplets was determined by Isard (1971) to be 1 to 3 times sphere radius in mm, in seconds. The validity of glassy jets or streamers breaking-up into discrete droplets is verified in observing the string of interconnected droplets (Pl. 23, fig. 1) which have the general configuration of

a sinuous glassy filament.

Spherical particles may also form by the rotation of a liquid mass with sufficient centrifugal force to overcome the force of surface tension (Marshall, 1954). When a droplet forms from a rotating liquid disk or filament it closely approximates the formation of a droplet from a capillary tube. The mass of the liquid hanging at the end of the capillary breaks into at least three parts when rupture occurs. One part remains attached to the host surface; the second which made up the "neck" of the drop is transformed into one or several smaller droplets; and the liquid which hung below the neck forms a large drop (Bikerman, 1958).

Small glass spheres may be produced by passing irregular glass fragments through or into a high temperature region of the lava fountain. Temperatures above the softening point, ($\sim 850^{o}C$) for a basaltic glass, are needed to decrease viscosity sufficiently to allow surface tension to shape the particle into a sphere. A similar process is used to make small glass spheres (ballotini) for commercial uses where powdered glass fragments are passed into a high temperature flame. The plausibility of this method requires that irregular particles are erupted and fall back into the fountain as indicated by Chouet (1973) or the particles are erupted from a lava fountain upwind and pass through or into a downwind fountain. The occurrence of several fountains operating similutaneously is documented in the opening phases of many Kilauean eruptions (Richter and Murata, 1966 and

Swanson, et al., 1971).

The large number of small spheres (Pl. 2, fig. 5) attached to host particles may represent the small droplet fraction formed due to spraying and jet break-up. The decreased number of spheres in the finer-grain size fractions (Table 4) suggests that smaller droplets have accumulated onto larger particles. Hobbs, et al., (1977) noted a similar trend for size distribution of smaller particles erupted from St. Augustine volcano, Alaska in Jan., 1976.

As particle size decrease surface tension increases (Carmichael, et al., 1974) allowing many of the small spherules to retain hemispherical platelet shapes when landing upon larger particles (Pl. 7, figs. 2,3). However, this may also be due to the spherules being cooler, more viscous and semirigid upon impact.

Elongate Particles

Elongate particles consist of streamers and filaments with a length to diameter ratio of greater than 2:1 and 10:1 respectively, which partially to completely solidify during flight. Acceleration of particles from the vent or strong air currents stretch and elongate fluid clots or irregular masses of lava into elongate forms (Pl. 3, figs. 1-6) and filaments or Pele's Hair (Pl. 4, figs. 1,2). Two major processes are responsible for formation of elongate particles: (1) aerodynamic streamlining (Heiken, 1972), and (2) stretching of glass particles into filaments (Duffield, et al., 1977). A variety of particle shapes and

features are produced by variations in temperature, viscosity, vesiculation and extent of crystal formation within the initial particle. Thermal properties control to a degree the viscosity and vesiculation of the glass and whether an elongate particle exhibits fluid to rigid characteristics. Filaments exhibit features suggestive of a wide range of temperature-viscosity values; some being fluid (Pl. 5, fig. 4), whereas others have cooled to a rigid state and fractured prior to or during impact (Pl. 6, fig. 2). Lava particles that contain vesicles or crystals prior to being stretched often develop as filaments with bulges where vesicles or crystals occur along filaments (Pl. 4, fig. 2 and Pl. 3, fig. 3). Fluid, non-vesicular particles produce small thread-like filaments (Pl. 6, fig. 4, area c, and fig. 1), whereas more viscous and vesiculated particles produce glass filaments with stretched or tubular vesicles and ribbing (Pl. 3, fig. 2, areas a,b, and c, and Pl. 16, fig. 4). Interiors vary from filaments that are solid (Pl. 3, fig. 1), to those with a small central tubular vesicle (Pl. 3, fig. 5), or those with numerous stretched vesicles. However, some glassy filaments contain spherical vesicles (Pl. 16, fig. 5) which suggests formation other than by stretching. One possibility is that particles with stretched vesicles are recycled through a hotter portion of the fountain and fused, allowing surface tension to reshape the vesicles, as well as round the ends of the filaments. Locally small filaments (Pl. 21, fig. 2) were observed with rigid walls which fractured during impact exposing

a continuous hollow core or "soda straw" filament. How this type of filament forms is uncertain but may be explained by the following possibilities: (1) a filament that contains a bundle of tubular vesicles which coalesce into a single continuous vesicle prior to impact (Duffield, et al., 1977), and (2) a mechanism similar to that hypothesied for lava tube formation, where a more fluid interior drains as the external surface becomes rigid forming an internal capillary vesicle. Glass filaments are observed to form around "sky-lights" in lava tubes (G. Heiken and M. G. Best, personal communication) indicating that air currents wafted small particles of fluid lava sputtered from the flow. Glassy filaments have also been observed to form at pahoehoe fronts where bulbous toes pull apart into interlocking fibers as more fluid lava flows out. Locally filaments are twisted (Pl. 16, fig. 4, upper figure) by air currents or particle rotation during flight. Air currents waft filaments downwind and often bend (Pl. 4, fig. 2), or form pretzels (Pl. 6, fig. 3, area b), closed loops (Pl. 4, fig. 1) and intertwine numerous filaments into web-like structures (Pl. 6, fig. 1).

Coated Mineral Grains

If lava particles are not homogeneous and contain crystalline phases, an additional force of attraction (adhesion -- attraction between dissimilar molecules) is added to surface tension in holding particles together. Adhesion is usually stronger than cohesion. When dissimilar substances are separated the rupture surface is not the contact plane but lies within one

of the substances. In the case of a liquid containing solid particles the rupture surface will be within the liquid. During eruption individual or crystal aggregates are separated from surrounding liquid by: (1) aerodynamic streamlining stripping glass away; (2) centrifical separation by density difference; and (3) liquid vesiculation until coherence is lost (Pl. 4, fig. 4). In each case, the rupture surface is within the glass (Pl. 20, fig. 3). Numerous examples were observed of glassy particles that contained mineral grain cores (Pl. 4, fig. 4; Pl. 16, fig. 1; Pl. 17, fig. 6; and Pl. 21, fig. 3). Mineral grains were not observed that lacked glass coatings, even though some coatings were not evident until studied by petrographic microscope or SEM (Pl. 4, fig. 3). The abundance and composition of coated mineral grains varies with eruption and occasionally with the phase and location of the eruption. Olivines and rare clinopyroxenes were observed as coated grains with olivine occurring as euhedral (Pl. 16, fig. 1, and Pl. 20, fig. 3) and corroded or resorbed (Pl. 20, figs. 1,2) crystals as was clinopyroxene (Pl. 21, fig. 3). Petrographically, Kilauean olivines represent two different stages of olivine crystallization (Richter and Murata, 1966) with the larger resorbed magnesium-rich crystals indicating crystallization at earlier periods at higher pressures and temperatures. The later formed euhedral olivines are in equilibrium with the surrounding glass and formed in a near surface magma chamber. During the 1959-60 Kilauea Iki eruption several phases (midpoint of phase 1, 2, 4, 5, 10, and 16) contain

10 to 20 percent more olivine crystals than other phases (Richter and Murata, 1966) suggesting eruption of lava from previously settled olivine rich layers within the magma chamber. The percentage of euhedral olivine grains is generally uniform for each eruptive phase and the increase in olivine content for the above olivine enriched phases being resorbed or corroded grains.

Composite Particles

Composite particles consist of several particles welded or held together and are usually formed by multiple particle impact within the fountain. Chouet (1973) observed that many particles have near vertical trajectories and fall back into the fountain. A wide range in particle temperatures can be expected since those which fall back into the fountain may have cooled to a rigid state and collect hotter less viscous particles (filaments, smaller spheres, debris, etc.,) (Pl. 4, fig. 5). In some cases the accreted particles will have cooled to a semirigid state prior to collection and retain their shape (Pl. 4, fig. 6). Composites or combinations (Pl. 16, fig. 6) of almost any kind can occur where a glassy "wish-bone" filament is attached to an irregular mass of vesicular glass. The lack of stretched vesicles within the filament and spherical vesicle shape suggests that this filament fell back into the fountain, was reheated above the softening point where the previously stretched vesicles reformed to their present shape and the ends of the filament were rounded. Some composite forms may form when hot semirigid particles land on the ejecta blanket and cement the underlying

debris to their surface.

Lithic Fragments

Lithic fragments consist of an inner crystalline core covered by an accreted coating of glass, surficial secondary crystals, and other debris (Pl. 5, fig. 1). Compositionally the interior consists primarily of a diktytaxitic intergrowth of plagioclase, minor pyroxene and glass (Pl. 5, fig. 2). The particles are generally rounded and vary in size from ~300 to 90 μ. Two mechanisms of formation may be considered: (1) crystallization of the particle during flight, and (2) eruption of a previously crystallized fragment which acquired a debris coating during flight. Cooling time for an average basaltic particle (Isard, 1971) is estimated to be ~1-3 times the particle radius in mm, indicating a maximum cooling time of ~1 sec for a 300 μ particle. This would be insufficient time to develop the observed texture (Lofgren, 1974). The second mechanism, or crystallization prior to eruption while within the magma chamber, is more plausible except for the abundance of plagioclase crystals. Two possible explanations can be suggested: (1) that the particles are relicts from previously crystallized magmas and were picked up during eruption; and (2) that the magma was held in an upper reservoir for some period of time where the magma differentiated and an upper layer of plagioclase crystals formed which during subsequent eruption were disrupted and ejected as somewhat rounded particles. Richter and Murata (1966) indicate that the initial composition

of the Kapoho (1960) flank eruption was considerably differentiated from that of the later phases which closely resemble the composition of the 1959 summit lavas. This data suggests that magma was stored within the flank conduit system from a previous eruption and was initially erupted when the magma from the 1959 summit eruption forced it from the underlying chambers. One sample noted during this study was collected from Kapoho, whereas the remainder were Mauna Ulu samples which may well have had the same relationship of magma storage from a previous eruption as the Kapoho lavas. A remote possibility exists that if a particle is cycled up and down within the fountain for sufficient time that crystallization could take place or alternatively if the particle was deposited in the ejecta blanket and remained at high temperatures for sufficient time crystallization would occur. However, neither of these possibilities can be seriously considered since if crystallization took place within the ejecta blanket the surface of the particle would be considerably altered which is not the case.

Constructional Surface Processes

Surface features observed on glassy particles provide a record of many of the processes active within a lava fountain and associated ejecta blanket. Fountain processes can be divided into two broad categories: (1) constructional if they add or accrete material to the surface; and (2) destructional if they remove or alter the surface of previously deposited constructional materials. Again it is important to note that particles produced

by lava fountains will have widely varying temperatures and attendant physical states depending upon what region of the fountain they are in or passing through. The microstratigraphy of a particle indicates its history of formation, the capture and accumulation of other particles, possible loss or removal of material, fracturing or breakage, and alteration by oxidation or hydration. The various stages of particle experience may be shortened, by-passed, reversed or repeated depending upon the flight history of the particle. Constructive features previously documented indicate that constructional processes accumulate material on particle surfaces by: (1) accretionary growth or accumulation of solid or liquid particulate materials; and (2) sublimation or condensation growth by sublimation of vapor phase crystals and micromounds or condensation of liquids onto the sample surface.

Accretionary Growth

Accretionary growth is accomplished by the addition of solid or liquid particles to a particle surface by glass splashes, attachment or welding of smaller particles, filaments, platelets, previously grown crystals, and other debris.

Glassy Splashes and Other Fluid Impacts. Glassy splashes are formed by fluid particles encountering a semirigid to rigid host particle. Fluid droplets, streamers or jets cover the underlying material in a uniform film or layer (Pl. 5, figs. 4,5). Since liquid particles have fluid characteristics, upon impact, they wet the surface due to forces of adhesion (Morey,

1954) and cover previously formed surface features. Holland (1964) reported that the balance between cohesion (surface tension) and adhesion determines whether a fluid flows over a surface or draws up into droplets. If adhesion is equal to or greater than cohesion, the surface will be wetted and flow will take place. Depending on temperature, degree of vesiculation, and crystal content, the viscosity of the fluid will determine the thickness of the film. Very low viscosity fluids develop thin films (Pl. 5, fig. 5), whereas viscous fluids produce thick layers (Pl. 5, fig. 4). Rarely were fluid films observed that contained microlites or crystallites which suggests that the liquid was above the liquidus temperature or that crystallites were sufficiently small to be unobserved or the liquid was supercooled below the liquidus prior to crystal nucleation. Locally "splash-soft impacts" contain semirigid cores and fluid exteriors (Pl. 5, fig. 6) which suggests that the particle had previously cooled to a semirigid or rigid state and was cycled back into hotter portions of the fountain where the exterior was heated prior to impact on the host particle. Alternateley, the semirigid grain may have accumulated an exterior layer of lower viscosity liquid by condensation prior to impact. Streamers or jets of fluid glass encounter host particles and form narrow "wetted" bands across the particle surface (Pl. 5, fig. 5, area a). Other semifluid streamer impacts produce wetted surfaces with parallel ridges (Pl. 5, fig. 4, area c and Pl. 6, fig. 4, area c) which indicates two possible mechanisms of formation:

(1) upon partial cooling and subsequent impact of a streamer, an outer semirigid glass skin retained its wall configuration while the fluid interior covered the intrawall area; or (2) due to higher temperature the fluid streamer had greater surface tension (McBirney and Murase, 1971) than the force of adhesion and began to draw up into a rounded form but was prematurely chilled producing the parallel "curled-up" ridges.

Some particles have accumulated a surface film of glass by the accretion of numerous fluid splashes (Pl. 7, fig. 1). The thickness of the film is determined by the temperature and viscosity of the fluid (Pl. 5, fig. 4, compare areas a and e). Other continuous glass films that contain numerous vesicles (Pl. 10, figs. 1,3) were formed by exposure to high temperature rather than accretion.

Glassy Filaments. Glassy filaments are streamers or jets of fluid glass that have cooled to a semirigid or rigid state prior to encounter with a host particle. A continuous range of thermal properties from the fluid to rigid states is possible (Pl. 6, figs. 2 and 3). Filaments which do not wet the surface will be considered here, whereas those which wet the surface have been considered under splashes and other fluid impacts. A single filament may exhibit a range of thermal states (Pl. 4, fig. 5) in that part of the filament is semifluid and wets the surface (left center), whereas the remainder is semirigid and forms an arch (far left). A two fold increase in width is noted when comparing semifluid-fluid versus semirigid-rigid filaments (compare

forms in Pl. 4, fig. 5).

Filaments are attached to host particles either by adhesion or by the host surface being sufficiently hot to weld the rigid filament (Pl. 6, fig. 2). The latter type of attachment may be somewhat weak allowing the filaments to "pop-off", producing surface impressions (Pl. 15, fig. 4). Filaments may be attached soon after formation, whereas others experience moderate to extensive oxide-sulfate alteration (EDAX analysis) prior to attachment (Pl. 12, fig. 2, area c; Pl. 12, fig. 3, area a; Pl. 15, fig. 3, area b; and Pl. 15, fig. 4, area a). Stratigraphically, filament attachment always occurs after surface rippling (Pl. 4, fig. 5 and Pl. 6, fig. 4), accumulation of most micromounds (Pl. 5, fig. 3 and Pl. 10, fig. 6), and platelets (Pl. 11, fig. 1). Filaments usually bridge fractures (Pl. 12, figs. 2,3) but occasionally are broken by them (Pl. 13, fig. 2). Shards typically occur after or contemporaneous with filament accumulation (Pl. 11, figs. 1,2). Crystal development (either by sublimation or subsequent accumulation) occurs after filament accretion. Particle history indicates, but is not limited to: filament accumulation after the surface of the host particle has cooled to a semirigid state, after formation of micromounds and platelets with concurrent fracturing, and probable contemporaneous accretion of filaments and shards with later deposition of sulfate crystals.

Platelets. Platelets are formed by small semirigid spheres impacting a particle surface and deforming into flattened

hemispherical shapes (Pl. 7, fig. 1). A continuous range from fluid splashes to semirigid platelets has been observed with the controlling factor being the thermal state of the impacting particle. Platelets usually occur in patches or fields suggesting a mechanism of formation that produces numerous droplets of similar size (Pl. 7, fig. 2). This along with their general association with larger spheres (Pl. 7, fig. 3) suggests formation by spraying where several smaller particles are formed simultaneously with the larger droplets. Some platelets occur in small groups suggesting that they may have formed by the break-up of filaments (Pl. 7, fig. 1 and Pl. 23, fig. 2). Platelets usually cover micromounds where present (Pl. 7, fig. 3) and in turn are locally fractured where they lie across fractures and are covered by later filaments, shards, and crystals.

Glass Shards. Glass shards form by impact of generally rigid particles onto a rigid host surface or by vesicles bursting through a thin semirigid to rigid outer shell. Further discussion of shard formation is considered under mechanical abrasion.

Sulfate Crystals. Gypsum and jarosite crystals occur as accreted crystals which have grown elsewhere and were later deposited on a host surface. The distinction between crystals grown elsewhere with later accretion to a host surface versus a crystal that has grown in place on a host by vapor phase growth is difficult to distinguish. Critera used in this study to determine crystal accretion were: (1) impact features on the

host particle directly related to crystal impact; (2) different micromound populations on the surface of the crystal to that of the underlying host (Pl. 9, fig. 2). Differences in micromound population or size may also be explained by secondary or multiple periods of micromound development. (3) geographic association of crystals with other accreted materials; and (4) large crystals located on only a few areas of the host particle (Pl. 2, fig. 3).

Gypsum crystals suggestive of accretion are generally larger than 5 microns, exhibit euhedral form and, although associated with others, are usually single crystals. They either rest on earlier formed surface features or are associated with clumps of surficial materials (Pl. 12, fig. 3). Jarosite crystals were observed as tabular to spindle forms which encrust filaments (Pl. 8, fig. 4) and larger gypsum crystals which have at a later time accreted to the host surface. Since gypsum and jarosite crystals usually cover previously accreted materials a late stage of accretion is suggested with attendant low temperatures ($\lesssim 320^{o}C$).

Amorphous Calcium Sulfate. Aggregates of amorphous or microcrystalline calcium sulfate with minor amounts of K, Na, and Fe (EDAX analyses) were observed as irregular masses, clumps (Pl. 4, fig. 6) or associated with other accreted debris (Pl. 11, fig. 3) suggesting formation prior to impact. Locally amorphous calcium sulfate forms as small irregular to blocky aggregates on semifluid filament impacts (Pl. 6, fig. 3, area d). A possible method of formation is that the semifluid filament was previously

semirigid or rigid; had accumulated an alteration coating of calcium sulfate such as (Pl. 15, fig. 3) or elemental sulfur; then recycled into a hotter region of the fountain by convective air currents and was fused. Akhtar and Cable (1968) report that when SO_3 is added to liquid soda -lime -silicate glass in amounts greater than the solubility of the liquid (usually a few percent) separation takes place with the excess sulfate forming a surface film of Na or Ca sulfates which reduces the surface tension from $\sim$300 dynes-cm^{-1} to about 150 dynes-cm^{-1}. A similar process may explain the formation of the small irregular masses which appear to "ball up" on the semifluid streamer due to an apparent difference in surface tension between a surface layer of sulfate and the underlying glass.

Sublimation or Condensation Growth

Sublimation or condensation growth on particle surfaces takes place by nucleation and growth of vapor phase crystals, sublimation or condensation of micromounds, and condensation of liquid films on cooler surfaces. Research on sublimate systems has been summarized by White and Waring (1963) with recent studies by Stoiber and Rose (1970) of encrusting sublimates around fumaroles or near volcanic vents in Central America. Fume collected from volcanic clouds was analyzed for particulates by Cadle, et al., (1969), Cadle and Frank (1968), Vonnegut, et al., (1966), and McClaine, et al., (1968). Several workers (Meunow, 1973, and Duffield, et al., 1977) have characterized gaseous components given off from Pele's Tears and Hair during heating

and have reported that some gases (CO_2, SO_2, etc.,) indicate decomposition of encrusting carbonates, sulfates, and sulfur sublimates. An important study (Naughton, et al., 1974) of gas-sublimate samples collected directly from the fume of the 1969-70 eruption of Mauna Ulu utilizes computer calculations to define reduced and oxidized conditions at 1 atm for the main gaseous components at approximately lava fountain temperatures (1400°K). They also studied the changes that take place in the oxidized mixture when the temperature is lowered to 400°K. To date few workers have undertaken the study of the above mentioned particulate sublimates as to morphology or habit and their relationship to host particles.

Vapor Phase Crystals. Four minerals have been identified based on crystal morphology and composition: (1) elemental sulfur; (2) gypsum; (3) jarosite; and (4) marcasite.

Elemental sulfur locally forms as fiberous to feather-like clusters (Pl. 8, fig. 1) and is associated with surficial debris which generally covers other surface deposits suggesting late stage and low temperature formation. Stoiber and Rose (1974) reported the formation of native sulfur sublimates at Central American fumaroles in regions below temperatures of 150°C.

Naughton, et al., (1974) indicate the formation at eruption temperatures of crystalline calcium and sodium sulfates which do not exhibit compositional change through a temperature range of 1400 to 400°K in both reduced and oxidized environmental conditions. Whether the calcium sulfate is anhydrous (anhydrite)

or hydrous (gypsum) is not specified. Calcium sulfate crystals (EDAX analysis) observed in this study have euhedral monoclinic forms (Pl. 5, figs. 1,3; Pl. 8, figs. 2,4 area b) characteristic of gypsum ($CaSO_4 \cdot H_2O$). Differential thermal analyses of gypsum (Kostov, 1968) indicate that gypsum dehydrates at temperatures greater than 150 to 250°C to anhydrite ($CaSO_4$). This further restrains the formation of gypsum to those regions within the fountain or plume that have low temperatures.

At higher temperatures (1400 to 400°K) anhydrite may be the crystalline calcium sulfate phase which alters by hydration at lower temperature to gypsum. Larsen and Chilingar (1967) noted that the conversion of anhydrite to gypsum requires ~40 percent increase in volume. The majority of the crystalline forms observed in this study indicate little expansive deformation; however, rarely crystals were observed which have expanded anhedral surfaces suggesting hydration of anhydrite to gypsum (Pl. 23, fig. 3). Therefore, it is suggested that vapor phase calcium sulfate crystals observed in this study formed on host surfaces as gypsum at low temperatures rather than anhydrite which formed at higher temperatures with a later low temperature hydration.

Jarosite, $K\ Fe_3\ (SO_4)_2 \cdot 6(OH)$ (Figure 10), was observed to form as initial hexagonal crystals (Pl. 8, fig. 2) with later tabular to lenticular shaped crystals forming on the surface of the hexagonal forms (Pl. 8, fig. 5). The reason for the development of an initial hexagonal habit with a later change to tabular

crystals is uncertain. However, tabular to lenticular crystals always form on previously formed jarosite or gypsum which suggests that they are lower temperature forms. Krauskopf (1967) reports that jarosite forms in oxidized, low temperature environments. In DTA studies of jarosite, Kulp and Adler (1950) found that jarosite decomposes by dehydration at temperatures greater than 460°C. These findings support the premise that the hexagonal variety of jarosite forms at temperature ranges between 460 and ~250°C. Lenticular to tabular shaped varieties form at temperatures lower than the dehydration temperature of gypsum (~150 to 250°C). An amorphous variety of jarosite was observed forming as ridge-like deposits along polygonal fractures (Pl. 14, fig. 5). The formation of jarosite in close association with polygonal fractures suggest that water vapor or hydroxide ions combines with K and Fe atoms exposed along fracture surfaces. Holland (1964) reports similar reactions in synthetic glasses with the released K and Fe migrating to the surface and in the presence of SO_3 forming alkali-iron sulfates (Sendt, 1962).

Marcasite (FeS_2) was observed on several particles as multiple sheath-like crystals (Pl. 9, fig. 5) with some crystals exhibiting serrated or cocks-comb structures on the ends of tabular forms (Pl. 5, fig. 6). Naboko (1959) reported the formation of marcasite in volcanic exhalations from volcanoes of the Kamchatka-Kuriles region. Little is known about the stability field of marcasite beyond that it is unstable above 300°C (Barnes, 1967) and converts to the higher temperature

phase pyrite. Krauskopf (1967) indicates that marcasite forms at lower temperatures and more acidic environments than pyrite or pyrrhotite. This information along with the occurrence of marcasite resting on top of micromounds (Pl. 5, fig. 6) and local association around the periphery of gypsum crystals (Pl. 9, fig. 5) suggests a low temperature and late stage of formation.

Micromounds. Surficial micromounds form as continuous to patchy accumulations of small (~500 to several thousand angstroms) irregular to hemispherical surfaces (Pl. 10, figs. 4 and 5) or interconnected slightly larger "beaded" micromounds (Pl. 10, fig. 6). Formation may occur by: (1) sublimation of silicate materials which produces the hemispherical type of mounds, and (2) disruption of a liquid film due to surface tension which produces the "beaded" variety.

Sublimation micromounds are present on most glassy particles and vary from closely to moderately spaced mounds (compare Pl. 10, fig. 5 with Pl. 8, fig. 3). Some surfaces exhibit micromounds of approximately the same size (fig. 3, above), whereas other surfaces exhibit some size variation between mounds but within an order of magnitude of the mean (Pl. 10, fig. 5). The size to which micromounds grow depends upon the length of time a surface is exposed for sublimination, compare areas (a) and (c) in Pl. 10, fig. 4, where area (a) is extensively covered while (c), an area exposed by later spalling, has sparse development of smaller individual micromounds. Microstratigraphy of particle surfaces indicates that micromound development was initiated

early and continued throughout most of the particles history; i.e. micromounds are covered by fluid splashes (Pl. 5, figs. 3,6), semifluid to rigid filaments (Pl. 6, fig. 3), and vapor phase or accreted crystals (Pl. 8, figs. 2,3,6). Features indicating continued development during later particle history are spalling (Pl. 12, fig. 6) and coated fracture surfaces (Pl. 12, fig. 2).

Chemically, micromounds are similar to host surface compositions with minor addition of sulfur, potassium, iron, copper, and zinc (EDAX analyses). Whether micromounds represent sublimated silicates, nitrides or oxides, etc., is uncertain since methods of analysis used in this study does not allow for the determination or presence of the lighter atomic number elements (oxygen, carbon, nitrogen, etc.,). If micromounds are produced by sublimated lava vapors (Vonnegut, et al., 1966) they would exhibit enrichment of the more volatile metallic elements. McKay, et al., (1973) suggested a similar mechanism for the formation of lunar micromounds in which the more volatile silicate fractions of high temperature lava are vaporized and subsequently sublimated or condensed onto particle surfaces in the cooler regions of lava fountains. The presence of micromounds coating fracture surfaces (Pl. 12, fig. 2) suggests that a gaseous phase released from the interior of the particle may be responsible for some micromounds.

"Beaded" micromounds represent a different mode of formation; one of disruption of a liquid film due to surface tension. Only three particles were observed during this study with this

type of mound development. Again, the micromounds have similar compositions to that of the host particle. The mechanism of formation for such micromounds is an initial coating of the particle by either a single or several simultaneous fluid splashes, or the condensation of a liquid layer of silicate material. In either case, the host surface would be cooler than the hotter film which would have a higher surface tension coefficient (McBirney and Murase, 1971) allowing the surface film to break-up into beads or strands as noted in (Pl. 10, fig. 6). The time of formation is early as indicated by later added surficial particles etc., but in some cases the micromound beads cover previously formed fractures indicating that the host particle cooled prior to the acquisition of the liquid film and bead formation.

Destructional Processes

Destructional processes break apart, remove and alter accumulated surficial debris or break the particle into fragments. Three broad categories constitute destructional processes: (1) mechanical disintegration which includes fracturing, abrasion and some phases of vesiculation; (2) chemical alteration which includes decomposition, and oxidation, and (3) surface modification by rippling, waving, vesiculation, and surficial rind formation. Destructional processes modify particle surfaces throughout their history but for the most part affect the particle near the completion of its history. A clear-cut time schedule is not to be expected for the various phases or stages of particle history:

usually there is an overlapping of several processes. Constructional processes may be operative during the same time interval that destructional processes are altering or removing previously collected surface debris. Particles may be cycled back and forth alternating the effects of the above processes.

Mechanical Disintegration

Mechanical disintegration is caused by three main processes: (1) fracturing; (2) abrasion; and (3) particle disruption due to extensive vesiculation. Particle size, cooling rate, degree of vesiculation, crystal content and flight path of the particle determine the extent of mechanical disintegration.

Fracturing. Glass fractures result from thermal stresses developed within the glass by rapid cooling (thermal shock), chemical corrosion, and rapidly applied loads (impacts). Fracture type depends on the thermal state of the particle and the nature of the applied stress. Thermal stresses are relieved and some fractures annealed by reheating and gradual cooling (Morey, 1954). When a particle cools rapidly permanent stress develops between adjacent regions (Jones, 1971) with the surface experiencing compressive stress, whereas tensional stress is developed in the interior of the mass (Kingery, et al., 1976). However, upon heating the stress fields are reversed. Once a fracture is initiated in a glass particle, usually at a flaw, point of surface damage, or region where surficial debris is bonded to the surface (Cameron, 1968), it continues unabated until a phase or other boundary provides resistance to its propagation.

Several types of fractures were observed in glassy particles: (1) radial which radiate outward from the interior (Pl. 18, fig. 4); (2) surficial polygonal fractures (Pl. 12, fig. 1); (3) minute shallow cracks (Pl. 12, fig. 2, area d); (4) local fractures related to particle impacts (Pl. 12, fig. 3); (5) concentric or peripheral fractures associated with surface rinds (Pl. 18, fig. 5); and (6) internal polygonal fractures (Pl. 22, fig. 1).

Radial fractures were observed in many smaller particles (mean size $\sim$0.45 mm) that have sparse but generally large vesicles (Pl. 18, fig. 4 and Pl. 19, fig. 5). Whereas particles that contain numerous vesicles of various sizes (Pl. 19, fig. 4, and Pl. 18, fig. 2), surficial rinds (Pl. 22, fig. 5), and mineral grains as central cores (Pl. 16, fig. 1) do not contain radial fractures. Radial fractures generally radiate outward from an internal origin (Pl. 16, fig. 3) and decrease in width towards the periphery and often do not reach the particle surface. Sparse, large vesicles are usually located along radial fracture paths suggesting that gases escaping from the ruptured vesicle may help propagate the fracture. Fractures of this type are due to tensional stress developed during cooling. Rapidly cooled particles with numerous multi-sized vesicles seldom contain radial fractures because once initiated they encounter vesicles which retard and stop their propagation (Kingery, et al., 1976). The lack of radial fractures may also be explained by the numerous vesicles being able to deform and absorb the stress.

Surficial polygonal fractures (Pl. 12, fig. 1) are produced by surface layers failing under tensional stress. Kingery, et al., (1976) indicate such forces develop during reheating of previously cooled particles. Other particles which are highly fractured and exhibit similar polygonal patterns (Pl. 1, fig. 6) consist primarily of silicon oxide (EDAX analyses) which suggests a unique formation for such particles. Murata (1966) reported that pumice fragments collected from the Kilauea Iki ejecta blanket shortly after eruption had decomposed by reaction with HCL into "opaline pseudomorphs" of the previous fragments. It can be suggested that occasionally some of this highly siliceous material slumped or fell back into the lava fountain, became heated and developed tensional fractures on heating. A second alternative is that these particles were selectively condensed from eruptive vapors (McClain, et al., 1968). Internal polygonal fractures observed in other particles (Pl. 22, fig. 1) represent tensional failure of the inner glassy area during initial rapid cooling of the particle.

Many particles contain numerous, small (< 0.5 μ wide) surficial cracks that are associated with tensional or compressional failure of surface materials. These fractures are produced primarily by differential contraction between compositionally different materials (Pl. 14, fig. 1) where small fractures have developed between troughs and ridges, expansion cracks produced by alteration or oxidation (Pl. 14, fig. 4), and dehydration of surface coatings (Pl. 12, fig. 2).

Concentric fractures occur near the outer margins of many particles (Pl. 18, fig. 5) and often form the boundary between surface rinds and undisturbed glassy interiors. Generally they have concave outward paths that either intersect other concentric fractures and stop or continue to the surface. A close association with internal ripples was observed with fractures paralleling the ripple pattern (Pl. 22, fig. 4). Some minute hair-like fractures form boundaries between light and dark ripple layers and locally develop small perpendicular fractures breaking each ripple layer into smaller tabular fragments. Large concentric fractures, which form boundaries between surface rinds and glass interiors, sharply truncate rind features and suggest formation by compressional stress due to cooling and aerodynamic drag which produced plastic deformation of the outer surface until failure occurred resulting in an upward curving fracture.

Abrasion. Abrasion is the removal of surface materials by scraping, spalling or chipping. In most cases this process occurs when the host particle is semirigid or rigid and is either scraped or impacted by a second particle. Scrapes vary in size and shape (Pl. 10, fig. 4, area b) and generally occur as a minor process in material removal.

Spalling and chipping are common processes (Pl. 12, fig. 4) and nearly always result from the impact (Pl. 12, fig. 3) of a second particle onto a rigid host surface. Mechanical failure results, producing a spall or chip that is characterized by steep to gentle conchoidal edge fractures (Pl. 12, fig. 5) and

a smooth to cuspate, slightly curved bottom surface (Pl. 12, fig. 6). Pl. 12, fig. 3 leaves little doubt that debris impacts produce spalls. Whether sufficient stress builds up between adjacent layers within a glass particle during cooling, as suggested by Jones, (1971), to initiate exfoliation type spalls is uncertain. However, this type of stress may be localized by thermal expansion and contraction (Margolis, 1971) and together with polygonal fractures produce polygonal shaped spalls (Pl. 1, fig. 6).

Fragments spalled or chipped from particle surfaces are termed shards which commonly accumulate onto other particles. Often spalling removes constant uniformly thick layers suggesting that in some cases each spall represents an accreted layer or glass film (Pl. 5, fig. 4, area e) with the underlying surface exhibiting surface features. Some shards have surface coatings of surficial materials suggesting spalling, etc., occurred near the completion of a particles flight path. Other shards may form by internal vesicle expansion until intervesicle walls become disrupted.

Particle Disruption Due to Vesiculation. Some particles containing mineral cores are remnants of an original spherical shape (Pl. 4, fig. 4) which was destroyed due to extensive vesicle development and subsequent loss of glass coherence (McBirney and Murase, 1971). Disruption occurred, with immediate chilling to a rigid state, as evidenced by the lack of rounding of vesicle walls. An alternative mechanism for formation of such particles

would be the mechanical breakdown of particles upon landing or later while within the ejecta blanket. However, the presence of accreted surficial materials on vesicle surfaces refutes this possibility.

Reticulite Formation. Reticulite (Wentworth and Williams, 1932) developes by eruption of lava that has vesiculated to such an extent that coherence is lost resulting in a disrupted liquid froth. Such a material was erupted at Kilauea Caldera (prehistoric) and is described by Heiken (1974) as a lattice-shaped network of triangular glass rods produced by the continued growth of vesicles in a very low viscosity magma producing an open network or froth. A similar type of particle (Pl. 1, fig. 1) is produced by the mechanical breakdown of glassy particles which have centers of extensive vesicle development or coalescence (Pl. 18, fig. 2). The comminuted fragments consist of highly irregular, triangular shaped glass strands (Pl. 19, fig. 6). Grain size analyses indicate a steady increase in reticulite frequency as grain size decreases (Table 3). Mechanical disintegration of vesiculated central portions of glassy particles as the source of the reticulite was verified by a simple experiment in which six fractured spheres ($\sim$1-3 mm dia.) were sieved for 20 minutes. Results indicate a parallel trend of increasing reticulite particles with each mesh of decreasing size. Although labeled as reticulite throughout this study this type of particle should not be mistaken for the lace-like reticulite described by Heiken (1974), but can be easily mistaken for

it if care is not taken. Further means of discerning reticulite formed during eruption versus that formed by mechanical commuition is the presence of accreted materials on the erupted forms and the lack of such features on mechanically formed reticulite. To resolve the problem of nomenclature it is suggested that erupted reticulite be termed "froth reticulite" and the mechanically produced analog labeled "friable reticulite".

Chemical Alteration

Chemical alteration of glassy particles consists of the removal of materials by chemical decomposition or solution; alteration of surficial debris by the formation of oxide or sulfate films; and development of other weathering products. In most cases these processes are surficial; however, locally complete particles have undergone alteration or partial digestion. Mineral grains or fragments within particles were rarely altered with the bulk of the alteration affecting only surficial glass areas.

Decomposition. Decomposition, as considered in this study, includes the removal of soluble ions throughout a particle or alteration restricted to surficial materials. Recently a study by Murata (1966) indicated an important difference between gases samples from recently deposited ejecta blankets and gases samples from volcanic vents and fumaroles (Macdonald, 1972). The largest difference was in the greater quantity of hydrochloric and to a lesser extent, sulfuric and hydrofluoric acid vapors or condensates, which were emitted from small fissures in the ejecta

blanket. In fact, Murata (1966) indicated that the gases contained a considerable amount of a condensate which proved to be essentially 2N HCL. Cadle and Frank (1968) found that liquid particulates collected from the fume of lava fountains consisted predominantly of dilute sulfuric acid. These findings suggest that both fountains and ejecta blankets contain reactive acidic vapor or condensates that are active agents of chemical attack; either as droplets that form etch depressions (Pl. 13, figs. 1,2) or as vapors that grossly alter glassy particles, similar in composition to those of Tables 9 and 10, by selective partial digestion to "opaline psuedomorphs" consisting of 95.2 percent SiO_2 (Murata, 1966). This type of partial digestion by selective removal of alkali oxides due to acid attack while the silica component resists attack has been confirmed by Holland (1964).

Silica glass is almost insoluble in water except at high temperatures ($> 250^{o}C$) and therefore the attack on glass at lower temperatures depends on the high concentration of soluble components such as alkali in the glass. Charles (1958) observed that water or water vapor assumes an important role in the corrosion of soda-lime glasses at moderate and elevated temperatures. Three steps are important:

(1) A typical hydrolysis reaction of the salt of a weak acid.

$$\left[-\overset{|}{\underset{|}{Si}}- O - Na\right] + H_2O \rightarrow -\overset{|}{\underset{|}{SiOH}} + Na^{+} + OH^{-}$$

An oxygen-sodium bond near the surface is broken, with

migration away of Na^+ ion, and subsequent oxygen dissociation of a H_2O molecule forming a free hydroxide ion.

(2) Breaking of the very strong Si – O – Si bond by a hydroxide ion.

$$[-\overset{|}{\underset{|}{Si}} - O - \overset{|}{\underset{|}{Si}}-] + H_2O \rightarrow [-\overset{|}{\underset{|}{Si}} - OH + OH - \overset{|}{\underset{|}{Si}}-]$$

This step procedes only after step (1) has taken place.

(3) Dissociation of another H_2O molecule.

$$[-\overset{|}{\underset{|}{Si}}O^-]^{+2} + H_2O \rightarrow -\overset{|}{\underset{|}{Si}}OH^{+3} + OH^-$$

The above reactions appear to be an important factor in the formation of an amorphous jarosite-like alteration material that is located adjacent to small polygonal fractures (Pl. 14, fig. 5). This is the probably mechanism for liberating potassium and iron ions noted in the ridge-like alteration products.

Encrustation remnants (Pl. 15, figs. 1,2) indicate the removal by solution of what previously were monoclinic crystals. The presence of potassium in surrounding alteration products suggests that potassium chloride or other similar soluble crystalline substance was responsible for their formation.

Oxidation. Freshly formed Na-Ca-Si-O glass surfaces have a high affinity for oxide formation (Holland, 1964, and Jones, 1971) as do fractured glass surfaces (Kingery, et al., 1976). Glassy particles produced by lava fountains have compositions roughly similar to those reported above and can be considered to have like affinities for oxide formation. Basaltic glass oxide films would be less developed or thinner due to shorter exposure

at temperatures and oxygen abundances suitable for oxide growth. Since the inner portion of a fountain consists of disrupted lava and gases that are mainly reduced in relation to the atmosphere (Naughton, et al., 1974, determined a value for oxygen of 10^{-8} atm); glass surfaces that retain sufficiently high temperatures during flight to outer regions of the fountain will adsorb reactive gas molecules (such as oxygen) onto the surface to satisfy surface charges. Trajectories at low angles would satisfy the above requirements as would particles ejected in trajectories that allowed them to be reheated in a region of high oxygen content. Swanson and Fabbi (1973) reported that oxidation of Fe^{+2} in the glass to Fe^{+3} occurs during high temperature exposure of pumice fragments to air during phases of high lava fountaining. The production of oxide scale (Pl. 13, fig. 1) is indicative of growth from the glass-oxide boundary which expands outward developing a nonprotective oxide film characterized by tensional fractures and a tendency to flake or spall (Fontana and Staehle, 1976). The diffusion rate of oxygen through an oxide film is faster than the diffusion outward of other elements from within the glass. Kofstad (1966) further substantiated that growth is at the glass-oxide boundary. Development of nonprotective oxides will expose fresh surfaces for oxidation as suggested by (Pl. 13, fig. 5). With further growth the surface develops rounded masses with intermound depressions and fractures (Pl. 13, fig. 6). The development of oxide coatings on particles containing ripple patterns (Pl. 14, figs. 1-4) suggests that ripple

crests develop oxides to a greater extent than ripple troughs (Pl. 14, figs. 3,4). This suggests that the crests may be of a different composition than the troughs.

Once oxides form at the surface, further chemical attack or reaction may alter the film or coating to other compounds. Whether oxide films have a uniform composition cannot be determined at present but it seems reasonable that the oxide film would contain the same elemental ratios as the host surface if allowances for differences in diffusion rates are taken into account.

Surface Modification

Surface modification of glassy particles is produced by rippling, surficial vesiculation and rind formation. Generally these processes produce an overprint or response of the particle surface to a external force that operates on its surface. The development of ripples and surface vesicles, however, may involve to a degree some internal processes that exhibit external expression.

Surface Ripples. Surface ripples (Pl. 15, fig. 6) are sufficiently small that observation is limited to SEM study at moderate magnification. They consist of a pattern of contorted ridges and valleys that cover partial to complete particle surfaces with minor areas of pattern disruption around vesicles. X-ray analysis of ridge areas does not indicate a difference in composition from that of the underlying sphere but this may be due to the large excitation volume of the electron beam in

comparison to the relatively small volume of the ripple crest.

Thin section study of glassy particle interiors indicates that approximately 20 percent of the particles contain what appears to be the internal equivalents of surface ripples. The internal laminae consist of alternating light (yellow) and dark (reddish-brown) layers (Pl. 18, fig. 4 and Pl. 22, figs. 3 and 4) that are folded. Some patterns are distorted as they pass around vesicles similar to the distortion of surface ripples. Where laminae intersect the surface only a vague suggestion of the pattern is noted on the periphery of the particle (Pl. 22, fig. 4). This may be due to surface removal during thin section preparation. Under high magnification (~1000X) the dark laminae consist of a string of minute particles (~0.1 to 0.05 μ dia.) of dark glass (?) in a lighter glass matrix. No birefringence was noted, nor were the particles bubbles, but seem to be a separate phase of higher index glass. The reddish-brown color and higher index suggests that this phase may have a higher iron content than the lighter laminae but in a highly disseminated minute nature. Heiken (1974) observed in thin section a sphere with similar light and dark bands on the outer margins of the particle and suggested that they were cooling joints deformed by air drag. This does not seem consistent with the wavy nature of the laminae as exhibited in (Pl. 18, fig. 4).

Several mechanisms can be suggested for ripple formation but none of the possibilities seem to be entirely feasible. Kingery, et al., (1976) report that glass slightly richer in SiO_2

content than basaltic glass can develop micro-domains of immiscible iron sulfide in a SiO_2 glass phase. This does not agree with the transparent nature of the dark particles unless the iron compounds are very small and disseminated throughout the laminae. How alternating layers form would still be difficult to expalin. A second possibility would be that the dark particles forming the dark layers are spherulites of olivine or pyroxene composition somewhat similar to the alternating laminae of light and dark layers in volcanic flows as noted by Christiansen and Lipman (1966) but on a much finer scale. A third possible mechanism of formation is suggested by noting that some particles with surface ripples also contain single or double tails suggesting that the particle was formed and modified by aerodynamic friction. Margolis, et al., (1971) observed that simulated tektite flanges formed by blowing a hot flame over a glass surface produced a system of ripple patterns with valleys and ridges somewhat similar to those noted in this study but on a larger scale. The fact that the surface of the particle was in a fluid or semifluid state is confirmed by the distortion of the internal and external patterns by vesicles that migrate toward the surface and explode. Once again the means of developing alternating laminae of light and dark bands is not easily explained unless the laminae separate during surface flow or deformation while the particle is in a semifluid or fluid state. A fourth possible mechanism of surface ripple formation would be the partial fusion of a previously formed and cooled oxide or sulfate layer that was rippled by

aerodynamic friction while fluid during particle flight. This may explain why the ridge material appears to consist of a brighter surface in SEM photographs due to either: (1) a "Z" effect produced by compositional difference such as the ridge areas having a higher average atomic weight and corresponding higher electron density, and (2) the ridges being topographically higher and closer to the electron detector and thus appearing brighter. If the initial surface was altered in such a way as to preferrentially collect iron or other heavy elements on the surface such as the formation of a oxide or jarosite deposit. The ridges may represent this deposit after fusion and deformation by aerodynamic drag has produced the "iron rich" ridges versus the lower average "Z" content of the glassy valleys. Further work is required to understand the relationship between surface and internal ripples, their mechanism of formation, and reason for the difference in the alternating of the light and dark layers.

Some particle surfaces contain wrinkles or waves (Pl. 3, fig. 6 and Pl. 15, fig. 5) formed by impact or collision with other particles or landing on a surface in a semifluid or semi-rigid state.

Surficial Vesiculation. Many particles exhibit circular surficial vesicles (Pl. 1, fig. 5; Pl. 3, figs. 4,5; Pl. 4, fig. 5; Pl. 10, figs. 1,2,3; Pl. 14, figs. 1,2; Pl. 20, fig. 3; and Pl. 22, fig. 6) formed by gas bubbles which migrated to the surface, rapidly expanded, and ruptured due to the rapid decrease in confining pressure. Depending upon surface conditions

(temperature, viscosity, etc.,) several types of surface expression were generated by the vesicles. Vesicles vary in size and areal extent from very small (~500 Å) closely spaced openings (Pl. 18, fig. 1) to large (~500 μ) widely dispersed or single vesicles. When vesicles are similar in size and closely spaced (Pl. 18, fig. 1) a common time and mechanism of formation is suggested. The small size and uniform dispersion of closely spaced vesicles strongly suggests formation as a unit from a thin layer or film of glass that was rapidly and uniformly heated above the vaporization temperature of a gaseous component that exsolved from the fused surface and formed a myriad of bubbles. After rupture rapid chilling preserved the surface. Similar surface development has been noted when a PVA-alcohol mounting solution is placed on a sample stub and rapidly heated until the alcohol reaches the vaporization temperature, exsolves from the solution, and forms a profusion of small bubbles throughout the layer which burst almost simultaneously. If the layer from which the bubbles nucleate is thick and sufficient time available, the bubbles generated will grow or go back into solution, in similar fashion to crystal nuclei, until they reach a critical size where growth continues (Carmichael, et al., 1974). In the above case the thin film would be on the order of 500 to several thousand angstroms to contain such a uniform vesicle size distribution. It is conceivable that a previously formed particle could pass through a very hot region of the fountain and be very rapidly cooled if the particle trajectory were at a high angle to

the fountain axis. Fontana and Green (1967) noted that alkali oxides are highly volatile at high temperatures. This would enable a particle surface coated by alkali oxides to be partially fused, vesiculated, and frozen by falling or passing through a fountain plume.

Other vesicles may form as individual bubbles, grow in size, and migrate to the surface where they arch or bow-up the surface (Pl. 18, fig. 6) or rupture at the surface. Circular openings with glass flanges (Pl. 14, fig. 1) often have overturned lips of sharp to rounded outlines (Pl. 10, figs. 2,3) depending upon the fluid and thermal state of the surface. A smaller sphere attached to a larger sphere (Pl. 7, fig. 4) exhibits a surface that indicates an episode of surficial vesiculation (represented by the large circular depressions) accretion of an oxide or sulfate coating, later partial melting of the surface and minor vesiculation (small grouped vesicles) within the accreted layer. The sphere just below the "d" arrow (Pl. 7, fig. 3) illustrates a nearly complete coating of oxide or sulfate which has not been exposed to sufficient heat to generate surface vesicles.

Thin section study indicates that only a few vesicles contained within a particle form surficial vesicle openings. This indicates the large influence that surface tension has on the formation of surface features. Compare a SEM view of a particle surface for external vesicle development (Pl. 4, fig. 5) to that of internal development (Pl. 22, fig. 5 or Pl. 19, fig. 4).

Even though the particles are different, a good comparison of the lack of surficial vesicle development is found in relation to the total number of vesicles within the particle.

Rind Formation. Approximately 22 percent of the particles studied petrographically exhibit peripheral rinds (Pl. 22, figs. 1,5) of optically darker glass which contain internal ripples, and concentric, or tensional fractures (Pl. 18, fig. 5). Rind thickness is usually constant for a given particle and is generally less than 0.02 mm and seldom greater than 0.05 mm. The boundary between the outer rind and particle interior is usually abrupt (Pl. 19, fig. 3) and formed by concentric to slightly convex fractures (Pl. 18, fig. 5). No alteration or devitrification was observed in the glass adjacent to the fractures. Particles with peripheral rinds are generally large (mean dia. 1.38 mm) as compared to rindless particles (mean dia. 0.59 mm). They also contain abundant phenocrysts or vesicles (Pl. 19, fig. 4) and often have attached surficial debris (Pl. 22, fig. 1).

Heiken (1974) illustrated a rind-bearing volcanic particle and suggested that it has a cooling rind composed of an oxidized surface layer that contains parallel contraction cracks which were deformed by air drag. Friedman and Irwin (1967) studied volcanic particles that contain hydration rinds consisting of curved fractures bounded by devitrified glass. However, the rinds they describe are substantially different than those of this study and may represent a significantly more advanced stage of alteration. Coleman (1976) studied weathering rinds, 0.2 to

4 mm thick, and found them to be a good relative age indicator. He observed several stages of rind development: an initial stage of oxidation and hydration of Fe-bearing minerals or mineraloids and intergranular staining; intermediate alteration of all constituents with alteration intensity being glass > olivine > pyroxene > amphibole > plagioclase > opaques; and abundant clay mineral development predominate with advanced rind formation. Swanson and Fabbi (1973) report that more particles with "skins" were developed in high versus less vigorous lava fountains. They also report higher oxidation values from particles produced by high fountains.

The findings of Coleman (1976) and Swanson and Fabbi (1973) substantiate Heikens observations that oxidation of the glassy outer layer produces the optically darker periphery. Ripple laminae as earlier discussed are not presently fully understood, except that they may be produced by deformation of the surface or interior by aerodynamic drag or viscous flow. Macdonald (1972) observed that curved cracks, oriented nearly normal to the flow surface and convex upstream, form by the pulling away of a portion of the lava from the rest of the flow. If sufficient aerodynamic drag is present, as the outer particle surface becomes viscous, similar cracks to those described by Macdonald could be generated. Isard (1971) reports that glass particles less than ~1 mm are transparent radiators and therefore cool as a single unit with the interior of the particle being at the same temperature as the periphery. Particles larger

than 1 mm or inhomogeneous particles that have numerous vesicles or phenocrysts, which tend to be obstacles to radiate heat transfer, would develop an outer periphery that cools faster than the interior and thereby develop a cooling rind. Surficial debris may act as heat radiators further increasing the difference between the internal and outer peripheral temperature of the particle. The development of a chilled zone or rind would establish a set of stress fields on the outer layer due to differential contraction that would produce concentric fractures parallel to the surface and tensional fractures at an angle to the surface.

Lava Fountain and Particle Models

This section will present a synthesis of observed data, and discussion of conceptual models of a lava fountain and formation of its glassy particles. From the model some constraints can be placed on where various processes operate within lava fountains and during what period of time these processes modify glassy particles.

Fountain Model

Figure 11 is a representation of a Hawaiian lava fountain. Scale is variable depending on the magnitude of the eruption and characteristics of the lava. Elements of the lava fountain model are: vent, fountain column, plume, spatter ramparts, and pumice cone and blanket.

Initial eruptions occur along linear fractures several

"Page missing from available version"

page 103

hundred meters to kilometers in length forming "curtains of fire" that within hours die out leaving a single fountain that plays for indefinite periods of time (Macdonald, 1972 and Swanson, et al., 1971). During the initial eruptive phase, spatter ramparts develop adjacent to the fissure and grow to heights of several meters depending upon the length of the eruption. Spatter refers to thick pasty globs of lava that travel short distances usually at a high angle to the fountain axis. Within a short time after an eruption begins, accumulation of molten spatter collects around the fissure and flows away from the vents as a rootless flow. If the vent becomes localized within a depression, often the fountain will continue to erupt through the accumulating lava lake until the lake drowns the vent.

The large temperature gradient between the fountain and surroundings generates an atmospheric low pressure ring around the eruption site. This sets into motion an inward rush of cooler air, which becomes heated and rises upward along the fountain. Prevailing winds generate a downwind plume consisting of fountain gases and fine-grained volcanic particles produced by the eruption. Depending upon fountain size and wind velocity, fine-grained particles may be transported tens of kilometers downwind. The majority of the pumaceous ejecta is deposited in close proximity to the fountain vent and grades outward from coarse to fine. Large pumice cones or blankets form downwind when the wind direction and fountain axis remain constant (Macdonald, 1972 and Richter. et al., 1966).

Information on temperature and pressure distribution within the fountain and immediate surroundings is lacking. Temperatures can be assumed to vary from $\sim 1200^{o}C$ near the vent with a gradual decrease to the outer edge of the fountain column. Prevailing winds carry hot particles and erupted gases in the downwind plume at temperatures between approximately 800 to $500^{o}C$. The downwind plume cools to ambient values some distances from the fountain. It should be noted that pumice deposited in the cone or blanket retains considerable heat with temperatures reaching $\sim 800^{o}C$ documented by the color of the cone interior during a slump of the 1959-60 Kilauea Iki pumice cone into the vent.

Pressures within the fountain are unknown but can be considered as being above ambient due to gas expansion. Pressure drops rapidly to ambient or lower values at the margins of the fountain. The vapor pressure of each gaseous species will vary depending upon many factors. Water vapor, a major component of eruptive gases (Naughton, et al., 1974, Heald, et al., 1963, Nordlie, 1971) is concentrated in the fountain column and diminishes outward due to atmospheric mixing.

Particle Formation and Modification Model

The formation and modification of glassy particles can be modeled as a process having three stages: (1) initial formation, (2) constructive material accumulation, and (3) destructive removal or alteration of existent surfaces (Figure 12). Factors that affect particles in these three stages are: (1) lava composition and viscosity, (2) vent configuration, (3) flight velocity,

(4) flight time duration at temperatures > 800°C, (5) surface tension, (6) gas concentration or expansion, (7) particle population within the fountain, and (8) convective cycling. After initial formation, a particle constructively accumulates other solid or liquid materials by accretion or sublimation and condensation of vapor phase crystals, micromounds and condensed liquids. The amount of accreted material depends upon the duration of particle flight within the fountain column and plume or upon the extent of its cycling within the fountain. Subsequent to but sometimes synchronous with constructive accumulation, particles experience destructive removal of surface materials. Destructive processes modify particles throughout their history but generally have a greater affect on the particle near the completion of its history. Furthermore, particles can be cycled back into any of the previous stages or may by-pass some processes without modification.

Vent Configuration. Vent configuration, along with the extent of gas dissolution during transport from an underlying magma chamber, will determine the extent of lava disruption as it travels through the vent and is accelerated outward by gas pressure. The main affects that vent configuration will have on the lava column will be to: (1) develop a spray rather than a single jet or column, and (2) to initiate a rotational character to the clots or blebs of disrupted lava. An excellent analogy of vent configuration is shown by the extent of liquid disruption when an obstacle is placed in the nozzle of a fire hose. If the

nozzle has a smooth and open bore a long continuous jet or fountain of water with laminar flow is produced which gradually breaks apart as the force of gravity overcomes the expulsion force of the liquid through the nozzle. When the nozzle has obstacles, a roughened surface, or is partially blocked a spray of highly disrupted water particles is produced. Obstacles may alter the orientation of the fountain axis and thereby modify other variables such as flight time and amount of flight time at elevated temperatures. Vent configuration therefore produces an initial segregation of lava into jets or streamers of lava, clots or blebs of lava consisting of liquid, liquid plus crystals, liquid plus vesicles, and a mixture of liquid, crystals, and vesicles.

Flight Velocity. Flight velocity partially determines the shape of disrupted lava particles after eruption. High velocities develop frictional resistance on the surface of the particle (aerodynamic drag) which pulls the liquid mass into elongate, twisted and curled forms or separates smaller particles from rapidly rotating masses. Often frictional resistance overcomes cohesive forces and strips-away the liquid periphery of mineral-cored particles. Low particle velocities do not develop a component of frictional resistance that is large enough to deform the particle or strip-off peripheral liquids.

Flight Time Duration at Elevated Temperatures. A close relationship exists between flight path attitude and the duration of flight time at elevated temperatures. Trajectories at low

angles to the fountain axis maximize the length of time at elevated temperatures and thereby experience the greatest amount of constructive accumulation. Conversely, particles with high angle trajectories to the fountain axis rapidly leave regions of high temperature, have short travel times and minimal constructive accumulation. Particles modified by surface tension and gas expansion are considered to have spent sufficient time at elevated temperatures for these processes to act upon and modify their shape or internal character. Particles not modified by surface tension or gas expansion are classified as having a short flight path at elevated temperatures and are quickly chilled to semirigid or rigid states.

Surface Tension. Surface tension (inward directed forces of cohesion) modifies irregular and elongate shapes into forms of minimal surface energy. Sufficient time at elevated temperature is required for molecular adjustment of the surface of the particle. This is most easily accomplished at low viscosities and elevated temperatures. Irregular particles develop rounded edges and attempt to become spherical. With sufficient time elongate streamers or jets break-up into droplets or spheres of nearly the same diameter. Basaltic lavas at temperatures greater than $\sim 800^{o}C$ remain fluid to semifluid and are acted upon by surface tension. At lower temperatures basaltic lava is semirigid to rigid and is unaffected by surface tension.

Gas Concentration or Expansion. Gas concentration or expansion is considered as the growth of existing vesicles or the

initiation of new vesicles by the exsolution of a gaseous phase from the liquid. The effect that gas expansion has on a particle depends on whether the vaporization pressure of the volatile phase is greater or less than the forces of surface tension. Two end points were considered in this model: (1) gas expansion force less than surface tension resulting in the development or growth of small, dispersed vesicles within the particle, and (2) gas expansion greater than surface tension resulting in vesicle coalescence and disruption of the interior of the particle or the development of a surface characterized by ruptured vesicles due to rapid heating of the exterior until the vaporization pressure of a surface component is exceeded.

Particle Population Within the Fountain. The population of particles within a lava fountain can be considered as the average number of particles across a given cross-sectional area of the fountain at a particular point of time during the eruption. Particle population depends on several factors: (1) type of fountain eruption, (2) amount of particle fall-back into the fountain, and (3) extent of small particle addition due to convective cycling of particles from the fountain periphery.

Fountain eruptions can be catagorized depending on the type and amount of eruptive products. Fumarolic eruptions consist predominantly of gases produced by either extensive exsolution of gas from the magma during transport to the vent or a combination of steam and gas produced by the partial flooding of the eruptive conduit by non-juvenile waters. Particle population within

fumarolic eruptions would be moderate. Spatter fountains contain significantly less gas and have fewer but larger erupted particles. Particle population would be low. Between fumarolic and spatter eruptions lies the normally observed lava fountain which consists generally of subequal amounts of gases and particles. Particle populations within this type of eruption would be high.

The variation of particle population within a fountain due to fall-back of previously erupted particles depends primarily on the orientation of the fountain axis. Near vertical axes have maximum fall-back due to gravity with correspondingly less fall-back as departure from a vertical orientation increases. An exception to the above would be where the axis of the fountain is inclined into the prevailing wind direction. This would allow erupted particles to be carried downwind above the axis and fall-back into the fountain.

Convective Cycling. Convective cycling of small particles back into the fountain column from peripheral areas depends on particle size, trajectory, and strength of convective air currents. Particles most likely affected by convective cycling would have maximum surface areas, i.e., streamers, ribbons, filaments, or particles which have interiors which contain abundant vesicles producing a low density to surface area ratio. Particles carried back into the fountain are those that are settling out of the downwind plume or falling around the periphery of the fountain. An additional particle source may be small, very-vesicular particles with large cross-sectional areas that are picked-up from

the pumics deposit by convective air currents. Whether this last possibility is operative is uncertain and should be considered in later studies. The addition of convectively cycled particles would depend on fountain size and thermal differential between the fountain and surrounding atmosphere. This addition would generally be small when considered to the large generation of particles produced within the fountain.

The general affect of convective cycling and increased particle population within a fountain would be the generation of composite forms where particles collide and remain together or the destructive removal of material by rigid particle collison.

Constructive and Destructive Processes. Particles produced by lava fountains have widely varying temperatures and attendant physical states depending upon what region of the fountain they are in or passing through. In this model of particle formation and modification these processes are noted by the presence or absence of specific features. Therefore the microstratigraphy of a particle indicates its history of formation, capture and accumulation of other particles, possible loss or removal of material by fracturing or breakage, and alteration by oxidation or hydration. The various stages of particle experience may be shortened, by-passed, reversed or repeated depending upon the flight history of the particle.

Based on the microstratigraphy of internal and external particle features, a sequential chain of events and associated attendant physical conditions can be determined for each

particle. This record or history describes the physical and chemical processes that operate on small particles within lava fountains. Four specific examples are as follows:

Example 1. Homogeneous spherical particle (Pl. 1, fig. 6).

I. Observations.

A. Large Scale Features (Pl. 1, fig. 6).

1. Spherical shape.

2. Accreted surficial debris.

3. Fractured and spalled surface.

4. Lack of surface vesicles.

B. Small Scale Features (Pl. 5, fig. 6, Pl. 12, fig. 6, and Pl. 9, fig. 6).

1. (Pl. 5, fig. 6).

a. Accretion of a dense growth of micromounds on the surface.

b. Impact of particle with semirigid core and fluid exterior which coats micromounds. Note minor to sparse micromound development on fluid splash area.

2. (Pl. 12, fig. 6)

a. Surficial accumulation of micromounds (lower left center).

b. Accretion of debris onto micromounds (lower left).

c. Spalling episode #1, central area, (left center).

d. Minor accretion of micromounds on new surface (left center).

e. Accretion of shard with micromounds and debris (center).

f. Accretion of debris onto spalled region and shard (upper right).

g. Spalling episode #2, right center, no micromound development.

3. (Pl. 9, fig. 6)

a. Sublimation or accretion of marcasite crystals on micromound surface. Note lack of micromounds on crystals.

II. Suggested Particle Formation and History.

A. Stage One: Particle Formation.

1. Particle appears to be homogeneous without vesicles. This indicates eruption as a homogeneous melt that remained hot long enough during flight to develop a spherical shape.

2. Flight velocity and associated surficial resistance was less than the cohesive strength of the liquid and therefore did not produce aerodynamic shape modification.

3. Gas concentration was low as indicated by the lack of vesicles suggesting that the surface tension of the melt was greater

than the force of gas expansion.

4. Internal character would be similar to the sphere shown in Pl. 16, fig. 2 which has minimal vesicle development or crystal content and concentric fractures.

B. Stage Two and Three: Constructive and Destructive History.

1. Accretionary growth of dense micromound covering while particle was within the fountain column or downwind plume. Particle has a cooled surface suitable for sublimation of micromounds.

2. The occurrence of a partially fluid particle impact suggests that the host particle was cycled back into a hotter region of the fountain. This is suggested also by surficial polygonal fractures and tensional spalls that developed during reheating of the particle.

3. Possible multiple cycling may have occurred as indicated by a second spalling episode and micromound development.

4. Additional debris (shards and amorphous material) was accreted to the surface of the sphere partially covering the newly spalled region.

5. Sublimation or accretion of marcasite on a fractured surface when the particle was in in a region of low temperature, i.e., fountain plume below $\sim 300^{o}C$. A ubiquitous coating of marcasite crystals would suggest sublimation, however the occurrence of small crystal clumps on only parts of the surface suggests that the crystals formed elsewhere and were later accreted to the host surface.

III. Correlation of This Particle With The Particle Formation Model.

The particle described above could be generated by three possible routes producting particles 1, 18, or 26 (Figure 12). These spheres have identical features but different pathways of formation.

Example 2. Irregular hetergeneous sphere (Pl. 4, fig. 5).

I. Observations.

A. Large Scale Features (Pl. 4, fig. 5).

1. Irregular oval spheroidal shape.
2. Numerous filaments draped across surface.
3. Possible development of filament tail (particle right) which has subsequently been detached or folded back onto the particle surface.
4. Numerous vesicles.

5. Surface ripples with minor disruption by surficial vesicles.

B. Small Scale Features (Pl. 6, figs. 3 and 4).

1. Sublimation of micromounds on host surface (Pl. 6, fig. 3).
2. Accretion of platelets onto micromounds, lower right, (Pl. 6, fig. 4).
3. Accretion of partially-fluid particle splashes, lower center (Pl. 6, fig. 3).
4. Development of surface ripples, upper and lower margins, (Pl. 6, fig. 4).
5. Development of small tension (?) cracks along ripple edges, upper center, (Pl. 6, fig. 4) and center (Pl. 6, fig. 3).
6. Accretion of numerous rigid to fluid filaments or filament splashes.
   a. Liquid filament splash with oxide-sulfate coating, area a, (Pl. 6, fig. 3).
   b. Later accretion of thread-like filaments, area c, (Pl. 6, fig. 3).
   c. Accretion of semifluid to semirigid filaments and debris, upper center and right (Pl. 6, fig. 3).
   d. Accretion of rigid filaments, area a, (Pl. 6, fig. 3 and 4).

II. Suggested Particle Formation and History.

A. Stage One: Particle Formation.

1. Irregular hetergenous sphere-like vesicular melt that remained sufficiently hot for its original shape to be modified by surface tension to that of an oval spheroid.

2. Sufficient flight velocity produced surficial resistance which formed surface ripples and a possible tail. Whether the elongation of the spheroid was produced by aerodynamic shaping or is due to the breakdown of a streamer into its present shape is unknown.

3. Gas expansion during flight at high temperature has allowed vesicle growth and movement to the surface where the vesicles have burst. No indication is given whether interior vesicles may have coalesced.

4. Internal character: The lack of radial fractures and numerous surficial vesicles suggest an interior similar to that shown in Pl. 22, fig. 5. From SEM observations it cannot be determined whether this particle contains small crystals. The presence of surficial ripples may have a similar relationship between the periphery

and the interior of the particle such as (Pl. 18, fig. 5).

B. Stage Two and Three: Constructive and Destructive History.

1. After initial particle formation, accretionary sublimation of micromounds occurred on a cooling surface. Additional accretion of semirigid spheres which flattened to form platelets and fluid splashes indicates that micromound development and subsequent accretion of platelets and fluid splashes occurred within a high temperature region of the fountain column.
2. The occurrence of surface ripples suggests that the particle experienced surficial resistance prior to the cooling of the surface to a rigid state. This suggests occurrence within a region close to the fountain axis where particles have high flight velocities and fluid exteriors.
3. Minute cracks appear to have formed prior to fluid or rigid filament accumulation. Areas of intense filament formation surround the periphery of the fountain column here strong updrafts combine with the stripping action of liquid removal by

high velocity flight to produce many liquid filaments. Generally large rigid filaments tend to accumulate after thin semifluid threadlike filaments. This suggests that smaller filaments are accreteted at higher temperatures closer to the fountain column and larger filaments accrete at low temperatures and at a greater distance from the fountain. A notable exception to this scheme is the occurrence of a large fluid filament impact which is covered by small equant masses. This filament initially formed, cooled, developed a surficial coating of sulfate or oxide; was cycled back into the fountain column where it was fused and developed a surface layer of material of lower surface tension which during impact separated into the equant masses due to the different surface tension values of the surface layer and the underlying liquid.

4. Subsequent to filament accretion further debris, shards, and amorphous sulfate, etc., was accreted to the surface.

III. Correlation of This Particle With The Particle Formation Model.

The particle described above could be generated by two possible routes, terminating as particle types 10 or 18 (Figure 12) which have similar features but different origins and paths of development.

Example 4. Irregular, twisted streamer with mineral grains (Pl. 3, fig. 3).

I. Observation.

A. Large Scale Features (Pl. 3, fig. 3).

1. Irregular twisted streamer shape with flutes and ridges.
2. Partially enclosed mineral grains.
3. Stretched vesicles.
4. Small filaments attached to surface.

B. Small Scale Features (Pl. 6, fig. 2).

1. Minimal development of micromounds.
2. Accreted materials consist primarily of filaments, shards and small platelets.

II. Suggested Particle Formation and History.

A. Stage One; Particle Formation.

1. Particle is composed of glass and sparse euhedral crystals and a few vesicles. This would suggest that the particle was initially composed of melt with some vesicles

and previously formed crystals.

2. Eruption disrupted the lava into a long spindle-shaped streamer of liquid, vesicles and crystals.
3. Flight velocity further modified the streamer by forming ridges and flutes due to fictional resistance between the surface and atmosphere.
4. Flight time was short as indicated by the irregular shape but rounded form. Note that sufficient time was not available for the streamer to break-up into droplets.

B. Stage Two and Three: Constructive and Destructive History.

1. Flight time was sufficiently short so that gas exsolution did not generate disrupted vesicles.
2. Minimal surficial debris was collected on the surface except for rigid filaments and small platelets which suggests that flight time was short and in regions of cooler temperatures (filaments and platelets were semirigid or rigid). The above features indicate a flight that occurred at a high angle to the fountain axis and across the fountain column where it was twisted and

subquently collected the partially hardened debris just prior to deposition.

3. Internal character would be similar to that of the upper figure in Pl. 16, fig. 4 which illustrates a twisted form with stretched vesicles and Pl. 17, fig. 2 which shows a stretched filament with small crystals in partial alignment.

III. Correlation of particle with Particle Formation Model.

This particle contains external and internal features suggestive of particle types 15 and possible 23 (Figure 12).

Particle Modification Within Pumice Deposits

Until now the discussion of the particle formation and modification model has addressed only those processes and modifications that take place within the lava fountain or downwind plume. Although outside of the initial scope of the model, it is important to consider the affects that particle impact and residence within a pumice deposit would have on the particles. Pumice deposits can be considered as either thick cone or thin blanket deposits (Figure 11). Cone deposits accumulate near the vent and grow in size depending on the amount of volcanic debris that is erupted and falls or is carried downwind. Particles deposited close to the vent often retain considerable heat. As deposit thickness decreases and distance from the vent increases

temperatures within the deposit decrease to ambient conditions. Other factors that determine the extent and nature of particle modification are: (1) type of impact, (2) surface area of particle, and (3) exposure to chemically active agents.

Particle Impact. The thermal nature of a particle will largely determine the extent that a particle deforms, fractures or remains unchanged. To a minor degree velocity of impact and thermal nature of the pumice deposit will also affect the amount of mechanical deformation or disintegration. Fluid particles on impact loose coherence and splash onto surrounding debris (Pl. 5, figs. 3 and 5). As the liquid cools some of the underlying pumice fragments will be welded together. Particles formed by splashes welding debris together were rarely observed but the validity of the mechanism is easily verified by observing attached pumice debris on the bottom surfaces of "cow-pie bombs". On impact semifluid particles flow and spread out or wet the surface of underlying particles (Pl. 5, fig. 4). Semirigid particles deform (Pl. 15, fig. 5) bend or drape over underlying debris (Pl. 6, figs. 1,3) but do not fracture on impact. Rigid particles often fracture into several pieces producing fragments, half spheres, broken filaments or "soda straws" (Pl. 6, fig. 2). Other rigid particles develop fractures but do not break apart (Pl. 1, fig. 6 and Pl. 12, fig. 1). Often particles falling earthward are cushioned by air currents rising from the hot pumice deposit and "soft" land rather than impact the surface at terminal velocity and thereby experience minor if any deformation due to

impact. Soft impacts also occur when the impacted surface is semirigid.

Surface Area. Particles that contain large surface areas experience greater amounts of chemical alteration or decomposition and some types of mechanical disintegration than those of minimal surface exposure i.e., spheres and rounded forms. As particles mechanically disintegrate the amount of surface area available for chemical alteration rapidly increases. Particles particularly susceptible to mechanical breakdown are long filaments and particles containing highly vesiculated interiors which breakdown into fragments termed "friable reticulite".

Exposure to Chemically Active Agents. Particles in pumice deposits and fountain plumes are exposed to a variety of aerosols, mists, and vapors of acids (hydrochloric, sulfuric, and hydrofluoric), sulfides, sulfates, chlorides, and water. As previously discussed chemical alteration and decomposition takes place not only within the fountain but also within the pumice deposit. Little doubt is left of the active nature of sulfur compounds observed coating fragments (Pl. 15, fig. 3) around fissures within recently deposited pumice blankets. Murata (1966) provided evidence of the presence of corrosive acid vapors which rise through the pumice cones and etch or decompose particle surfaces (Pl. 13, figs. 1,3 and 4). Volatile cations (Na, K) can be expected to combine with prevalent anions to form soluble crystalline forms which remain stable until exposed to water vapor. Such soluble salts may well explain the presence of

surficial encrusting remnants observed on some particles (Pl. 15, figs. 1 and 2).

CHAPTER 5

COMPARISON OF TERRESTRIAL AND LUNAR GLASSY PARTICLES

Introduction

Terrestrial glassy particles produced by low viscosity basaltic lava fountains and glassy particles collected from lunar soils have been observed to contain many similar surface and internal features. This section will discuss these similarities as well as differences observed between the two types of particles. Reasons will be suggested which explain why the particles have similarities or differences and why some particle types and surface features are abundant in one environment but lacking in the other.

Terrestrial glassy particles and associated external and internal features have been documented by SEM and petrography (this report; Heiken, 1971, 1974; Duffield, et al., 1977). Glassy particles of lunar origin have been extensively studied by SEM and petrography (McKay, et al., 1973; Carter, et al., 1973; Carusi, et al., 1972; Agrell, et al., 1973; Chao, et al., 1973; Reid, et al., 1973; and Heiken, et al., 1974). Features common to particles of both environments suggest formation by similar processes. Conversely, if particles from only one environment contain a particular feature it is suggested that (1) the process responsible for that feature does not operate in both environments, (2) physical

and chemical conditions within the environment are not suitable for the preservation of the feature, or (3) the feature is time dependent (i.e., devitrification) and insufficient time was available for the feature to develop. Differences in the abundance of a particle type or feature suggests that the processes responsible for their formation functioned at different rates or over longer periods of time. Substantial differences between lunar and terrestrial physical and chemical environments suggest a wide variation of particle types and associated features. Such variability is surprisingly small. This suggests that environmental conditions during particle formation and modification were similar and does not reflect the large difference between environments.

For comparative purposes, Table 11 lists particle types and constructive or destructive features in terms of observed abundance; abundant = (A); common = (C); few = (F); and rare = (R). Data for lunar glassy particle comparison were compiled from previously mentioned sources, several of which were co-authored by myself, as well as data acquired during membership on the Preliminary Examination Teams for Apollo 11 and 12 samples.

In comparing lunar and terrestrial glassy particles, it is important to realize that although some lunar glassy particles were formed by the eruption of magma from the lunar subsurface, continuing generation of molten rock is produced by meteorite bombardment. Meteorites impacting the lunar surface have considerable kinetic energy which is transformed into heat during

TABLE 11.

COMPARISON OF TERRESTRIAL AND LUNAR GLASSY PARTICLES

Particle Type or Feature	Abundance (A=abundant, C=common, F=few, R=rare) Terrestrial	Lunar
Particle Type		
Spherical	A	A
Elongate-Streamer	A	C
Glassy Filament	A	R
Coated Mineral Grain	C	C
Composite	C	C
Shard	F	C
Reticulite	A	F
Agglutinate	R	C
Lithic Fragment	F	C
Constructional Features		
Splash	A	A
Filament	A	F
Smaller Sphere	A	C
Platelet	C	A
Micromound	A	A
Iron-Nickel Mound	R	C
Iron-Sulfur Mound	R	C
Vapor Phase Crystal	C	C
Hydrous Calcium Sulfate	A	R
Jarosite	C	R
Marcasite	C	R
Elemental Sulfur	F	R
Apatite	R	C
Iron Crystal	R	F
K-Na Chlorides	R	C-F
Surficial Debris (shard, amorphous material)	C	C
Destructional Features		
Fractures	A	A
Gouges	A	A
Surficial vesiculation	C	C
Etch Depressions	C-F	R
Decomposition Surfaces	C-F	R
Surface Films (oxides)	C	R
Devitrification	R	C
Palagonitization	F	R
Ripples	C	R
Wrinkles	F	F
Rinds	C	C

impact and thus produces a region of fused rock. Much of this molten rock is ejected from the impact site as jets and streamers which are then acted upon by processes similar to those that form liquid droplets under terrestrial conditions. Large meteorite impacts generate a short-lived cloud or "atmosphere" of volatilized lunar material which enshrouds the impact site and acts in a similar manner to terrestrial or lunar volcanic eruption clouds.

Particle Similarities and Differences

Formational Processes

Lunar and terrestrial glassy particles experience generally similar formational processes, constructional growth, and destructional removal or alteration of particle materials. Independent of how a particle forms (i.e., meteorite impact or volcanic eruption), once that it has become a high temperature, low viscosity, liquid particle it can be acted upon by modifying forces.

Compositional Affects. Lunar lavas can be considered to have similar compositional characteristics to those of terrestrial lavas (a homogeneous to hetergeneous mixture of melt, vesicles and crystals). It has been difficult to determine the composition of initial lunar lavas due to modification by meteorite impact, resultant fusion and recrystallization. An average composition is suggested to be that of a basalt with enrichment of Fe and Ti (Reid, et al., 1973) with associated eruption temperature, viscosity and volatile content somewhat similar to terrestrial basalts. Like terrestrial lavas, heterogeneous mixtures of liquid,

crystals and vesicles would be most common with homogeneous melts being an infrequent exception.

Liquid particles formed by terrestrial or lunar impacts usually exhibit petrographic and chemical heterogeneity. Impact-produced particles commonly contain partially fused mineral or rock fragments which contain schlieren or bands of glass of different refractive index (Chao, 1967 and Heiken, 1972). If an impact is sufficiently small to only affect a single mineral fragment or is sufficiently large to fuse large volumes of material, it may be possible to produce chemically homogeneous liquid particles that are free of vesicles and crystals. If sufficient time is available at elevated temperatures, crystallization or volatile exsolution will take place producing a heterogeneous mixture of melt, vesicles, and crystals.

Vent or Impact Configuration. Volcanic eruption whether terrestrial or lunar will have similar disruptive affects on the lava. Melts produced by impact will experience varying amounts of disruption depending on the angle of particle impact with that of the host surface or the size of the impact. High velocity impacts produce impact craters with irregular edges which can disrupt liquid particles which deflect from their surfaces. During flight, liquid particles may be impacted by debris or other liquid particles which will also cause disruption. Analogs of impact events (raindrop or fountain droplet impacts) indicate that disrupted liquids are thrown outward from the impact site as annular or semi-annular sheets, splashes, jets or streamers

depending on the angle and force of impact.

Flight Velocity Affects. Aerodynamic drag or particle elongation is due to the surface of the particle responding to the frictional resistance of an encasing atmosphere. Terrestrial particles experience aerodynamic distortion depending upon the length of time that a particle has a fluid or semifluid surface. Lunar particles experience less distortion or elongation because of the virtual absence of an encasing atmosphere during flight. Previously, it was stated that impacts generate a short-lived cloud of volatilized material that may act momentarily as an atmosphere. Similarily, the length of time that a cloud or atmosphere, produced by a lunar eruption, would take to dissipate is unknown. Thus even if a lunar particle remained fluid during flight, the short-lived atmosphere would produce minimal aerodynamic distortion when compared to terrestrial particles. The lack of a persistant lunar atmosphere would have the greatest affect on the development of elongate particles, streamers, glassy filaments, and particles with surface features produced by frictional resistance or aerodynamic drag.

Length of Flight Time at Elevated Temperature $> 800^{o}C$. Flight time for comparable sized terrestrial and lunar particles has been calculated by McGetchen and Head (1973) with lunar particle flights lasting approximately one minute or 8 times longer than terrestrial flights. Flight time at elevated temperature is important when considering other modifying processes such as frictional resistance, surface tension, and gas expansion or

exsolution. These processes must also be viewed in terms of the size of an eruption or impact produced cloud and the temperature distribution within the cloud. Particles formed by impact will have flight paths at elevated temperatures that depend on the size of the impact. Particles formed by micrometeorite impacts will have short flight times at $> 800^{o}C$. Conversely, in large impacts the region of elevated temperature may be large with a considerable portion or all of the flight of a particle occurring at temperatures $> 800^{o}C$.

Surface Tension and Gas Expansion Affects. Both of these processes are basically compositionally controlled and should be similar for lunar and terrestrially produced particles. A possible exception would be a molten particle produced by lunar impact which would contain considerably less dissolved gases and have correspondingly fewer internal vesicles.

Summary. In general, very similar particle types are produced in both environments except for the paucity of elongate forms, glassy filaments, and reticulite in lunar samples and the dearth of agglutinates (pumice fragments welded together by a liquid droplet that lands on a lunar soil surface, McKay, et al., 1971) in terrestrial samples.

Constructional Processes (Similarities and Differences)

Terrestrial and lunar particles exhibit surficial materials that suggest similar constructional processes: (1) accretionary growth, and (2) sublimation or condensation growth.

Accretionary Growth. Accretionary growth in both lunar

and terrestrial environments is accomplished by the addition of solid or liquid particles to a host surface by liquid splashes, attachment or welding of smaller particles, platelets, shards, and other debris. Accretionary surfaces on lunar particles have greater abundances of fluid to semifluid splashes or soft impacts when compared to terrestrial particles. The reason for their greater abundance is the extreme length of time that a particle resides on the lunar surface where it collects additional fluid impacts produced by micrometeorite impacts. Surface gardening of the lunar soil by meteorite impact eventually removes particles from the surface and active surficial collection. A second factor that enhances lunar accretion is that when lunar particles are exposed at the surface they are in a virtually unreactive environment. This is greatly contrasted with terrestrial conditions where particle surfaces start to alter soon after formation. In perspective, terrestrial particles may reside on the pumice deposit surface and collect surficial debris and splashes for a few to 10's of years prior to mechanical breakdown or chemical decomposition. Lunar particles may be exposed on the surface with accompanying accretion taking place for tens of thousands to millions of years. Also the length of time available for accretion must be thought of in terms of flight time within a fountain produced cloud and surface exposure, which for lunar particles is longer in both cases when compared to terrestrial analogs. However, convective cycling of particles during terrestrial eruptions may significantly increase their residence

time within fountain columns.

Accretionary products are similar for both types of particles with the exception that few filaments or elongate forms are observed on lunar particles. Conversely, lunar particles exhibit higher abundances of platelets and smaller spherical particles on host surfaces which is due primarily to extensive meteorite impact, resultant fusion, liquid ejection, shape modification by surface tension, and semifluid to semirigid soft impacts. A third difference is noted in the lack of accreted crystalline material which would form within the fountain column or plume of lunar eruptions or impact clouds. The short-lived nature of the eruption or impact clouds does not allow sufficient time for formation of vapor phase crystals and later accretion to a host surface. Furthermore, the stability of any hydrous vapor phase crystals would be greatly reduced due to the P_{H_2O} of the lunar environment being ~ 0.

Sublimation or Condensation Growth. Sublimation and condensation of volatile material occurs in both lunar and terrestrial environments. Micromound development is observed on both types of particles. Lunar particles contain micromounds and mounds that differ in composition from terrestrial analogs which generally have the same composition as the host particle. Lunar micromound composition depends on the mechanism of melt production, i.e., volcanic eruption or meteorite impact. Micromounds on volcanically produced particles are similarily enriched in iron and titanium when compared to host particles (McKay, et

al., 1973). However, micromounds sublimated on particles produced by impact may have significantly different compositions. Their composition depends not only on the chemical nature of the lunar material that was fused and volatilized during impact, but they also reflect the composition of the volatilized impacting meteorite, i.e., iron-nickel, stoney, or carbonaceous. Iron-nickel meteorites produce the largest variation in micromound composition and morphology with the formation of iron-nickel mound-strings, iron-sulfide (troilite) mounds, or iron and phosphorus enriched micromounds (Carter, 1971).

Vapor phase crystallization of volatiles onto lunar host surfaces is infrequent. However, the occurrence of minute iron crystal-platelets was observed on Apollo 15 particles (McKay, et al., 1973). By far the most frequent occurrence of vapor phase crystallization occurs within thick tephra or pumice blankets produced by large meteorite impacts. Vapor phase crystals of iron, apatite, plagioclase, pyroxene, troilite, ilmenite, whitlockite, and iron-nickel were observed in vugs and crevices of Apollo 14, 15, and 16 breccias (McKay, et al., 1972, 1973).

Agglutination. A process of importance in the mechanics of lunar soil development is the production of agglutinates. This process is constructional in that it recombines previously disintegrated lunar materials. During micrometeorite impact, fused lunar material is ejected as a molten drop or streamer which lands as a fluid mass on the lunar surface and welds underlying fragmental particles together. McKay, et al., (1972)

termed particles produced in such a manner as agglutinates. A similar process operates during terrestrial volcanic eruptions but at a much smaller scale since a very short flight time is required if the particle is to remain fluid enough to weld previously erupted pumice fragments.

Destructional Processes (Similarities and Differences)

Destructional processes for lunar and terrestrial particles are generally the same. However, the agents or operators which produce the destruction or modification of lunar particles are considerably different in type and magnitude. Terrestrial destructional processes consist primarily of mechanical disintegration, chemical alteration or decomposition, and surface modification. Lunar particles experience all three operators but are predominantly altered by mechanical means.

Paramount in lunar particle modification or destruction is the process of meteorite or micrometeorite impact. Impact diameter ranges in size from less than 0.03 microns (Carter, 1971) to over hundreds of km. The extent that an impact affects a particle is determined by its velocity. Hypervelocity (>7 km/sec.) impacts form impact sites characterized by a central glass pit and numerous radial and annular fractures (see McKay, 1970 and Carter, 1971 for detailed discussion of microcrater types and associated features). Lower velocity impacts, formed by either meteoritic or secondary particles produced during meteorite impacts, indicate a wide velocity as well as thermal range. Features commonly produced by lower velocity impacts are

spalls, chips, fluid or semifluid splashes, and particle accretion by welding or attachment to a host surface. These later particle features most closely approximate terrestrial particle impacts and collisions during eruption.

Thermal cycling between day and night temperatures (130° to -153° C) has a more pronounced effect on the disintegration of lunar particles as compared to terrestrial counterparts.

The lack of a lunar atmosphere also has a pronounced affect on the preservation and modification of lunar particles. The absence of an atmosphere allows incoming meteorites to impact the lunar surface, whereas a terrestrial atmosphere allows few meteorites to impact the surface. The near perfect vacuum of the lunar environment significantly impedes chemical alteration or decompositional processes. It also generates a greater pressure differential between internal gas vesicles of lunar particles and the particle surface. This would significantly affect the extent of surficial disruption due to vesiculation. Surface modification by aerodynamic processes is of minor importance in the lunar environment and is developed only within eruption or impact clouds. The absence of an atmosphere significantly reduces the number of elongate particles formed in the lunar environment. Two plausible explanations can be suggested for the disparity of their respective abundance. During terrestrial eruption strong convective air currents rise along the edges of the fountain column and enhance the formation of particles with tails or

filaments. Conversely, the lack of such currents in the lunar environment reduces filament or elongate particle generation. Secondly, the fragile nature of glass filaments and particles with filament tails decreases their durability and preservation in the lunar soil because of constant meteorite impact.

A third general difference between lunar and terrestrial environments can be considered as a time factor. The length of resisdence of a glassy particle on the lunar surface is considerably longer when compared to its terrestrial counterpart. Estimates of particle residence on lunar soil surfaces range from millions to billions of years. A terrestrial particle is rapidly attacked by chemical agents within the atmosphere and is altered or decomposed within less than a few hundred years. Such extended periods of lunar particle life allow time dependent processes (devitrification, etc.,) to occur, whereas most terrestrial particles do not survive long enough for devitrification to take place. The time factor also determines where the majority of the destructional processes takes place. Terrestrial particles experience most of their destructional modification during the later part of particle flight and during particle impact onto the pumice blanket. Lunar particles experience greatest modification after deposition due to meteorite impact processes during surface exposure.

Particle histories for lunar particles are somewhat more complex than their terrestrial counterparts if the processes of chemical alteration are excluded. Lunar particles develop an

initial sequence of stratigraphic features which delineates their formation, flight, and impact onto the lunar surface. During residence on the surface the particle will be modified by micrometeorite impact and associated destructional or constructional processes. The particle may be cycled back and forth from burial to surface exposure where it receives further generations of destructional and constructional features.

Mechanical Disintegration. Mechanical disintegration processes are similar for both terrestrial and lunar particles: (1) fracturing, (2) abrasion, and (3) surficial disruption due to vesiculation. Although the processes of fracturing and abrasion are similar, a different mechanism (meteorite impact) is primarily responsible for lunar particle disintegration. Extensive impacting, several hundred impacts have been observed on some particles, indicates that the major cause of fracture or abrasion of lunar particles is impact produced. Thermal cycling also affects particles that have heterogeneous or crystalline textures, where the difference in the coefficients of expansion and contraction for the different phases would assist in the process of disintegration. Spalls and shards produced by impacts are commonly observed on lunar particles.

Surficial disruption due to vesicle bursts would be more pronounced on lunar particles due to the greater difference between the internal vesicle gas pressure and the virtual absence of a confining atmosphere.

Solar wind abrasion can be considered to be a minor agent

of mechanical removal of surficial material but is unknown as to what extent it has modified particle surfaces. Likewise, particle damage (fusion tracks) due to bombardment by solar neutrons and protons has been observed in some lunar minerals but again the extent to which this process modifies particle surfaces or interiors is unknown.

Chemical Alteration and Decomposition. Chemical alteration or decomposition of lunar particles is for the most part insignificant when compared to terrestrial particles. However, the presence of iron-oxide minerals within a few Apollo 16 samples indicates that oxidation and to some extent chemical alteration does occur during either eruption or impact. The release of water vapor from the lunar surface has been detected in minor amounts and suggests that the release of volcanic gases from the subsurface may well be responsible for some local chemically active areas. Lunar particles and volcanic gases released during eruption are considerably more reduced than their terrestrial counterparts (Naughton, et al., 1972).

Probably the greatest chemically different characteristic of terrestrial versus lunar particles is the abundant formation of hydrated mineral species on terrestrial particles and their dearth on lunar particles. Conversely, lunar particles contain more iron, iron sulfide and iron-nickel minerals than terrestrial particles.

Chemical alteration of glassy particles within pumice deposits occurs in both environments. Vapor phase transport and

recrystallization of volatile elements as silicates, oxides, phosphates, and native elements was observed by McKay, et al., (1972) in lunar breccias. Similar vapor phase crystals have been observed in several terrestrial pumice deposits (Smith, 1960).

CHAPTER 6

CONCLUSIONS

Terrestrial Glassy Particles

The following are the important and significant conclusions of this study of terrestrial glassy particles.

1. Glassy particles produced by basaltic lava fountains consist predominantly of sideromelane glass with minor to moderate amounts of vesicles and crystals.

2. Glassy particles are classed on the basis of morphology and consist of the following types: (a) reticulite, (b) shard, (c) spherical, and (d) elongate. Other particles common to lava fountains are: (e) glass-coated mineral grains or fragmens, (f) composite particles, and (g) lithic fragments.

3. The internal texture and surficial microstratigraphy of a glassy particle produced by basaltic lava fountains indicates its history of formation, the capture and accumulation of other particles, the possible loss or removal of material by fracturing or abrasion, and its decomposition or alteration by solution, oxidation or hydration.

4. The formation and modification of glassy particles can be modeled as a system with three main stages: (a) initial formation, (b) constructive material accumulation, and (c) destructive removal or alteration of existent surfaces. The various stages of particle history may be shortened, by-passed,

reversed, or cyclically repeated depending on the flight of a particle.

5. Factors that affect particle formation and modification are: (a) melt composition, (b) vent configuration, (c) flight velocity, (d) flight time duration at temperatures $>800^{o}C$, (e) surface tension, (f) gas exsolution or expansion, (g) particle population within the fountain, and (h) convective cycling.

6. The major components of a lava fountain model are the vent, spatter ramparts, fountain column, downwind plume, and associated pumice deposits.

7. The amount and type of surficial debris collected by a particle is a function of the length of time spent within the various regions of the fountain as well as the particular areas that the particle passed through during its flight history.

8. Two major processes active within a lava fountain and associated pumice deposit are: (a) constructional accumulation by addition of material to the surface by accretion and sublimation or condensation, and (b) destructional removal or alteration of the initial particle or subsequently accreted surficial materials by mechanical disintegration and chemical decomposition or alteration. Constructional accumulation usually precedes but may be synchronous with destructive removal of surface materials.

9. Descriptive glass terminology (between the liquid and solid states) is defined based on temperature, viscosity, and physical properties for a basaltic glass as tentatively

correlated with synthetic soda-lime-silicate glass:

rigid: where glass behaves as a solid; viscosity $>10^{13}$ poise, temperature $\sim 700^{o}C$.

semirigid: where glass deforms and bends without fracturing under gradually applied stress but fractures under instantaneous stress and does not wet a host surface; viscosity $\sim 10^{7}$ poise, temperature $\sim 850^{o}C$.

semifluid: where glass flows, spreads out, does not retain its shape, deforms under instantaneous stress without fracturing, wets a host surface; viscosity $\sim 10^{5}$ poise, temperature $\sim 950^{o}C$.

fluid: where glass behaves as a fluid; viscosity $<10^{5}$ poise, temperature $\sim 1250^{o}C$.

10. Spherical glassy particles are formed by: (a) the break-up of liquid cylinders (jets or streamers), (b) rapid rotaion of a liquid mass forming a spray of smaller droplets, and (c) shape modification of previously formed irregular particles by surface tension at elevated temperatures $> 800^{o}C$. Condensation does not appear to be an effective particle forming mechanism for particles > several thousand angstrom diameter. However, condensation is responsible for the development of beaded micromounds.

11. Glassy filaments or elongate particles form in response to rapid acceleration of a liquid mass from a vent where frictional resistance (aerodynamic drag) stretch lava particles into elongate forms. Strong convective air currents rising at the periphery of the fountain column causes longer times of particle motion and drag.

12. Glass-coated mineral grains are formed by the

disruption of crystal-bearing lava during eruption. Glass-coat thickness depends on flight time at elevated temperatures where liquid is stripped away or thinned by centrifical separation, aerodynamic drag, and vesicular coalescence.

13. Composite particles are formed by multiple particle impacts or collisions within the fountain and are a function of particle population within the fountain and the amount of convective cycling.

14. Other particles observed but not formed by the eruption of a liquid are lithic fragments (prior magmatic crystallization), shards (formed by mechanical breakage of cooled particles), and reticulite. Reticulite must be carefully distinguished as either friable reticulite (formed by mechanical breakage of vesicular particles) or froth reticulite (formed by a liquid that vesiculates to a point where coherence is lost).

15. Accretionary growth is accomplished by the addition of solid or liquid particles to a particle surface by glass splashes, attachment or welding of smaller particles, filaments, platelets, previously grown crystals, shards, and other debris.

16. Sublimation or condensation growth takes place on a particle surface by the nucleation and growth of vapor phase crystals, sublimation or condensation of micromounds, and condensation of liquid films on cooler surfaces.

17. Destructional processes break apart, remove and alter accumulated surficial debris or break the particle into fragments by: (a) mechanical disintegration which includes fracturing,

abrasion and surficial vesiculation, and (b) chemical alteration which includes decomposition, oxidation and hydration. Surfaces are also modified by rippling, waving, and rind formation.

18. Glassy particles are further modified by addition to or residence within pumice deposits by: (a) the type of particle impact, (b) the amount of surface area that is available for chemical alteration, and (c) the exposure to chemically active vapors, aerosols, etc., either during surface exposure or residence within the pumice deposit.

19. Additional studies and research needs to be conducted in the following areas:

a. Surface ripple formation and their relationship to internal ripple laminae.

b. Mechanism of internal ripple laminae formation.

c. Characterization and mechanism of oxide development on glass.

d. Mechanism and conditions under which particles develop peripheral rinds.

e. Effect that convective air currents have on particle removal from pumice deposits and convective cycling within fountains.

f. Temperature and pressure distributions within lava fountains, downwind plumes, and pumice deposits.

Terrestrial - Lunar Glassy Particle Comparisons

The following are the important and significant conclusions made in comparing terrestrial and lunar glassy particles.

1. Terrestrial and lunar glassy particles have generally similar abundances of particle types, internal texture and surficial features. Notable differences are the dearth of glassy

filaments and elongate particles in lunar soils and the paucity of agglutinates in terrestrial pumice deposits.

2. Similar particle types, surface features, etc., suggest similar methods of particle formation, constructive accumulation and destructive removal of materials. However, the lack of some surface features on both lunar and terrestrial particles indicates that additional processes operate within the lunar environment which do not operate to a significant degree on terrestrial particles (i.e. meteorite impact and thermal contraction or expansion). Likewise, processes active in the terrestrial environment (chemical alteration, etc.,) do not operate under lunar conditions.

3. Two liquid particle forming processes are active in the lunar environment: (a) volcanic eruption, and (b) meteorite impact which is the predominant means of liquid particle formation on the moon.

4. Accreted materials are similar for both terrestrial and lunar particles except that lunar particles contain more fluid to semifluid splashes, platelets, and smaller spheres than terrestrial glassy particles. Two notable reductions in particle forms accreted to lunar particles are filaments and previously grown vapor phase crystals. Reasons for this disparity are:

a. Greater length of particle residence time on lunar pumice deposits allows greater accumulation of meteorite produced glass.

b. Absence of atmospheric conditions in the lunar environment allows particles to remain chemically unaltered for vast periods of time and secondly causes a marked

decrease in aerodynamically produced particles, i.e., filaments and elongate forms.

c. Lower gravitational attraction extends particle flight time by a factor of 8 when compared to terrestrial particles. This allows irregular particles (jets, streamers) produced by impact or eruption to break-up into droplets or modify their shapes to spherical forms which further reduces elongate particle abundance.

d. Eruptive or impact produced atmospheres or clouds are short-lived and do not exist long enough for vapor phase crystals to nucleate and grow before the cloud is dissapated. However, sufficient time is available for micromounds to sublimate onto particle surfaces.

5. Terrestrial and lunar micromounds have similar shapes but differ in composition. Lunar micromound composition depends on the mechanism of melt production i.e., volcanic eruption or meteorite impact. Meteorite produced particles often contain micromounds with compositions enriched in Fe, Ni, and S which reflects not only the composition of the volatilized lunar material but that of the impacting meteorite (i.e., iron-nickel).

6. Destructional processes for lunar and terrestrial particles are similar except that the dominant method of mechanical disintegration of lunar samples is meteorite impact. Minor break-up of lunar glassy particles may also be caused by thermal expansion and contraction, solar wind abrasion, and particle disruption by solar or galactic cosmic particles. Surficial vesiculation would cause greater lunar particle disruption due to the greater pressure differential between vesicles and the surface. Little chemical alteration or decomposition was found on lunar particle surfaces formed during particle flight or surface

exposure. However, particles contained within thick pumice blankets experienced thermal decomposition and subsequent re-crystallization as vapor phase crystals that formed in crevices and vugs of pumice-breccia blankets.

EXPLANATION OF PLATE 1.

RETICULITE, FRAGMENTS, SHARDS AND DEBRIS-FREE SPHERES

Figure 1. Reticulite fragment. Note glass strands have triangular cross-sections and join together in triple-junctions. Reticulite surfaces exhibit little debris accumulation and fractures have sharp edges. Kilauea Iki; (1959-60) sample, 100X.

Figure 2. Glass shard with characteristic conchoidal fracture and lenticular to sliver-like shape. Note accumulation of superficial debris on surface. Kilauea Iki; (1959-60) sample, 100X.

Figure 3. Sideromelane sphere with light coating of surficial debris. Note that debris occurs as patches (a), individual particles (b), and large clumps of material (c). Mauna Ulu; (1969-73) sample, 600X.

Figure 4. Oblate spheroid with minor amount of surface debris which includes glass filaments (a), crystals (b) and fine-grained coating of micromounds (c). Mauna Ulu; (1969-73) sample, 600X.

Figure 5. Debris-free sphere with abundant sharp-edged surface depressions. Note appearance of light colored halos around depressions. Kilauea Iki; (1959-60) sample, 60X.

Figure 6. Highly fractured sphere containing both radial and concentric fractures. Note spalled regions (a) between fractures and minor amount of accumulated surficial debris patches (b) and small glass shard (c). Mauna Ulu; (1969-73) sample, 400X.

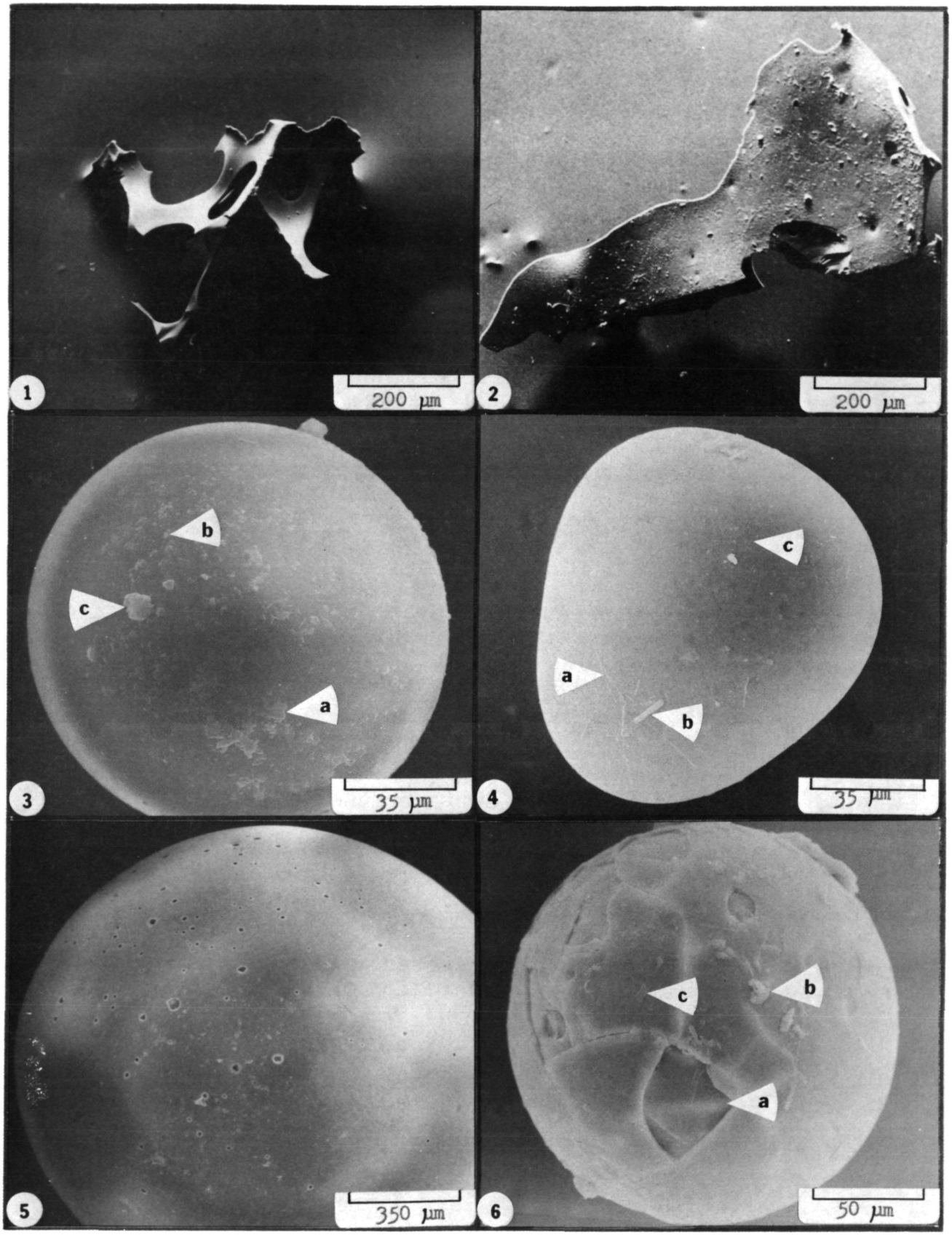
1
200 µm
2
200 µm
b
c
a
3
35 µm
c
a
b
4
35 µm
5
350 µm
c
b
a
6
50 µm

EXPLANATION OF PLATE 2.

DEBRIS COVERED SPHERES

Figure 1. Sphere with groups of smaller spheres as well as small individual spheres, also note the minor amount of glass filaments and crystals. Mauna Ulu; (1969-73) sample, 700X.

Figure 2. Egg-shaped spheroid with partial coating of fragments of glass filaments (Pele's Hair). Glass filaments were rigid at time of attachment to surface of sphere. Note occurrence of spheres (a), crystals (b), debris patches (c) and shards (d). Mauna Ulu; (1969-73) sample, 500X.

Figure 3. Sphere with several large gypsum crystals. Surface has a very fine-grained coating of micromounds. Note development of polygonal fracture pattern. Mauna Ulu; (1969-73) sample, 500X.

Figure 4. Sphere with surface covered by a mat of interlocking crystals of gypsum and other sulfur compounds as well as other debris (spheres, filaments, and irregular-shaped material). Mauna Ulu; (1969-73) sample, 1,000X.

Figure 5. Sphere partially coated by a composite mixture of all of the above surface materials (a). This sphere contains over 100 smaller spheres in this field of view. Note glass filaments (b), and "etched" surface (c). Mauna Ulu; (1969-73) sample, 800X.

Figure 6. Sphere completely covered with surficial debris, sublimates, and alteration products. Mauna Ulu; (1969-73) sample, 300X.

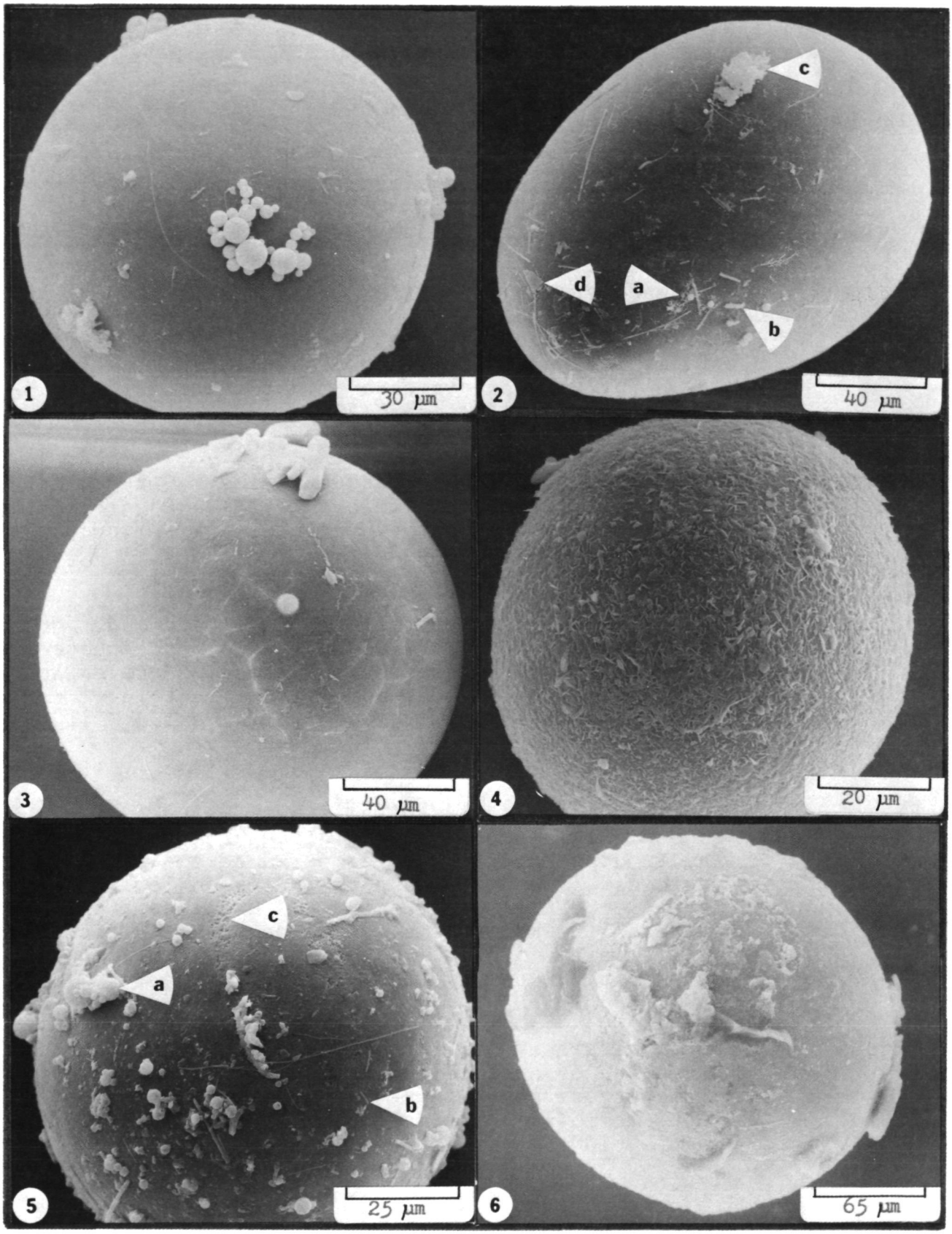
1
30 µm
2
c
d
a
b
40 µm
3
40 µm
4
20 µm
5
c
a
b
25 µm
6
65 µm

EXPLANATION OF PLATE 3.

ELONGATE PARTICLES

Figure 1. Elongate particle consisting of numerous strands of stretched glass. Note roundness of surfaces (a) with only minor deformation of vesicles. Broken strands (b) have solid interiors. Kilauea Iki; (1959-60) sample, 60X.

Figure 2. Elongate-stretched particle composed of several strands of glass. Note stretch marks (ribs) along strand surfaces (a), elongate vesicles (b), fluting of particle edges (c) and hollow nature of strand (d). Surface is covered by minor coating of superficial debris. Kilauea; (July, 1974) sample, 60X.

Figure 3. Glassy spindle with enclosed olivine. Surface has attached smaller glass filaments (a). Note stretched vesicles (b) and twisted particle (c). Kilauea; (July, 1974) sample, 60X.

Figure 4. Streamlined glassy particle with pointed end. Note light coating of surficial debris on both rounded surface as well as fractured surface. Note extent of vesicle development, but lack of vesicle coalescence at fractured end of fragment. Kilauea; (July, 1974) sample, 100X.

Figure 5. Two rounded particles with either a single or double filament tail. Note circular gas vesicles (a) in upper particle as compared to smaller vesicles (b) and ripple pattern (c) on lower particle. Filament fragment (d) overlies ripple pattern. Broken filaments (e) on upper particle are nearly solid with only minor inner-tube development. Mauna Ulu; (1969-73) sample, 100X.

Figure 6. Rod-like glassy particle with compressional deformation of surface and interior. Note that some vesicles are not deformed, whereas glass surface shows definite compression. Kilauea; (July, 1974) sample, 100X.

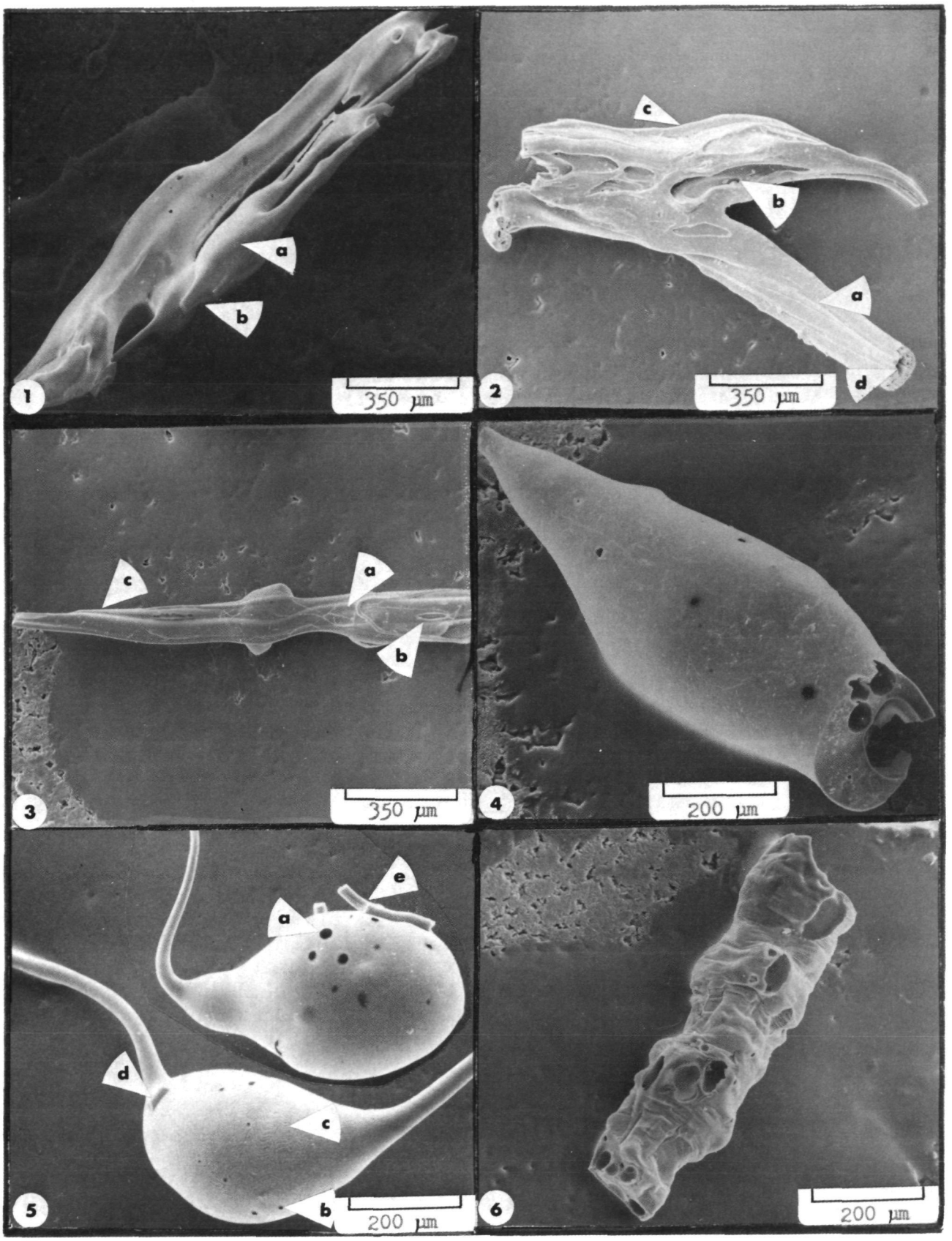
1
a
b
350 µm
2
c
b
a
d
350 µm
3
c
a
b
350 µm
4
200 µm
5
e
a
d
c
b
200 µm
6
200 µm

EXPLANATION OF PLATE 4.

GLASSY FILAMENTS, COATED MINERAL GRAINS

AND COMPOSITE PARTICLES

Figure 1. Glassy filament (Pele's Hair) shaped like a bobby-pin. Note the lower arm of the particle has filament doubled back forming a loop. Several other small filaments are attached to the surface. Kilauea; (Dec., 1974) sample, 80X.

Figure 2. Bent glass filament with two glass bulges. Note stretching of vesicles at the surface but minor vesicle development at fractured ends of filament. Kilauea; (July, 1974) sample, 60X.

Figure 3. Glass coated olivine crystal. Glass coating almost entirely masks grain shape. Note size and abundance of circular vesicles on glass surface. Compare vesicle size and abundance with Figure 4. Kilauea Iki; (1959-60) sample, 60X.

Figure 4. Mineral fragment (clinopyroxene?) coated by coarsely vesiculated glass. Note coalescence of vesicles forming triangular strands of glass (a) and smaller vesicle intersection of larger vesicle walls (b). Vesicle walls have coating of surficial debris. Upper left and right hand surfaces (c and d) are remnant portions of rounded glassy surface. Kilauea; (July, 1974) sample, 100X.

Figure 5. Composite grain consisting of vesiculated sphere with abundant coarse glass filaments wrapped around and over surface. Note filaments cover previously formed ripple surface. Filament cross-sections indicate solid rather than hollow fibers. Note general lack of longitudinal ribbing along filament surfaces. Mauna Ulu; (1969-73) sample, 100X.

Figure 6. Composite particle consisting of a large sphere with several smaller spheres welded to the surface. Note that smaller spheres were sufficiently rigid to retain their shapes upon impact. Note accumulation of large debris patches (a) and minor small filaments (b). Mauna Ulu; (1969-73) sample, 50X.

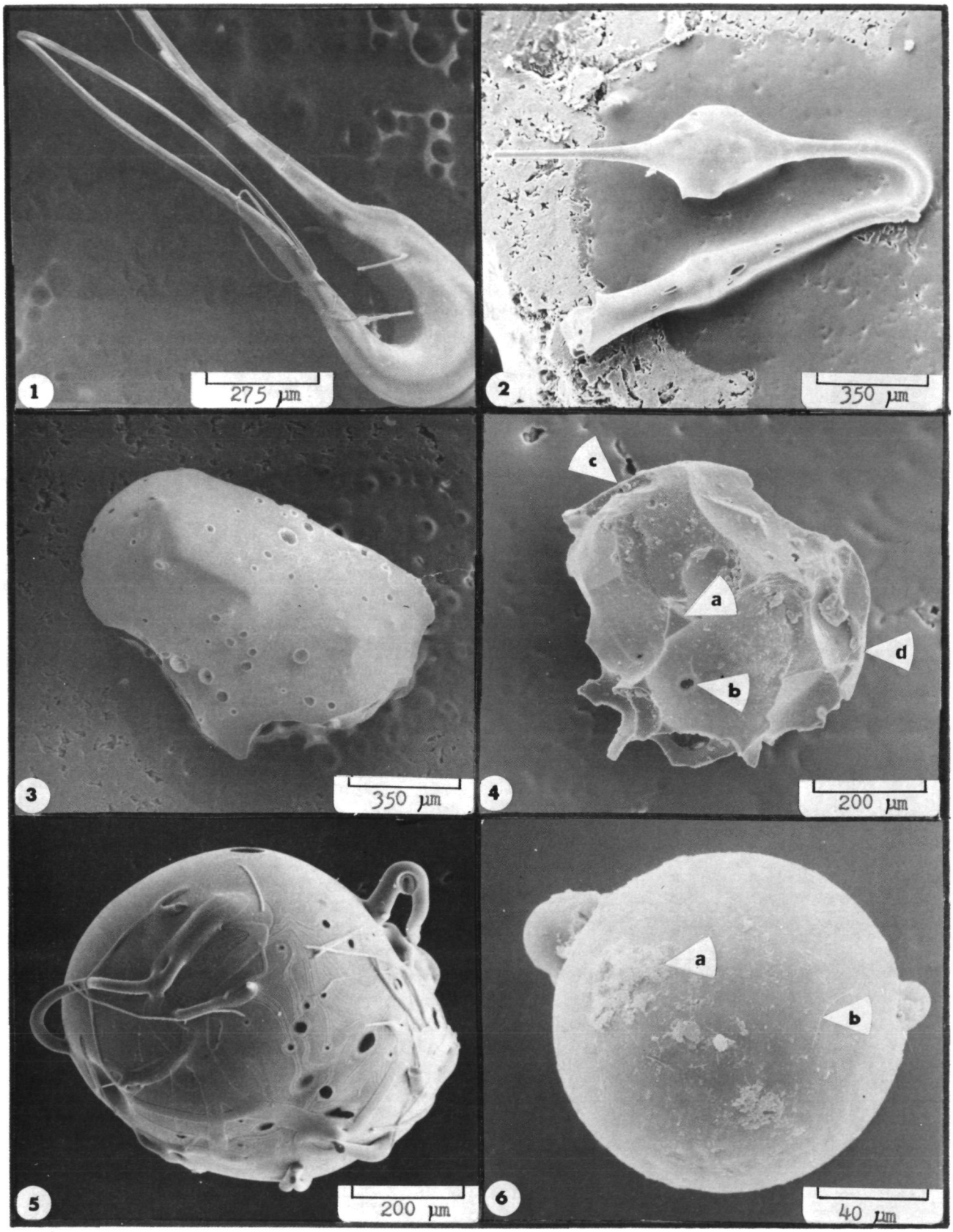
1
275 µm
2
350 µm
3
350 µm
4
c
a
d
b
200 µm
5
200 µm
6
a
b
40 µm

EXPLANATION OF PLATE 5.

ROCK FRAGMENTS AND SURFACE SPLASHES

Figure 1. Crystalline rock fragment covered by glass and surficial debris. Kapoho; (1960) sample, 400X.

Figure 2. Fractured rounded-rock fragment with central void lined with a diktytaxitic intergrowth of plagioclase crystals and glass. Note glass surface (a) in void area and minor accumulation of debris on void and fractured surfaces. Mauna Ulu; (1969-73) sample, 300X.

Figure 3. Constructive surface consisting of fluid splashes (a), glassy filaments (b), micromounds (c), platelets (d), crystals (e), and shards (f). Mauna Ulu; (1969-73) sample, 5,000X.

Figure 4. Glassy surface partially covered by numerous fluid to semifluid splashes. Central splash (a) is circular in shape and has a moderate thickness ($\sim 0.5\ \mu$), whereas doughnut shaped impact (b) has more hemispherical shape with central depression. Several semifluid filament soft impacts produce patterns characterized by parallel outer ridges (c). Fluid filament splashes form uniformly thin road-like surfaces (d). Nearly all of the surface viewed is covered by an accumulated veneer of glassy material. Note spalled glass area (e). Mauna Ulu; (1969-73) sample, 7,000X.

Figure 5. Fluid to semifluid filament impacts on glassy surface. Fluid filament splash (a) is characterized by a thin, uniformly-wide surface coating. Semifluid soft impacts exhibit deformed filament surfaces with partial retention of original wall configuration (b). Note that impact features have secondary coating of debris. Kilauea Iki; (1959-60) sample, 5,000X.

Figure 6. Impact of particle that contained an inner semi-rigid core (a) surrounded by a fluid exterior. Note the fluid splash covers fine-grained micromound surface (b). Mauna Ulu; (1969-73) sample, 10,000X.

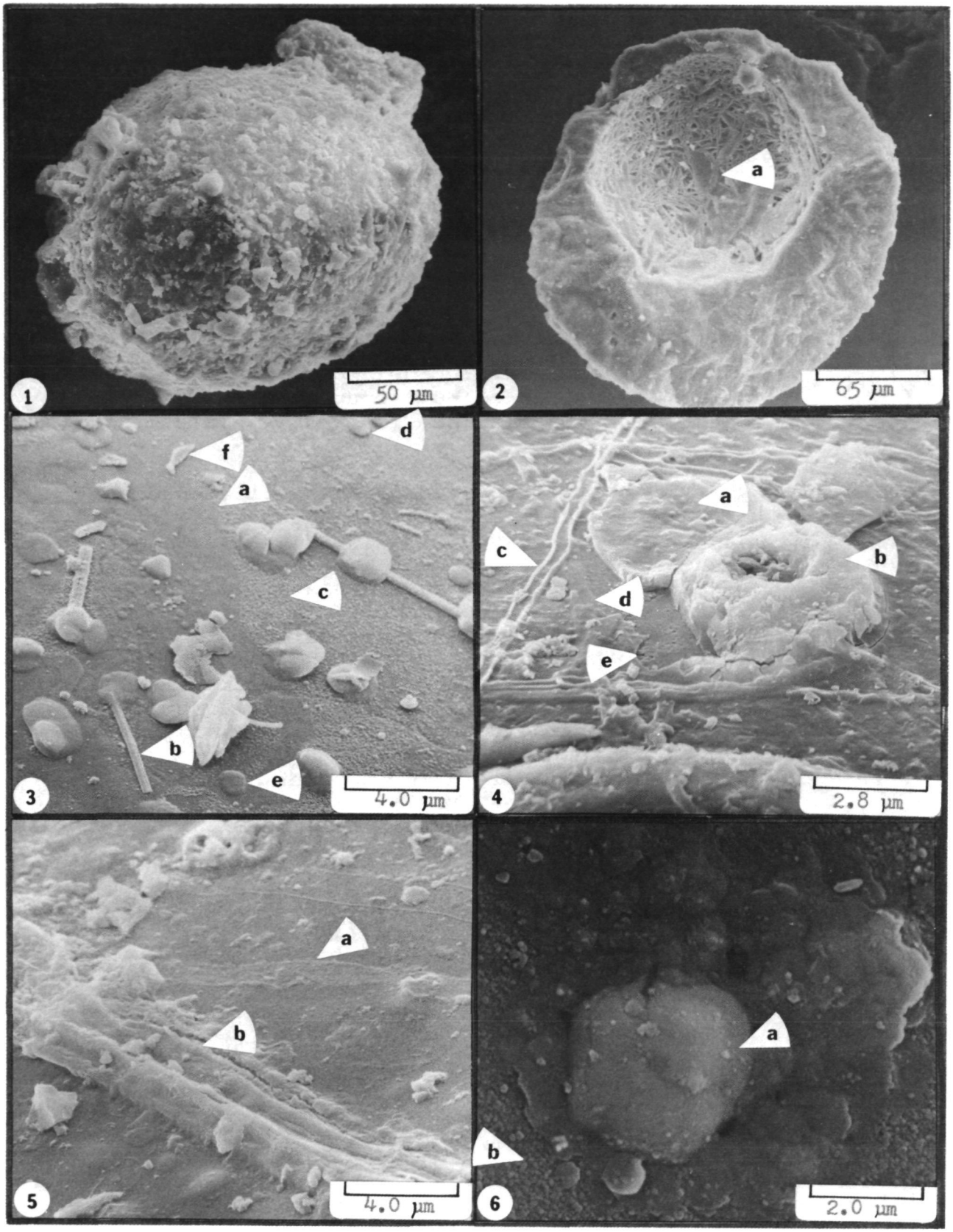
1
50 µm
2
a
65 µm
3
f
a
d
c
b
e
4.0 µm
4
a
c
b
d
e
2.8 µm
5
a
b
4.0 µm
6
a
b
2.0 µm

EXPLANATION OF PLATE 6.

SURFICIAL GLASSY FILAMENTS

Figure 1. Cluster of intertwined glassy filaments with general uniform thickness (~0.2 μ). Note small particles of debris attached to filaments (a) and other larger debris patches (b) superimposed on filaments. Kilauea Iki; (1959-60) sample, 5,000X.

Figure 2. "Soda Straw" filaments that have hollow cores and uniform wall thickness over considerable lengths. Note nature of filament fracture, both cross sectional (a) and longitudinal (b) fractures. Surface is generally free of debris and non-wetted around filaments. Kilauea Iki; (1959-60) sample, 1,600X.

Figure 3. Particle surface covered by glass filaments and filament impacts. Rigid filaments retain their shape on impact and do not "wet" the surface, whereas semifluid filament impacts are noticeably flattened, "wet" the glass surface and often indicate the nature of the underlying surface. Note glassy filaments (a) with several smaller filaments forming loops and pretzel shapes (b). Thin thread-like filaments (c) drape across larger filament splash with oxide-sulfate alteration mounds (d). Semifluid debris (upper right) has several filaments that retain their shapes at some localities (e) but exhibit splash features at others (f) indicating temperature variation within the particle. Kilauea Iki; (1959-60) sample, 15,000X.

Figure 4. Surface illustrating numerous glass filament types: filaments that retain their shape and have no associated surface wetting (a), filaments with upper surface depression (b), accreted filaments that "wet" the surface in long narrow strips (c) or twisted filaments (d). Note surface ripples (e) covered by filaments. Kilauea Iki; (1959-60) sample, 5,000X.

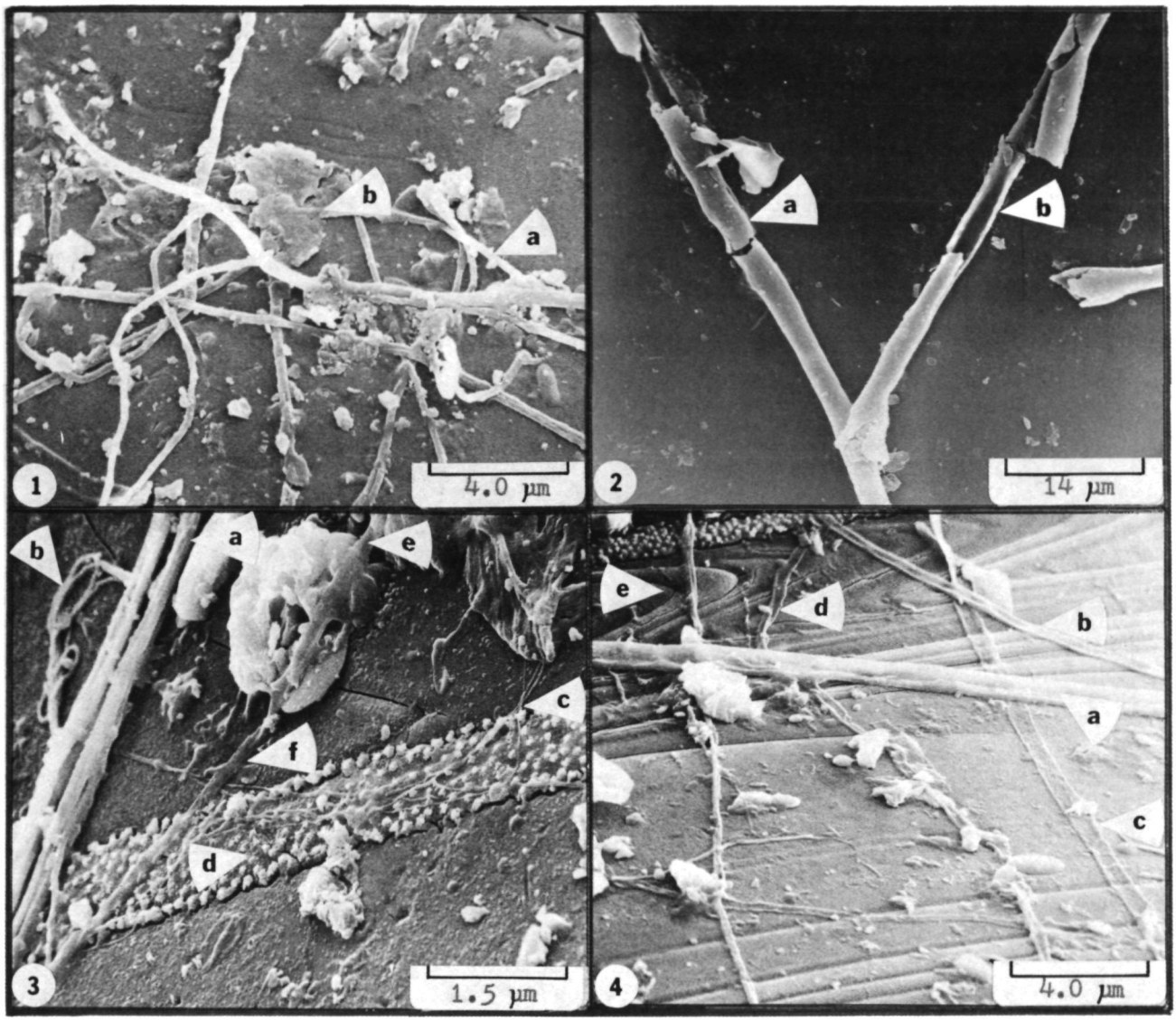
1
b
a
4.0 µm
2
a
b
14 µm
3
b
a
e
c
f
d
1.5 µm
4
e
d
b
a
c
4.0 µm

EXPLANATION OF PLATE 7.

PLATELETS AND SPHERES

Figure 1. Three large platelets (a) attached to surface composed of numerous fluid splashes (b) and other accumulated debris. Platelets have circular shapes and rounded upper surfaces with some debris. Note circular and flatter platelets at (c) and splash near (d). Kilauea; July, 1974 sample, 7,000X.

Figure 2. Surface covered with individual platelets (a) with later accumulation of gypsum crystal (b) and still later covering of crystal, platelets and glass surface by debris (c). Note general uniform size of platelets and hemispherical shape. Kilauea; (July, 1974) sample 15,000X.

Figure 3. Smaller spheres attached to a large sphere. Spheres occur as individuals or within groups. Note that some spheres have smaller platelets on surface (a) whereas others are free of debris (b). Small platelets (c) are often associated with sphere groups. Note that large glass shard (d) in upper center of photo has accumulation of surficial platelets. Mauna Ulu; (1969-73) sample, 3000X.

Figure 4. Attached sphere with two sets of surface depressions; larger smooth edge depressions (a), and smaller, closer-space holes (b) that are often grouped together in fields. Mauna Ulu; (1969-73) sample, 7,000X.

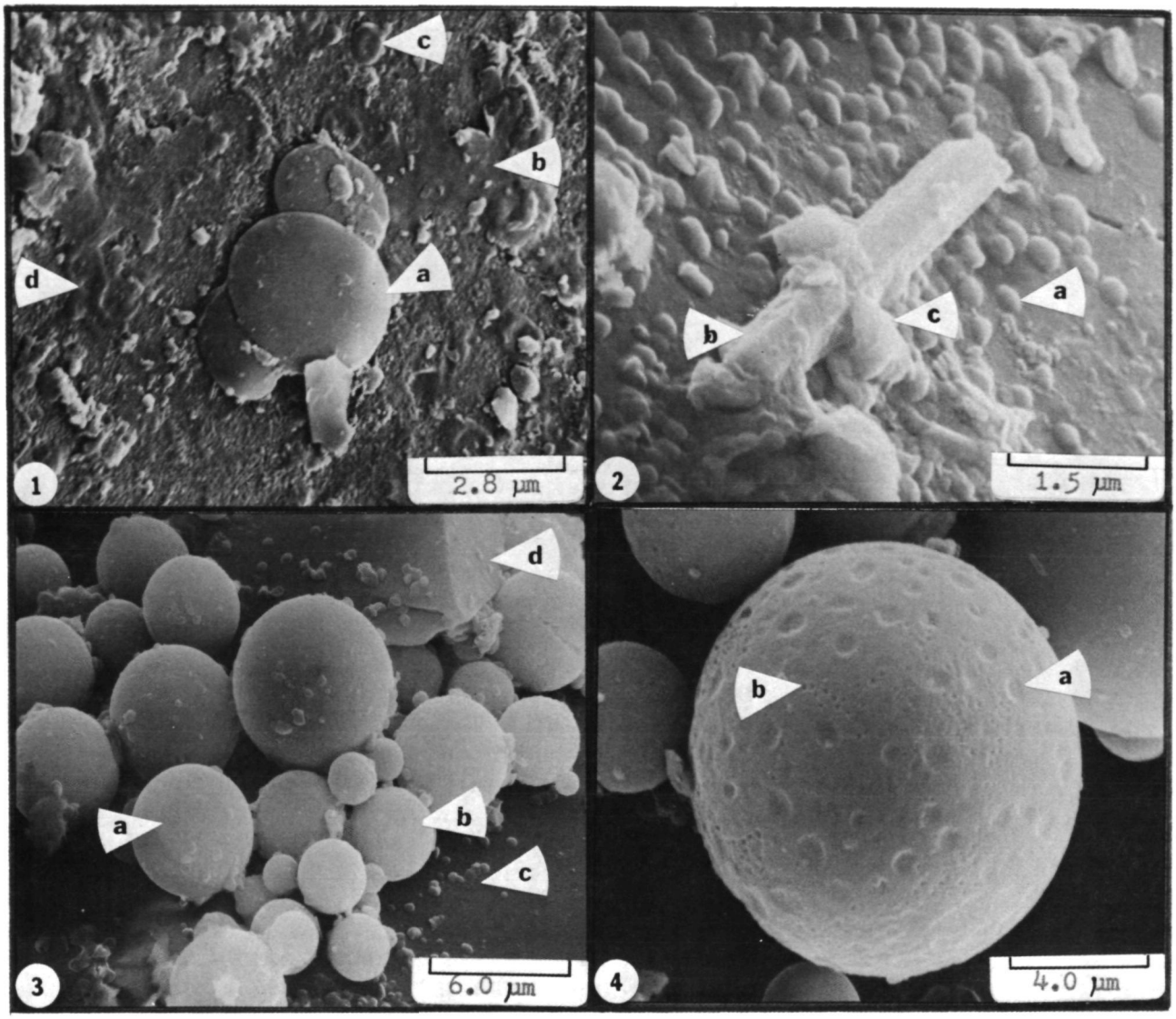
c
b
d
a
1
2.8 µm
a
b
c
2
1.5 µm
d
a
b
c
3
6.0 µm
b
a
4
4.0 µm

EXPLANATION OF PLATE 8.

SURFACE CRYSTALS

Figure 1. Elemental sulfur cluster (a) covering a surface fracture. Note surface splash (b), platelets (c) and sphere (d). Mauna Ulu; (1969-73) sample, 10,000X.

Figure 2. Jarosite, $KFe_3(SO_4)_2 \cdot 6(OH)$, with crystal habit of hexagonal ditrigonal pyramidal class (a). Crystals often form in close association with gypsum (b) and previously splashed surfaces (c). Smaller crystals are virtually platelets (d) but develop pyramidal growth with size. Note that some crystals have minor amounts of surficial debris on surfaces. Mauna Ulu; (1969-73) sample, 5,000X.

Figure 3. Jarosite crystal (a) with euhedral hexagonal shape which is attached to gypsum crystal that has smaller crystals (b) and micromounds (c). Jarosite has few micromounds, whereas the underlying glass surface shows individual micromound growth (d). Mauna Ulu; (1969-73) sample, 20,000X.

Figure 4. Jarosite developed as a secondary or encrusting phase of tabular to lenticular crystals (a) on a larger gypsum crystal (b). Note numerous spheres (c) that are attached to a gypsum crystal but are not covered by jarosite. Note platelets (d), curved fracture (e) and "wetted" versus splash free area (f). Mauna Ulu; (1969-73) sample, 4,000X.

Figure 5. Interwoven mesh of jarosite (a) that has developed on a previous hexagonal crystal habit (b). Note "wetted" surface near crystal development with some crystals grown over a fracture (c). Mauna Ulu; (1969-73) sample, 6,000X.

Figure 6. Mat-like surface of jarosite crystals covering sphere surface. Note occurrence of hexagonal crystals (a), however most crystals exhibit euhedral to anhedral tabular outlines. Note presence of fine-grained micromound growth (b) between crystals. Mauna Ulu; (1969-73) sample, 10,000X.

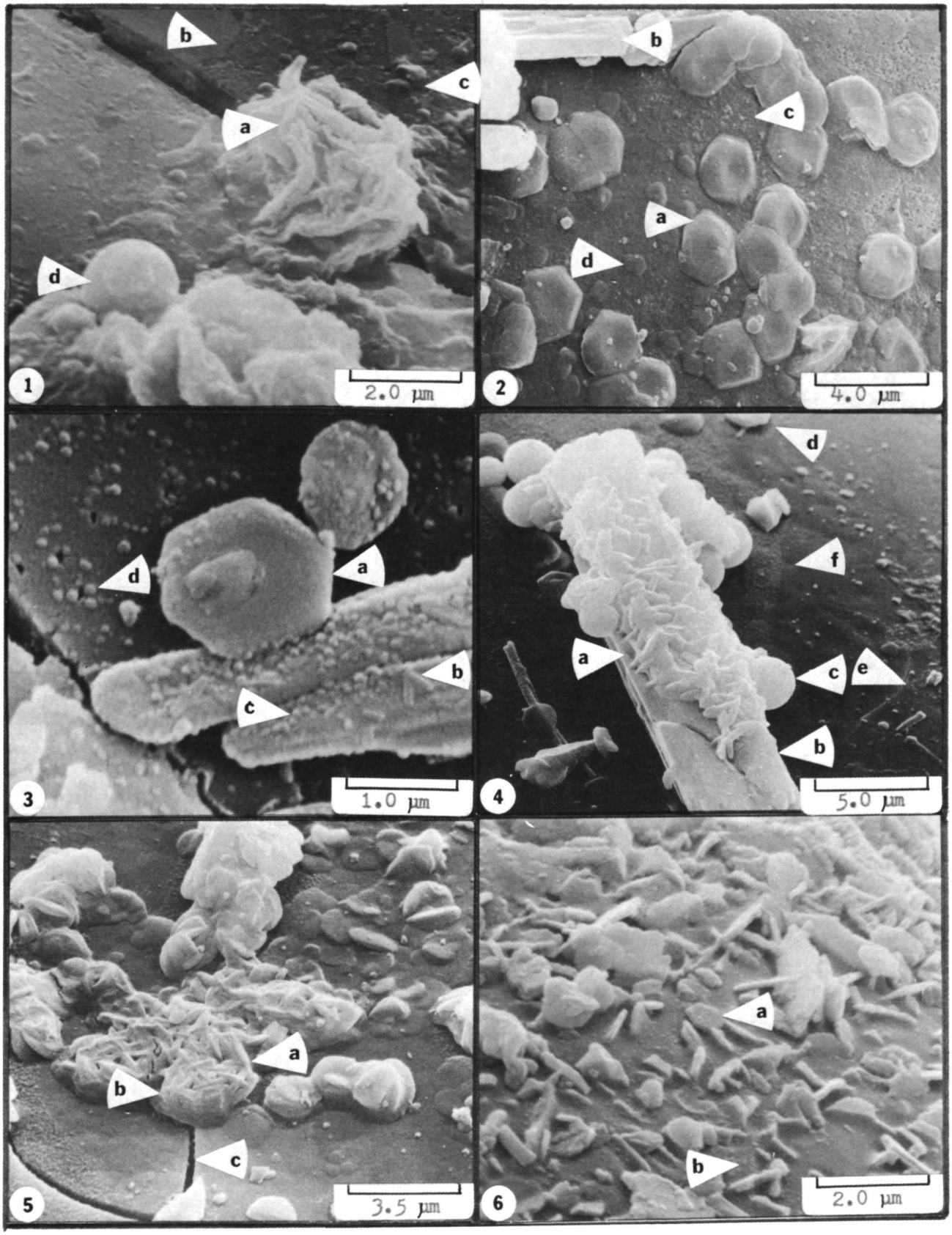
b
c
a
d
1
2.0 µm
b
c
a
d
2
4.0 µm
d
a
b
c
3
1.0 µm
d
f
a
c
e
b
4
5.0 µm
a
b
c
5
3.5 µm
a
b
6
2.0 µm

EXPLANATION OF PLATE 9.

GYPSUM AND MARCASITE CRYSTALS

Figure 1. Tabular clusters of gypsum crystals (a) on partially crystalline surface (b). Note amorphous accumulations of calcium sulfate (c). Mauna Ulu; (1969-73) sample, 5,000X.

Figure 2. Gypsum crystal. Note higher degree of micromound development on crystal than on glass background. Glass surface is fractured and exhibits many spall regions. Mauna Ulu; (1969-73) sample, 5,000X.

Figure 3. Large gypsum crystal overlying "beaded micromound" surface and glass filament. Note euhedral development of {110} prisms (a), {010} clinopinacoids (b), and partial development of {111} pyramids (c). Note crystal surface with minor micromound development (d) that is different from glass surface, and a scrape or gouge on upper right surface (e). Mauna Ulu; (1969-73) sample, 7,000X.

Figure 4. Radial cluster of gypsum crystals. Note relatively clean glass surface with only scattered micromound development. Mauna Ulu; (1969-73) sample, 15,000X.

Figure 5. Anhedral platelet masses of marcasite. Note arrangement around exterior of gypsum crystals. Marcasite masses have similar micromound development as glass surface. Mauna Ulu; (1969-73) sample, 10,000X.

Figure 6. Marcasite exhibiting compact sheath-like clusters with serrated or cocks-comb structures on ends of tabular forms. Note extensive development of micromounds beneath crystals, whereas the crystals have only minor development. Mauna Ulu; (1969-73) sample, 10,000X.

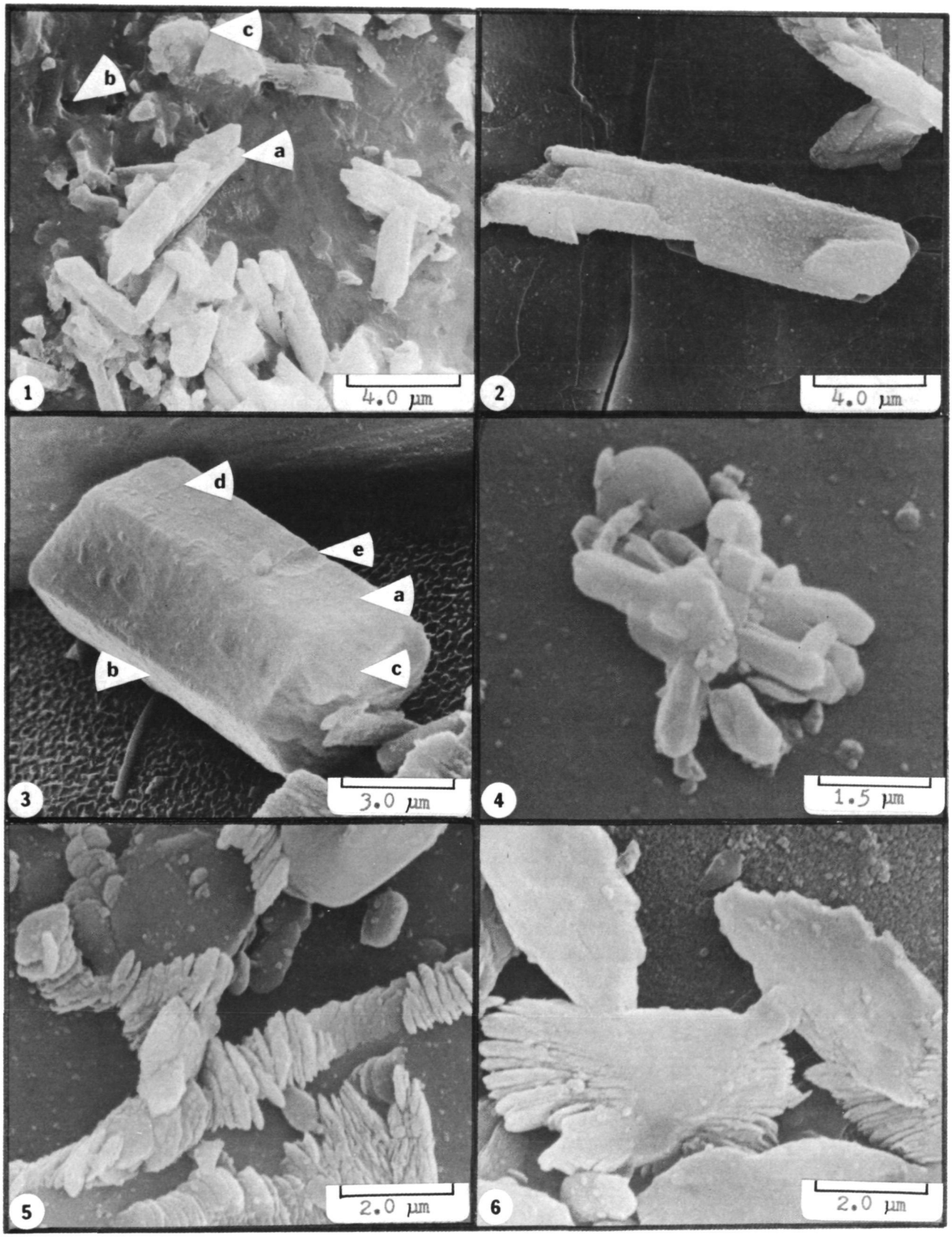
c
b
a
1
4.0 µm
2
4.0 µm
d
e
a
b
c
3
3.0 µm
4
1.5 µm
5
2.0 µm
6
2.0 µm

EXPLANATION OF PLATE 10.

GLASSY FILMS AND MICROMOUNDS

Figure 1. Enlarged view (Pl. 1, fig. 4) exhibiting glassy surface consisting of thin film with numerous evenly spaced vesicles. Note presence of splash material (a), platelets (b) and small spheres (c). Mauna Ulu; (1969-73) sample, 20,000X.

Figure 2. Fractured glass surface with development of widely-spaced small vesicles. Note presence of euhedral jarosite crystal (a), minor development of micro-mounds (b) and fractured larger overlying jarosite crystal but not to the same extent as the glass surface. Note multiple growth stages of jarosite crystals (c). Mauna Ulu; (1969-73) sample, 8,000X.

Figure 3. Glassy surface with grouped vesicles that exhibit rounded surfaces. Note skeletal development of crystal (photo center) and minor amount of debris on glass surface. Mauna Ulu; (1969-73) sample, 16,000X.

Figure 4. Surface covered with numerous micromounds (a), compare with scraped surface (b). A third surface, further right, has minor micromound development (c). Note splash area (d) and polygonal ridge development (e). Mauna Ulu; (1969-73) sample, 20,000X.

Figure 5. Extensive micromound growth area. Micromounds vary in size from 500 Å to several thousand Å. Note the growth of some mounds at the expense of smaller mounds. Surface area in upper center is covered with splash material which partially to wholly covers the mounds. Mauna Ulu; (1969-73) sample, 20,000X.

Figure 6. Micromound surface that exhibits interconnected mounds or "beaded micromounds", clearly a different micromound texture than those previously noted. Note micromounds cover fractures (a) but are over-lain by filaments (b) and sulfate crystals (c). Note the presence of very small individual sphere mounds (d). Mauna Ulu; (1969-73) sample, 10,000X.

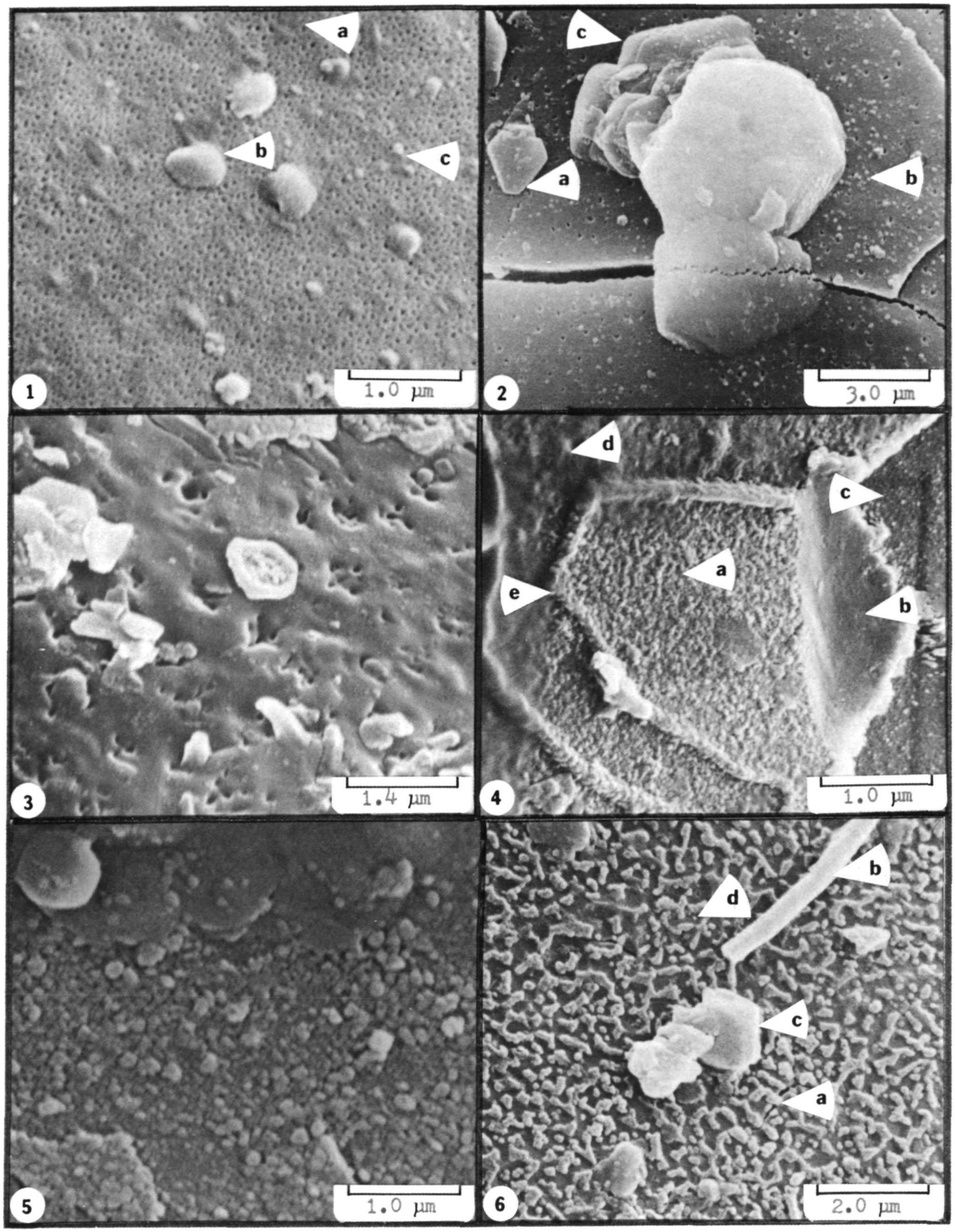
a
b
c
1
1.0 µm
c
a
b
2
3.0 µm
3
1.4 µm
d
c
a
e
b
4
1.0 µm
5
1.0 µm
b
d
c
a
6
2.0 µm

EXPLANATION OF PLATE 11.

GLASS SHARDS AND OTHER DEBRIS

Figure 1. Accumulation of lenticular glass shards indicating several periods of accumulation i.e. (1) platelet accumulation (a), (2) glass shard #1 (b), (3) impact of rigid glass filament (c) (4) impact of shard #2 (d). Mauna Ulu; (1969-73) sample, 5,000X.

Figure 2. Constructional surface composed of successive accumulation of: (1) splashes (a), (2) platelet (b), (3) shard with extensive micromounds (c), and (4) deposition of shard with minor micromound accumulation (d). Mauna Ulu (1969-73) sample, 10,000X.

Figure 3. Accumulation on sphere surface of debris mixture: (a) sphere (b) shard (c) intermixed deposits of platelets and amorphous calcium sulfate. Mauna Ulu; (1969-73) sample, 5,000X.

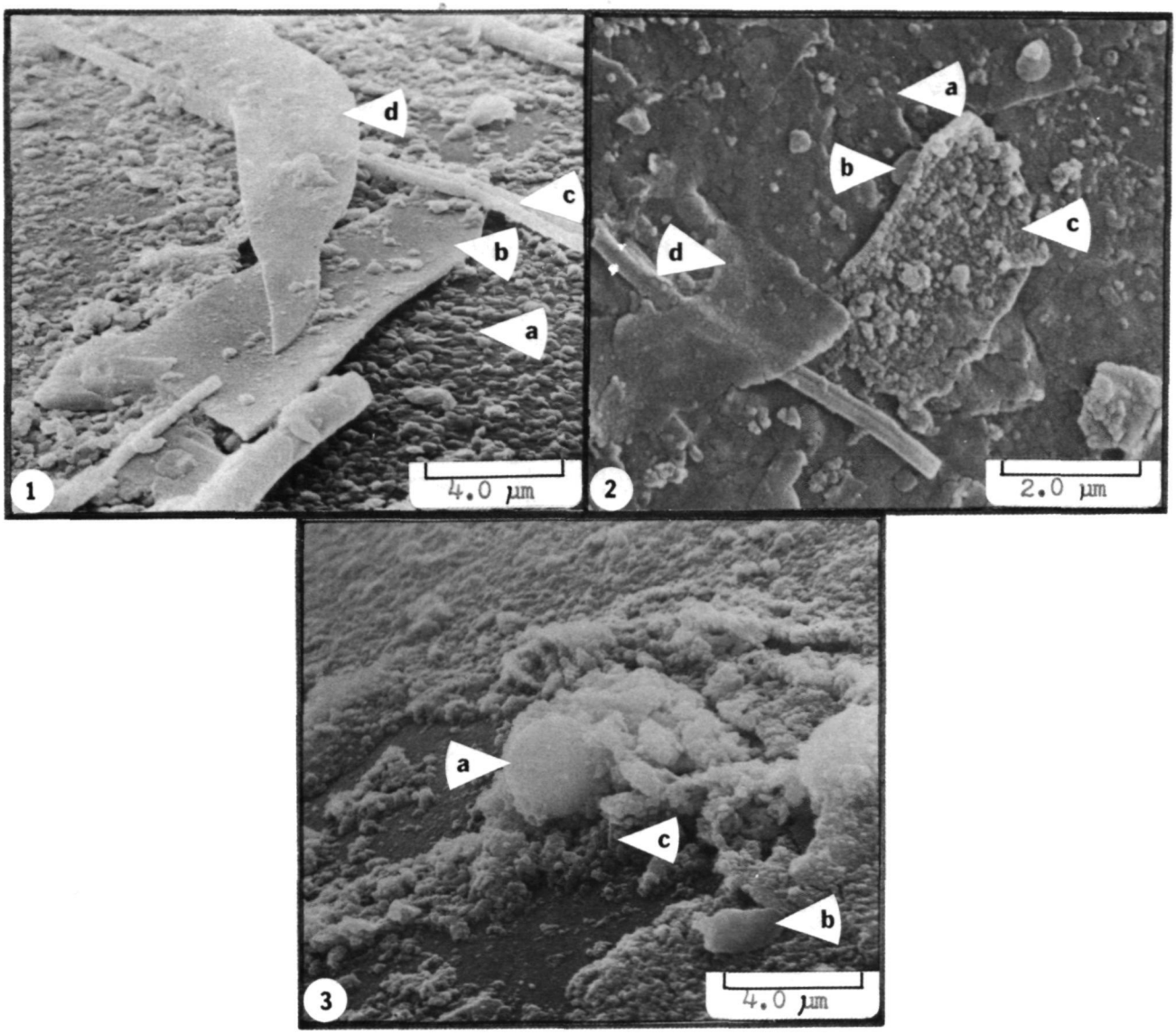
d
c
b
a
4.0 µm
1
a
b
c
d
2.0 µm
2
a
c
b
4.0 µm
3

EXPLANATION OF PLATE 12.

PARTICLE FRACTURING AND SURFICIAL

CHIPPING OR SPALLING

Figure 1. Surface fracture pattern on glassy sphere forming partial polygons with many of the fractures meeting at triple-junction with $\sim 120^{o}$ angles (a). Note crystals or other debris that bridge across fracture (b). Note fine-scale development of "beaded micromound" surface. Mauna Ulu, (1969-73) sample, 1,600X.

Figure 2. Fracture with coating of micromounds on sides (a) and exterior surface (b) areas. Note bridging filament strand (c) and other broken filaments accumulated on the surface. Note minor secondary fracture (d) parallel to larger fracture. Mauna Ulu; (1969-73) sample, 10,000X.

Figure 3. Several glass shards formed from surface covered by impacting debris consisting of sulfate encrusted filaments (a), spheres (b), deformed semirigid particles (c). Note the presence of constructive features on glass surface: platelets, hexagonal jarosite crystals, micromounds, and glass filaments. Mauna Ulu; (1969-73) sample, 5,000X.

Figure 4. Glass surface with twisted glass filament exhibiting plastic deformation. Note area of glass shard formation (a) and spalled areas (b). Surface exhibits platelets (c) subhedral crystal cluster (d), and semifluid splash (e). Kilauea Iki; (1959-60) sample, 10,000X.

Figure 5. Spalled glass surface exhibiting conchoidal fracture (a) and cuspate fracture surface (b). Note development of micromounds (c) on unspalled surface and their absence on spalled area. Kilauea; (July, 1974) sample, 8,000X.

Figure 6. Spall region exhibiting several generations of multiple spalls. Micromound development is greatest on outer surface and decreases with spall depth. Mauna Ulu; (1969-73) sample, 5,000X.

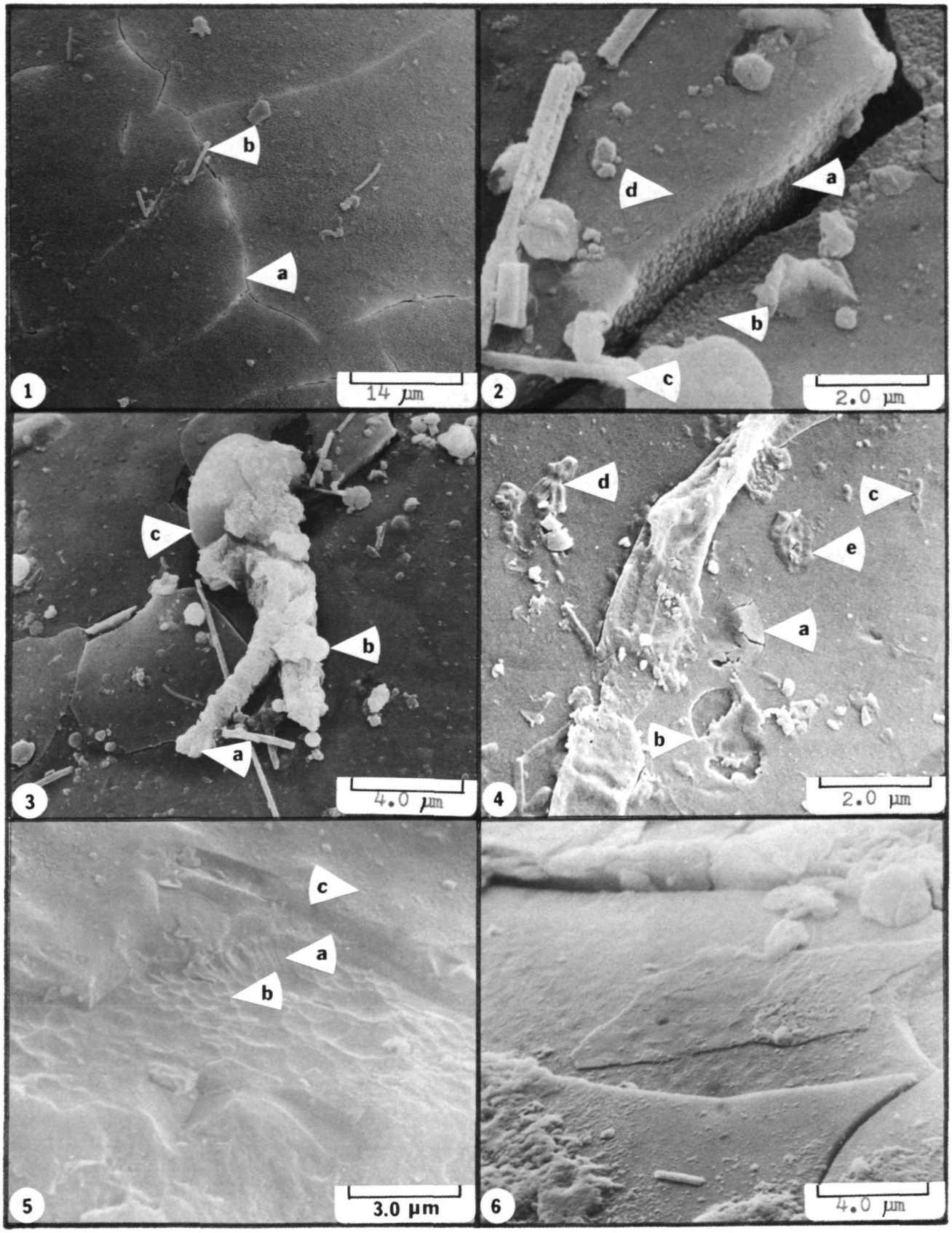
b
a
1
14 µm
d
a
b
c
2
2.0 µm
c
b
a
3
4.0 µm
d
c
e
a
b
4
2.0 µm
c
a
b
5
3.0 µm
6
4.0 µm

EXPLANATION OF PLATE 13.

ALTERED AND OXIDIZED SURFACES

Figure 1. Elliptical depressions exhibiting multiple terraces. Depressions have uppermost steps in common (a) and deeper steps (b) local to each depression. Note debris on depression surfaces. Small irregular single thickness depressions (c) are observed in foreground. Kilauea Iki; (1959-60) sample, 10,000X.

Figure 2. Fractured surface exhibiting small semicircular depressions (a). Note general polygonal pattern (b) of fracture system and wavy ripple surface beneath glass coating (c). Glassy filaments (d) have partial coating of debris. Note polygonal fractures break overlying glass filaments. Kilauea Iki; (1959-60) sample, 5,000X.

Figure 3. Highly decomposed particle surface exhibiting abundant cavities and branching fractures. Note the increase in surface area due to removal of material. Kilauea Iki; (1959-60) sample, 15,000X.

Figure 4. Oxidized surface exhibiting numerous scalelike masses and small cracks. Note volume increase due to expansion. Kilauea Iki; (1959-60) sample, 10,000X.

Figure 5. Oxidized surface consisting of small globular masses of oxidized material (a). Note accumulation or growth of globular material into a surface film (b) and partial covering of the oxide layer by later semifluid particles (c) and (d). Kilauea Iki; (1959-60) sample, 20,000X.

Figure 6. Particle surface covered with oxide film consisting of intergrown globular masses. Note that film expands surface, increases surface area, and has local areas covered by later semifluid material. Kilauea Iki; (1959-60) sample, 30,000X.

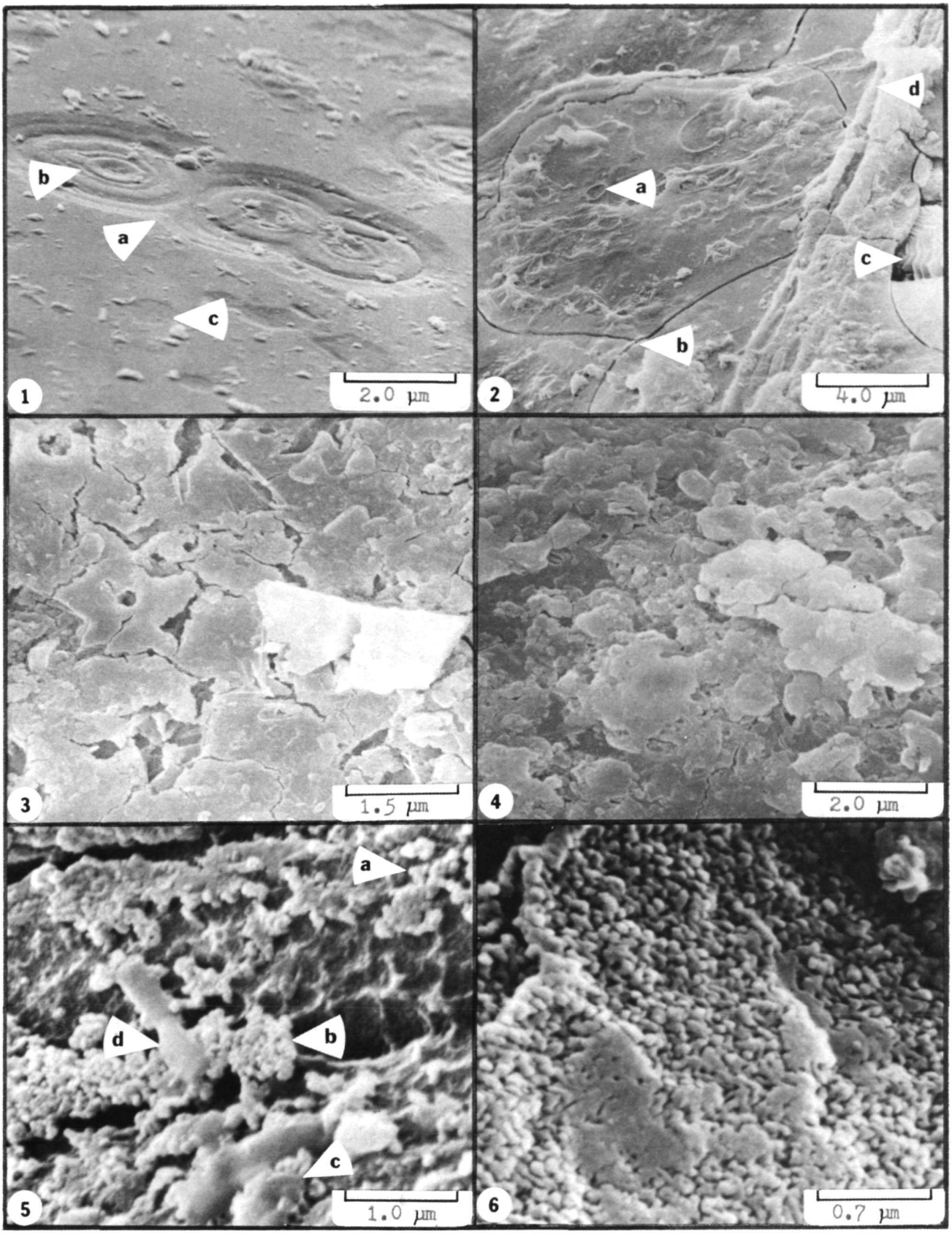
1
a
b
c
2.0 µm
2
a
b
c
d
4.0 µm
3
1.5 µm
4
2.0 µm
5
a
b
c
d
1.0 µm
6
0.7 µm

EXPLANATION OF PLATE 14.

OXIDE AND COMPOSITE ALTERATION SURFACES

Figure 1. Higher magnification view of ripple surface (Pl. 3, fig. 5) exhibiting ripples with small cracks (a) in troughs, whereas ripple crests have small oxide mounds (b) and in some cases mounds which have developed on top of cracks (c). Note glass flange, raised lip and radiating fractures that formed when vesicles burst at the surface. Mauna Ulu; (1969-73) sample 3,000X.

Figure 2. Particle surface with partial oxide film. Compare lower right portion of photo with ripple pattern at center of Figure 1. Oxide film has developed massive cap (a) on ripple crests and flange areas of vesicles (b). Note that the circular openings (c) disrupt both ripple pattern and oxide coating. Kilauea Iki; (1959-60) sample, 1,000X.

Figure 3. Intermediate magnification of Figure 2, exhibiting an oxide layer on ripple crests and troughs. Note compact character of crest (a) and blocky nature of film in trough (b). Kilauea Iki; (1959-60) sample, 6,000X.

Figure 4. High magnification of an oxide film exhibiting a scalelike mass at upper right (a) and "sponge" like expanded surface containing numerous small cracks and cavities (b). Note rounded mass (c) separated from material on ripple crest, whereas troughs contain blocky angular pedestals and deep valleys (d). Kilauea Iki; (1959-60) sample, 20,000X.

Figure 5. Composite surface exhibiting polygonal fractures and adjacent ridges composed of material enriched in Fe, K and S, whereas interridge areas are covered by oxide coating which has a similar composition to that of the underlying glass. Note later fluid splashes at upper left and photo center. Kilauea Iki; (1959-60) sample, 10,000X.

Figure 6. Lower magnification view exhibiting second oxide coating covering previously formed fractured and ridged surface (a). Note the formation of "dimples" or surface depressions where second film drapes over previously formed ridges (b). Spalled regions remove uppermost oxide layer exposing earlier formed surface (c). Kilauea Iki; (1959-60) sample, 3,000X.

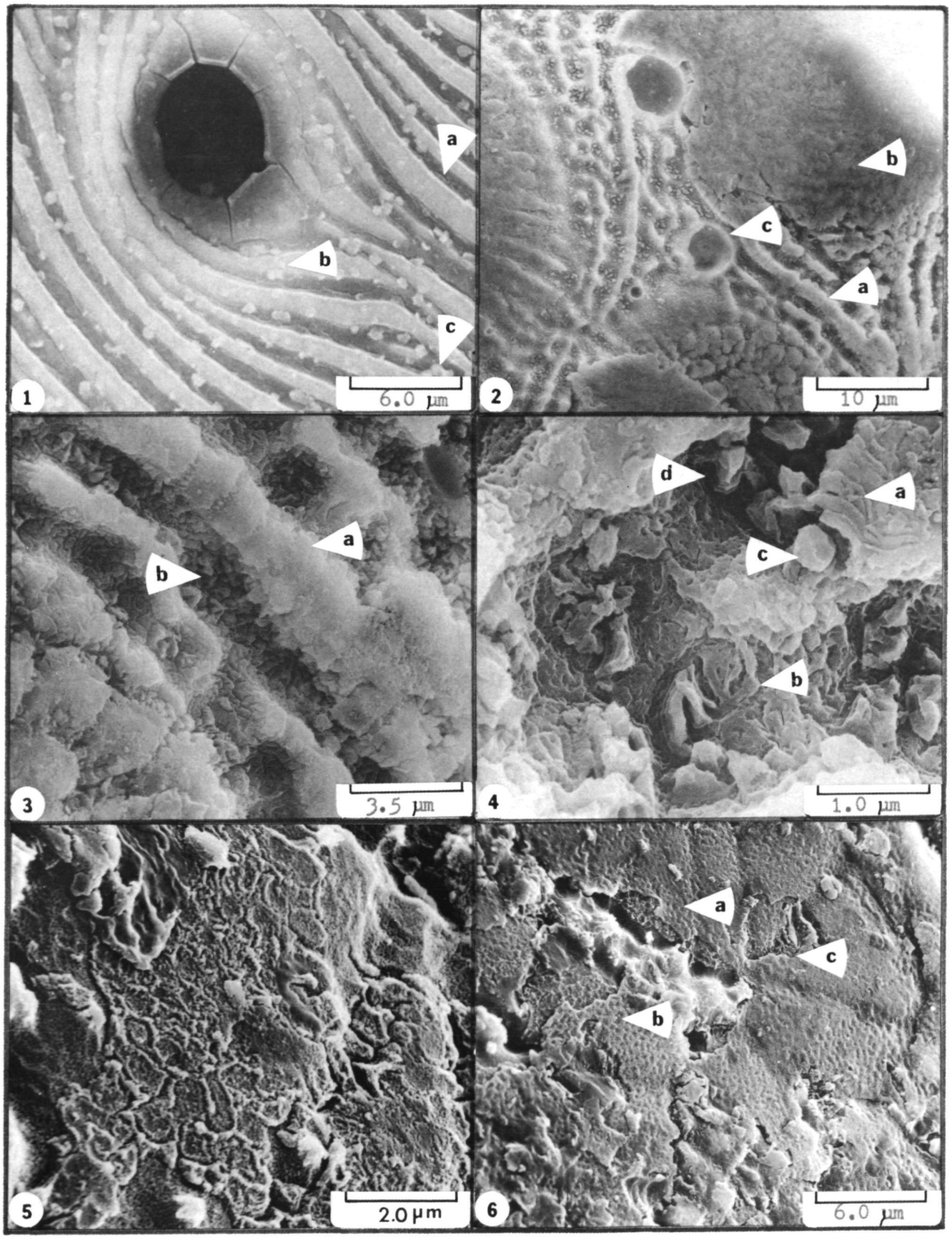
a
b
c
6.0 µm
1
b
c
a
10 µm
2
a
b
3.5 µm
3
d
a
c
b
1.0 µm
4
2.0 µm
5
a
c
b
6.0 µm
6

EXPLANATION OF PLATE 15.

CRYSTAL IMPRESSIONS, ENCRUSTATION REMNANTS

WRINKLES AND RIPPLES

Figure 1. Surficial encrustation remnants of previous crystals outlined by calcium sulfate. Outlines exhibit a monoclinic prismatic habit (a) and have tendency to develop as clusters rather than individuals. Note that several clusters (b) have calcium sulfate blebs as centers. Kilauea Iki; (1959-60) sample, 1,500X.

Figure 2. Crystal impressions outlined by small "spherules" of calcium sulfate or jarosite. Crystal outlines exhibit hexagonal characteristics or possible twinned monoclinic outlines. Note development of small micromound spheres (a) and platelets (b). Mauna Ulu; (1969-73) sample, 20,000X.

Figure 3. Glassy filament encrusted with calcium sulfate (a) with cavities (b) of previously formed minerals. Note debris accumulation on underlying surface. Kilauea Iki; (1959-60) sample, 1,600X.

Figure 4. Glassy surface exhibiting small needlelike impressions. Note surficial debris platelets and filaments cover some of the impressions (a). Note fine-grained micromounds (b) and calcium sulfate coated debris (c). Mauna Ulu; (1969-73) sample, 10,000X.

Figure 5. Glassy particle exhibiting wrinkles. Note that some areas are slightly deformed (a) as compared with intensely deformed areas (b). Circular vesicle (c) does not exhibit deformation when compared to adjacent areas. Kilauea; (July, 1974) sample, 700X.

Figure 6. Glassy particle showing surface ripples. Surface vesicles interrupt or obstruct the ripple pattern causing the ripples to accumulate or pileup around the vesicle (a). The remainder of the ripple refracts around the vesicle and becomes stretched and locally broken (b). Note surficial development of small alteration masses between and on ripple crests (c). Contrast ripple morphology and pattern with that of wrinkles in Figure 5. Mauna Ulu; (1969-73) sample, 1,500X.

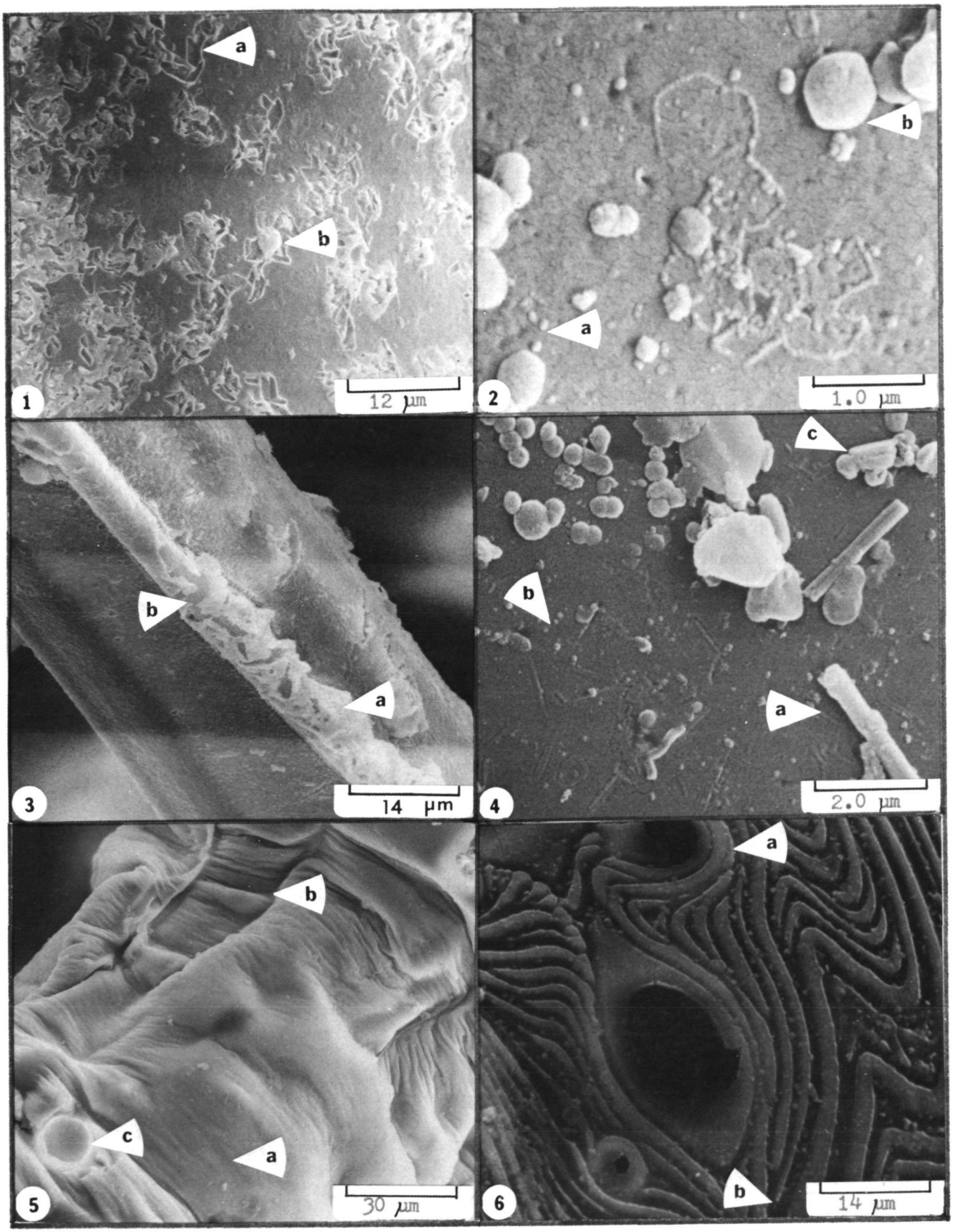
a
b
12 µm
1
b
a
1.0 µm
2
b
a
14 µm
3
c
b
a
2.0 µm
4
b
c
a
30 µm
5
a
b
14 µm
6

EXPLANATION OF PLATE 16.

PHOTOMICROGRAPHS OF THE

INTERNAL STRUCTURE OF GLASSY PARTICLES

Figure 1. Elongate sphere with euhedral olivine grain forming particle core. Note olivine cleavage {010} (a) and {100} (b). Glass coating has been disrupted by vesicle bursts near the surface (c). Some of the vesicles in the same region exhibit drag to the right. Several elongate vesicles form bulges in the glass coating (d). Kapoho; (1960) sample, 80X.

Figure 2. Small spherule composed of nearly all glass except for a few vesicles (a) and an olivine phenocryst (b). Note concentric fractures but lack of radial fractures. Kilauea; (Dec., 1974) sample, 125X.

Figure 3. Glassy sphere exhibiting vesicles, phenocrysts (a), radial fractures (b), and ripple pattern (c). Note paucity of phenocrysts. Surficial debris forms dark mounded surface on upper left of sphere. Dark circles are bubbles in the mounting medium. Kilauea Iki; (1959-60) sample, 40X.

Figure 4. Upper view illustrates twisted strands of glassy filament with elongate vesicles (a). Lower ribbed form exhibits numerous stretched vesicles (b). Kilauea; (Dec., 1974) sample, upper view 125X, lower view 30X.

Figure 5. Glassy filament exhibiting minimal stretching or vesicle elongation. Note spherical vesicle (a) and possible compression of filament end at right center. Particle contains few large fractures but numerous fine-scaled cracks (b). Kilauea (Dec., 1974) sample, 125X.

Figure 6. Composite sample consisting of glassy filament shaped like a wishbone and a rounded to irregular glassy particle containing numerous vesicles. Note the unstretched nature of the filament and spherical vesicles in both filament and glassy particle. Kapoho; (1960) sample, 50X.

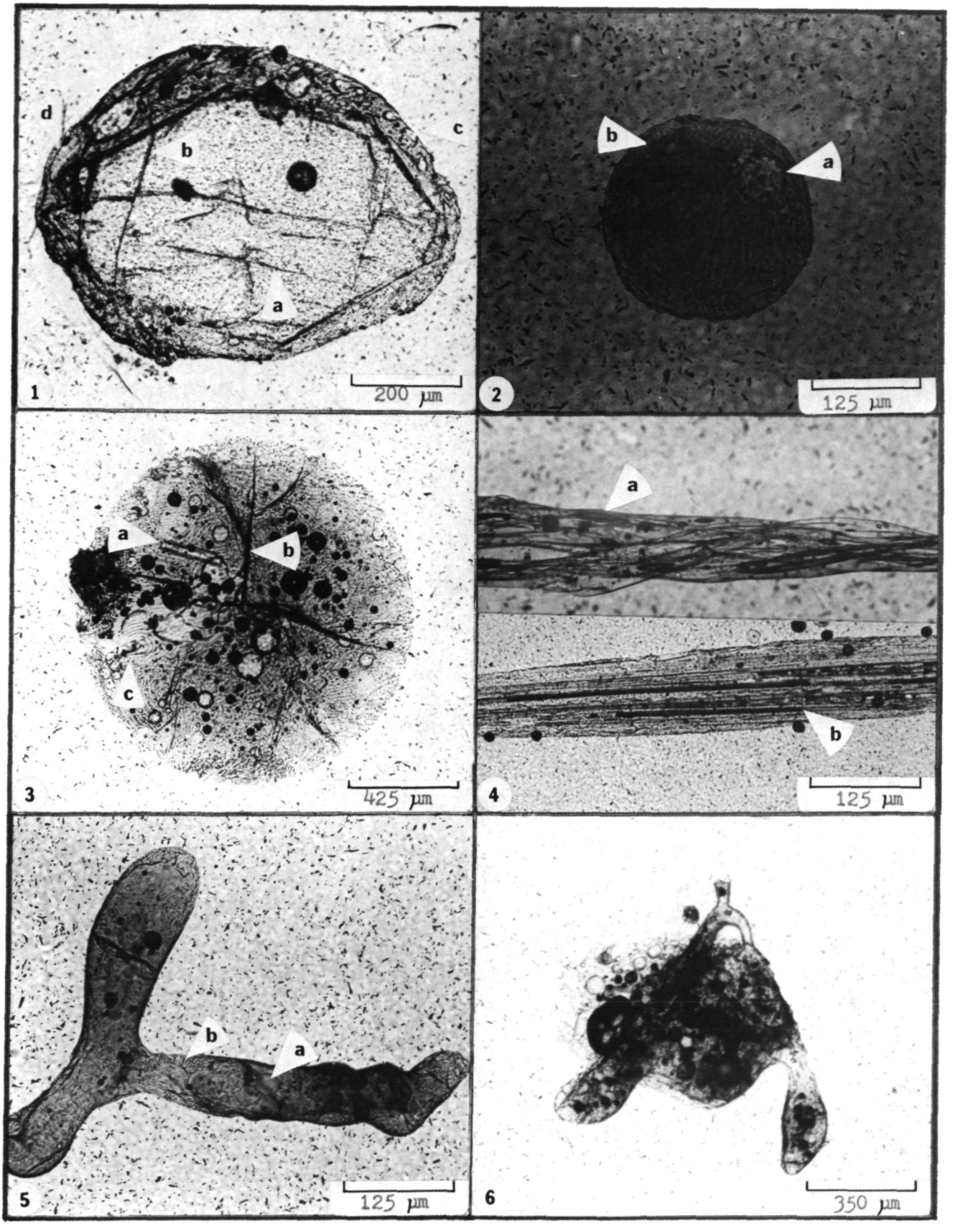
d
c
b
a
200 µm
1
b
a
125 µm
2
a
b
c
425 µm
3
a
b
125 µm
4
b
a
125 µm
5
350 µm
6

EXPLANATION OF PLATE 17.

TEXTURE OF GLASSY PARTICLES

Figure 1. Holohyaline particle consisting of glass with vesicles. Note presence of radial fractures and smaller concentric cracks near outer margins of particle. The particle does not exhibit evidence of twisting or surface rippling. Kilauea; (Dec., 1974) sample, 80X.

Figure 2. Hypocrystalline particle exhibiting aligned crystals. Note presence of radial fractures with local fracture oriented along the long axis of the particle (c). Note alignment of crystals at (a) and (b). Kilauea; (Dec., 1974) sample, 125X.

Figure 3. Intersertal particle with numerous olivine and clinopyroxene crystals. Note impingement of crystals into vesicles, whereas others are clumpled together (a). Mauna Ulu; (1969-73) sample, 320X.

Figure 4. Note radial cluster of several small olivine crystals (a) with smaller clump at (b). Kilauea Iki; (1959-60) sample, 320X.

Figure 5. Intersertal fabric with small vesicles. Crystals are predominantly olivine and augite. Mauna Ulu; (1969-73) sample, 320X.

Figure 6. Glassy particle with resorbed olivine and enclosed spinel grains (a). Note that fractures in the olivine do not continue into the glassy matrix suggesting fracture prior to particle formation. Kilauea Iki; (1959-60) sample, 80X.

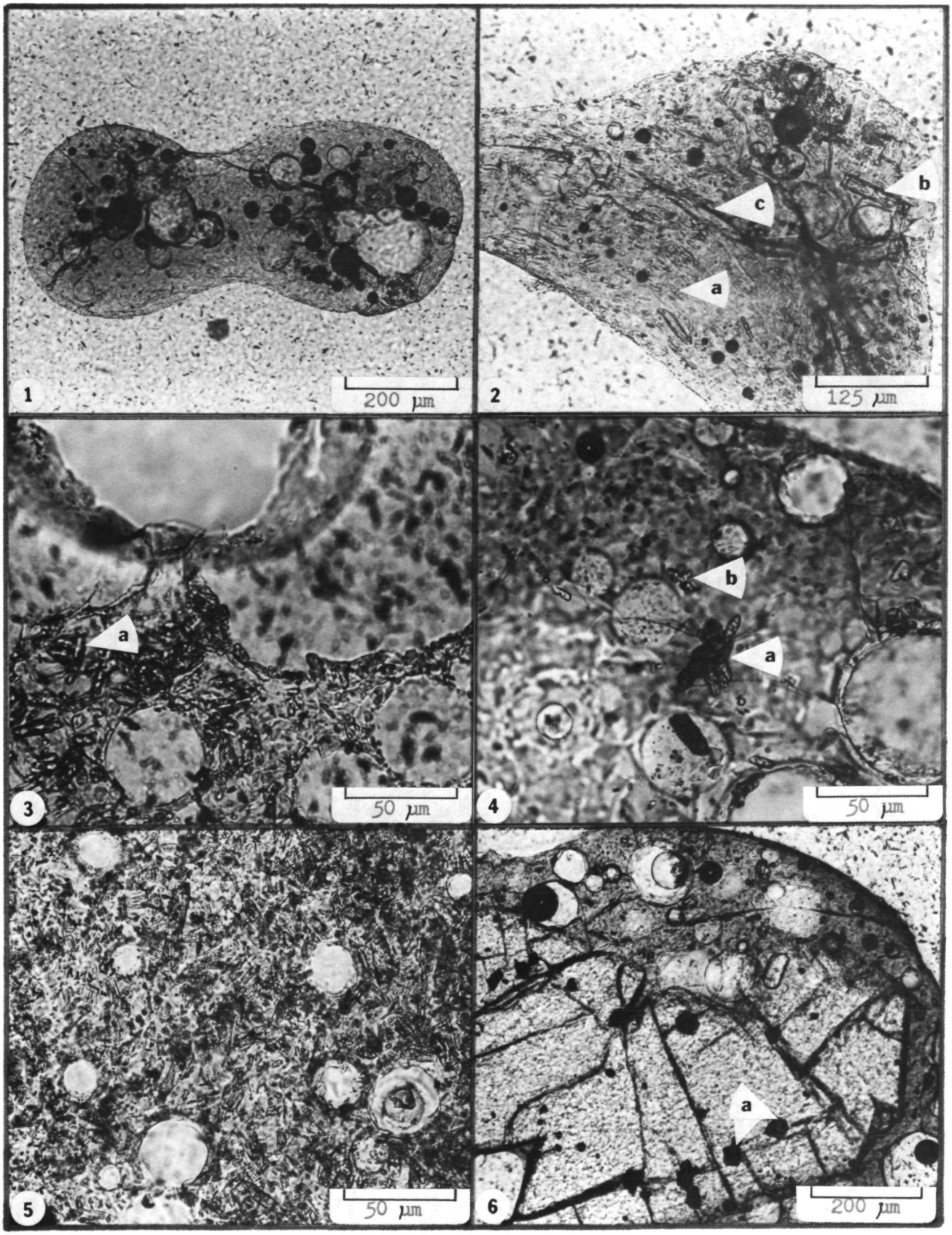
1
200 µm
2
a
b
c
125 µm
3
a
50 µm
4
a
b
50 µm
5
50 µm
6
a
200 µm

EXPLANATION OF PLATE 18.

PHOTOMICROGRAPH OF VESICLE SHAPE

AND FRACTURE TYPES

Figure 1. Elongate vesicles in glassy filament. Note lack of coalescence and formation of internal vesicle tubes. Kilauea Iki; (1959-60) sample, 260X.

Figure 2. Glassy particle exhibiting coalesced vesicles which form irregular larger bubbles. Note the lack of radial fractures. Kilauea Iki; (1959-60) sample, 30X.

Figure 3. Glassy particle containing several large subhedral olivines and large vesicles that are contained within the space between the crystals. Note shape modification and partial vesicle coalescence. Small euhedral spinel cluster at upper right. Kilauea Iki; (1959-60) sample, 80X.

Figure 4. Glassy particle with radial fractures that selectively break around vesicles within the glass matrix. Note development of ripple pattern of alternating light and dark layers and lack of crystals. Note fractures cut across ripples without displacement (a). Kilauea Iki; (1959-60) sample, 80X.

Figure 5. Close-up view of concentric cracks (a) and small fractures or cracks (b). Kilauea Iki; (1959-60) sample, 320X.

Figure 6. Longitudinal fracture oriented along major axis of particle. Many vesicles exhibit small polygonal cracks around their outer margins that are interconnected forming fracture polygons. Kilauea Iki; (1959-60) sample, 100X.

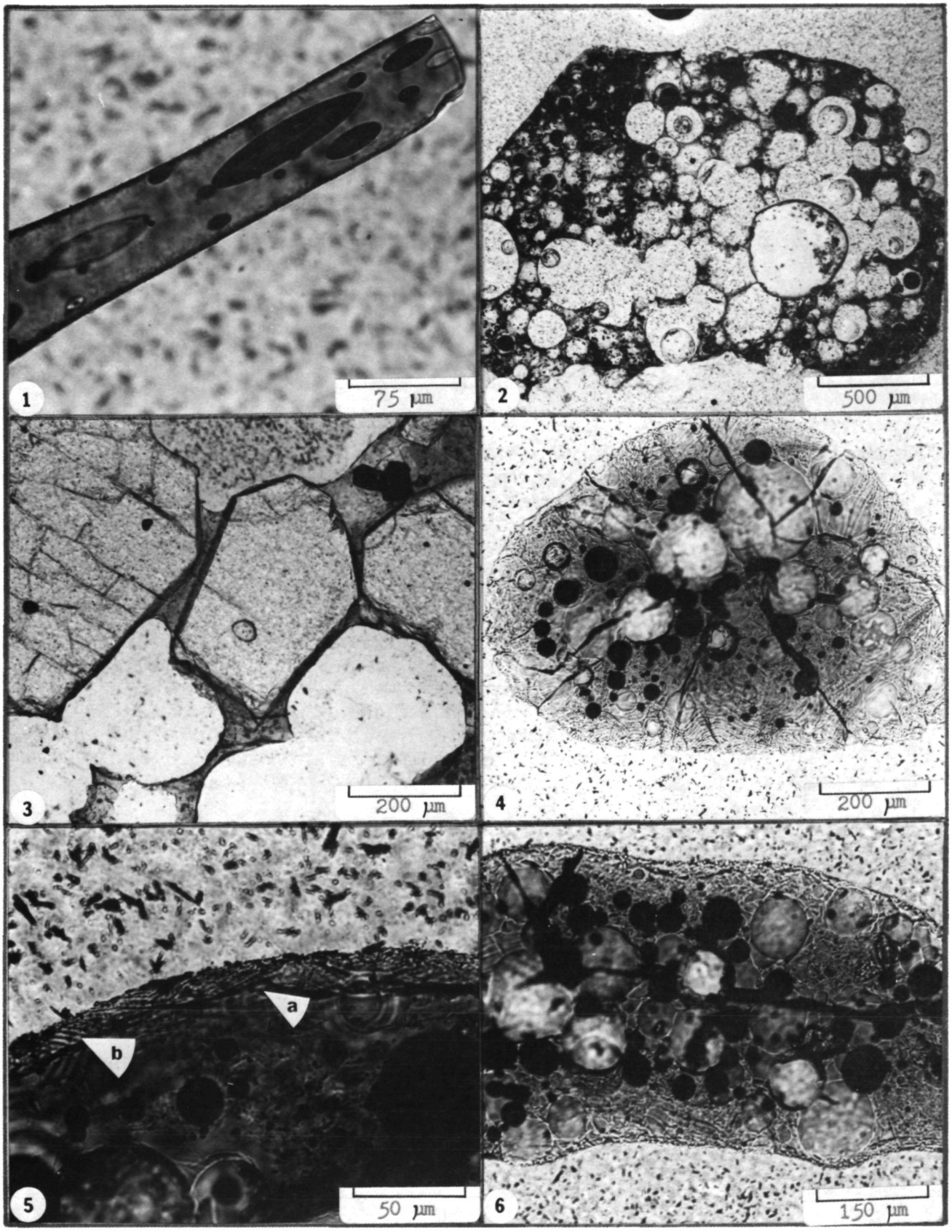
1
75 µm
2
500 µm
3
200 µm
4
200 µm
a
b
5
50 µm
6
150 µm

EXPLANATION OF PLATE 19.

PHOTOMICROGRAPHS OF PLAGIOCLASES, ORTHOPYROXENES AND VESICLES

Figure 1. Euhedral plagioclase (a) with rhombic-pinacoidal shape and negative relief. Note abundant crystals of olivine (b) pyroxene (c) and oval vesicle shape (d). Kapoho; (1960) sample, 320X.

Figure 2. Twinned (?) plagioclase (a) in glassy groundmass. Kapoho; (1960) sample, 320X.

Figure 3. Large elongate hypersthene (a) with basal partings (b). Note coalesced vesicles (c) and attached sphere (d). Note development of surface rind (e). Under polarized light the orthopyroxene exhibited compositional zonation. Kilauea Iki; (1959-60) sample, 125X.

Figure 4. Glassy particle with abundant vesicles that range in size from ~7Ø (8 μ) to -1.5Ø (~3000 μ) with major mode at +4.5Ø (~44 μ). Minor vesicle coalscence was observed. Note large subhedral olivine phenocrysts (a) and smaller euhedral olivines (b). Particle does not exhibit radial fractures. Kilauea Iki; (1959-60) sample, 30X.

Figure 5. Holohyaline particle with uniform vesicle size (~0.1 mm) and radial fractures. Kilauea Iki; (1959-60) sample, 125X.

Figure 6. Reticulite fragment exhibiting large vesicle size (1-2 mm) with thin triangular shaped glass strands connecting vesicles. Note the development of smaller vesicles within the connective glass strands. Conchoidal fracture is exhibited at cross sections of broken strands (a). Kilauea Iki; (1959-60) sample, 50X.

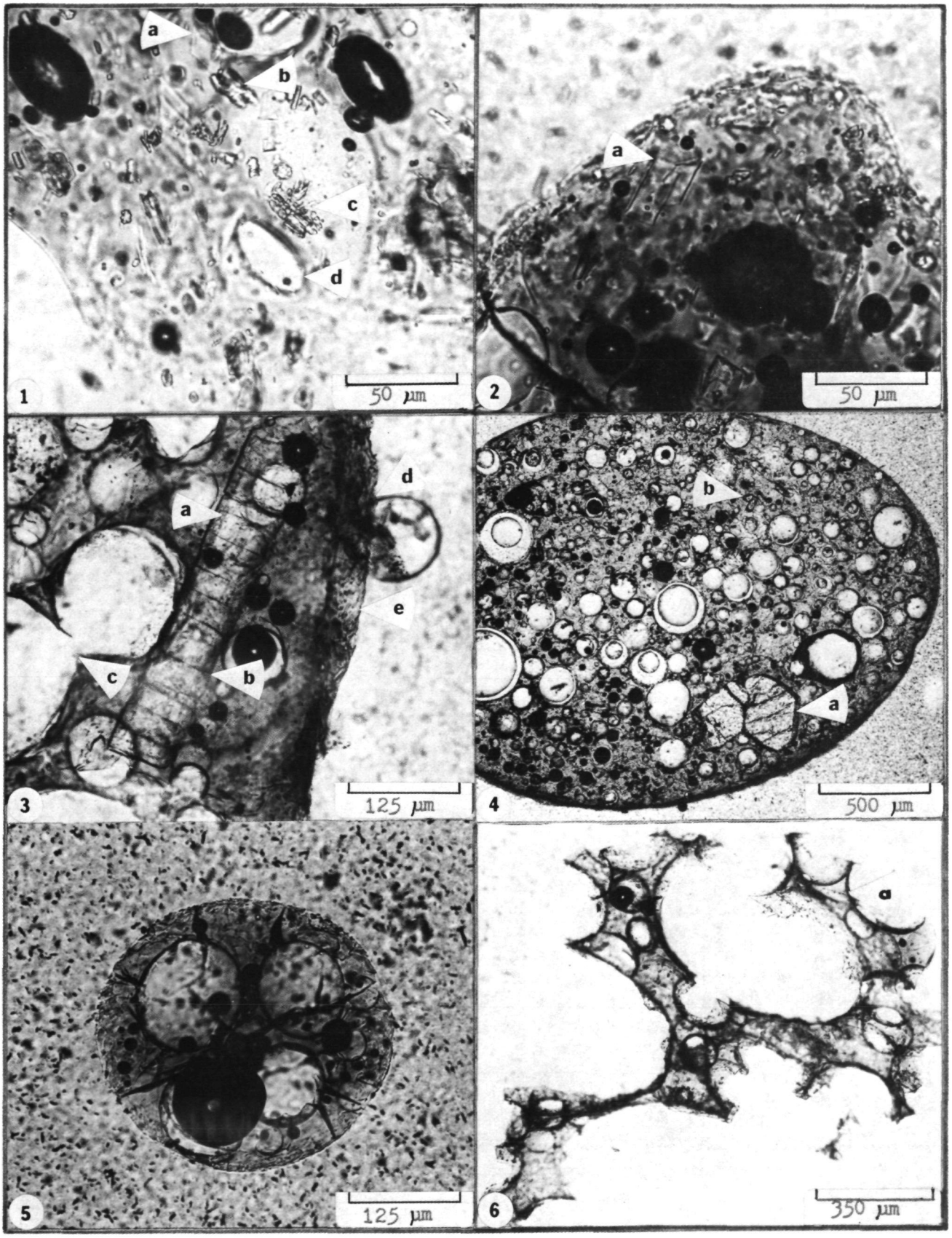
a
b
c
d
50 µm
1
a
50 µm
2
d
a
e
c
b
125 µm
3
b
a
500 µm
4
125 µm
5
a
350 µm
6

EXPLANATION OF PLATE 20.

PHOTOMICROGRAPHS OF OLIVINES

Figure 1. Large corroded olivine grains in vesiculated glass groundmass. Grains were fractured prior to glass solidification. Note size variation of vesicles and presence of a few smaller crystals Kilauea Iki; (1959-60) sample, 80X.

Figure 2. Large olivine exhibiting several liquid inclusions or embayments. Note fractured vesicular surfaces at upper left and lower right. Kilauea Iki; (1959-60) sample, 80X.

Figure 3. Large glass coated euhedral olivine grain with prominent cleavage. Note development of {110} faces and growth of {100} and {010} faces. Several anhedral spinel grains are enclosed within the grain. Note that a thin glass coating still encloses the grain even though the highly vesiculated. Kilauea Iki; (1959-60) sample, 40X.

Figure 4. Olivine phenocryst that exhibits both cleavage as well as a fracture that breaks both glass and mineral (a). Note more equant shape of grain along the {010} and {001} faces. Numerous crystals of clinopyroxene (b) and an isolated plagioclase (c) are contained in a moderately vesiculated glass matrix. Kapoho; (1960) sample, 200X.

Figure 5. Clusters of small euhedral olivines next to edge (lower right) of corroded earlier formed large olivine phenocryst. Note small liquid inclusions (a) and enclosed spinel grain (b). Glass matrix has numerous small fractures. Kilauea Iki; (1959-60) sample, 320X.

Figure 6. Skeletal euhedral olivine exhibiting prominant {110} faces and liquid inclusions parallel to the {110} face. Kilauea Iki; (1959-60) sample, 320X.

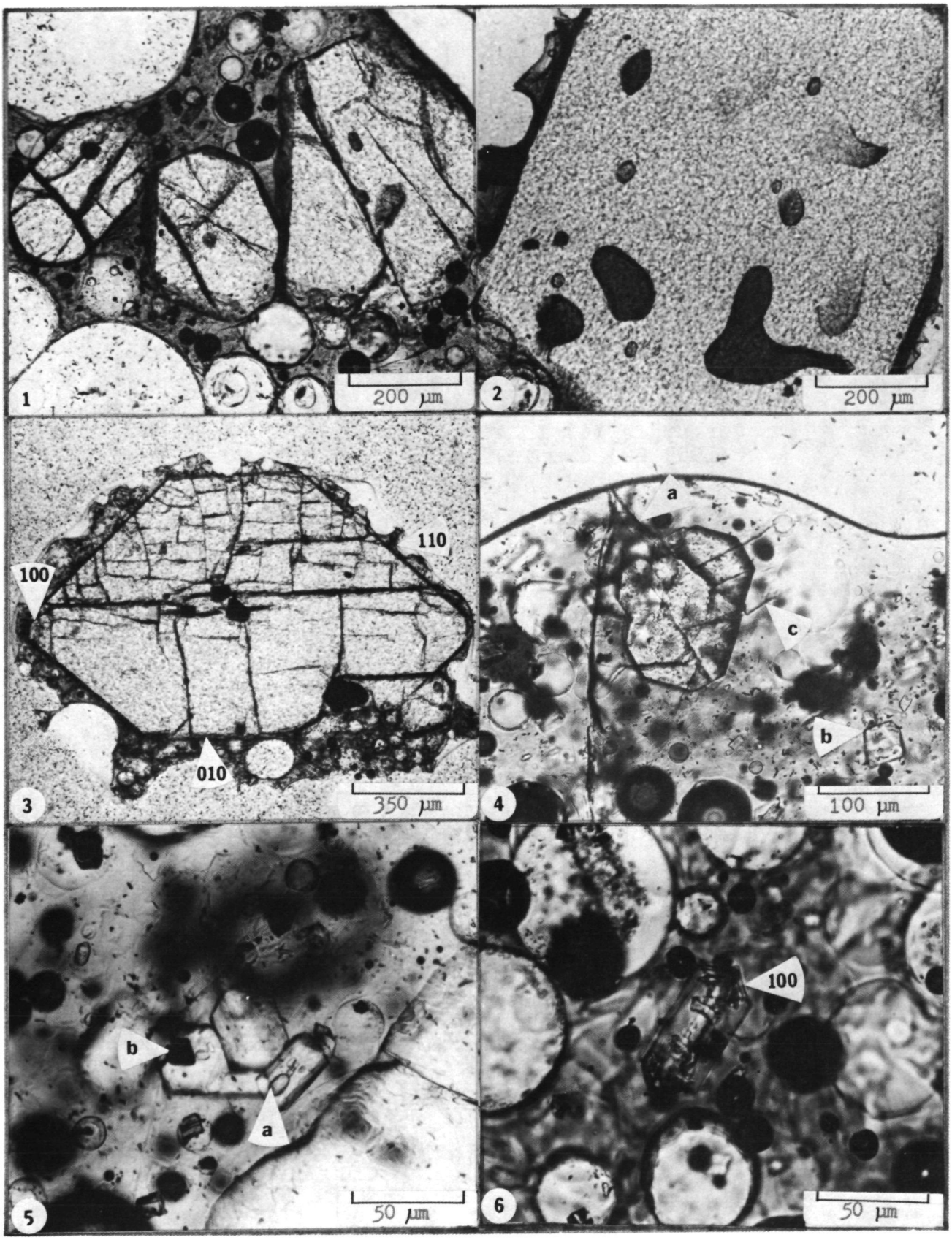
1
200 μm
2
200 μm
100
110
010
3
350 μm
a
c
b
4
100 μm
b
a
5
50 μm
100
6
50 μm

EXPLANATION OF PLATE 21.

PHOTOMICROGRAPHS OF SPINELS AND

CLINOPYROXENES

Figure 1. Euhedral spinels (a) with well developed cubic habit. Note smaller cluster (b) in moderately vesiculated glass. Note olivine crystals associated with spinel clusters (c) and (d). Kilauea Iki; (1959-60) sample, 125X.

Figure 2. Euhedral olivine crystal with enclosed spinel grains (a). Note numerous clusters of pyroxene crystals (b) in glassy matrix. Kilauea Iki; (1959-60) sample, 200X.

Figure 3. Corroded pyroxene crystal containing numerous liquid and mineral inclusions. Note glassy coating, smaller crystals and vesicles. Kapoho; (1960) sample, 80X.

Figure 4. Euhedral skeletal crystal of clinopyroxene with well developed hourglass inclusions. Kilauea Iki; (1959-60) sample, 125X.

Figure 5. Radiating cluster of skeletal pyroxenes with liquid inclusions forming partial hourglass structures. Kilauea Iki; (1959-60) sample, 320X.

Figure 6. Skeletal clinopyroxenes exhibiting partial development of "H" structure (a). Note abundance of small crystals and smaller beaded crystallites (b). Note the occurrence of fractures around vesicles and in glass matrix. Olivines at (c) exhibits non-tabular habit, whereas most pyroxene crystals show rectangular to rhombic shapes. Kilauea Iki; (1959-60) sample, 320X.

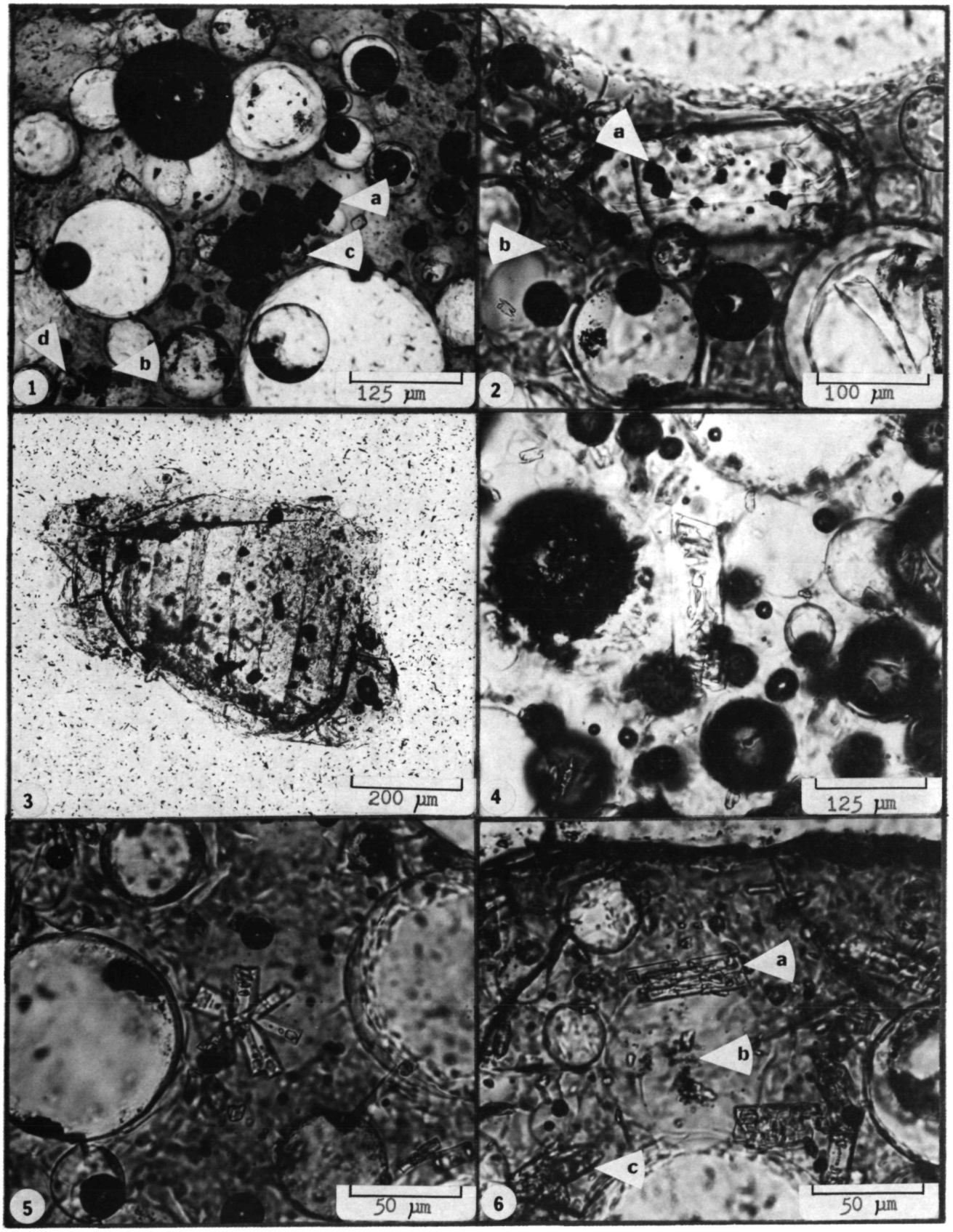
a
c
d
b
1
125 µm
a
b
2
100 µm
3
200 µm
4
125 µm
5
50 µm
a
b
c
6
50 µm

EXPLANATION OF PLATE 22.

PHOTOMICROGRAPHS OF FRACTURE TYPES, RIPPLES AND POSSIBLE DEVITRIFICATION TEXTURE

Figure 1. Glassy particle exhibiting internal polygonal fractures that break around vesicles. Note presence of attached irregular shaped debris on particle surface and dark rim of particle. Kilauea Iki; (1959-60) sample, 80X.

Figure 2. Glassy particle exhibiting fractures with later glass filling (a). Note unusual fracture pattern and presence of possible devitrification crystallites (b). Kapoho; (1960) sample, 320X.

Figure 3. Holohyaline particle with minor vesicles and extensive ripples. Note that ripples bend around spherical vesicles (a). Possible small spinel crystal (b). Kilauea Iki; (1959-60) sample, 100X.

Figure 4. Higher magnification of ripple surface. Note development of concentric fracture along ripple pattern (a). Kilauea Iki; (1959-60) sample, 200X.

Figure 5. Surface rind consisting of concentric and tensional (?) fractures. Note presence of attached spheres, one of which contains several small pyroxenes. Kilauea Iki; (1959-60) sample, 50X.

Figure 6. Possible "devitrification" texture of microcrystalline pyroxene (?) intergrowths. Note difference in internal character between portions of sphere. Kilauea Iki; (1959-60) sample, 80X.

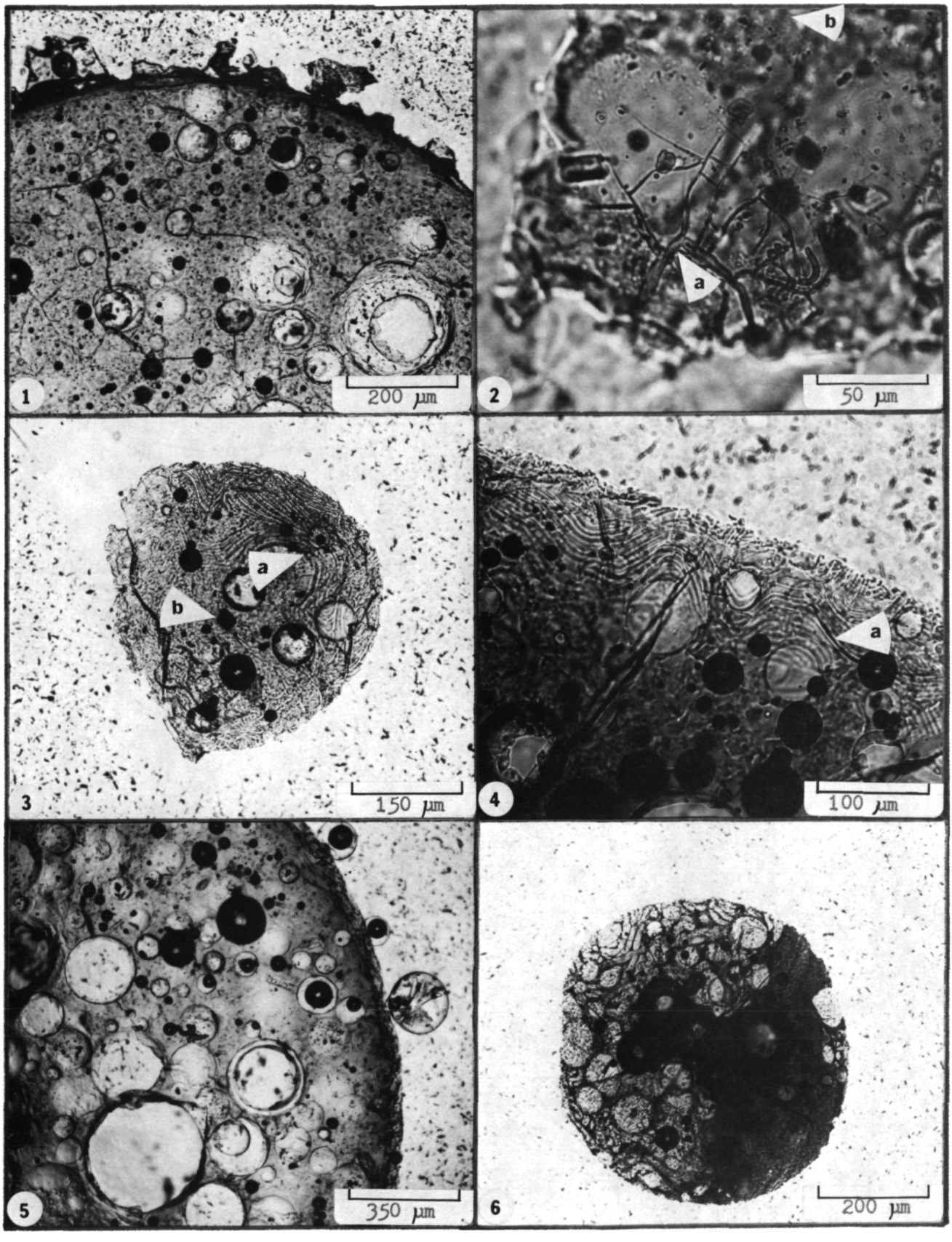
1
200 µm
2
b
a
50 µm
3
a
b
150 µm
4
a
100 µm
5
350 µm
6
200 µm

EXPLANATION OF PLATE 23.

PHOTOMICROGRAPH OF DEVITRIFICATION TEXTURE AND SEM VIEW OF DROPLET STRING AND HYDRATED ANHYDRITE (?) CRYSTAL

Figure 1. Enlarged view of Pl. 22, fig. 6 illustrating devitrification (?) texture of microcrystalline pyroxene (?) intergrowths (right 1/2). Left portion of sphere contains abundant round vesicles plus several flattened and deformed vesicles at upper left. Kilauea Iki; (1959-60) sample, 160X.

Figure 2. SEM view of glassy surface exhibiting a string of fluid particle splashes that appear to have been connected or were formed from the same filament which separated into droplets just prior to particle impact. Kilauea Iki; (1959-60) sample, 5,000X.

Figure 3. SEM view of calcium sulfate crystal that illustrates external expansion. This crystal may have been initially anhydrite which later has hydrated to gypsum. Mauna Ulu; (1969-73) sample, 5,000X.

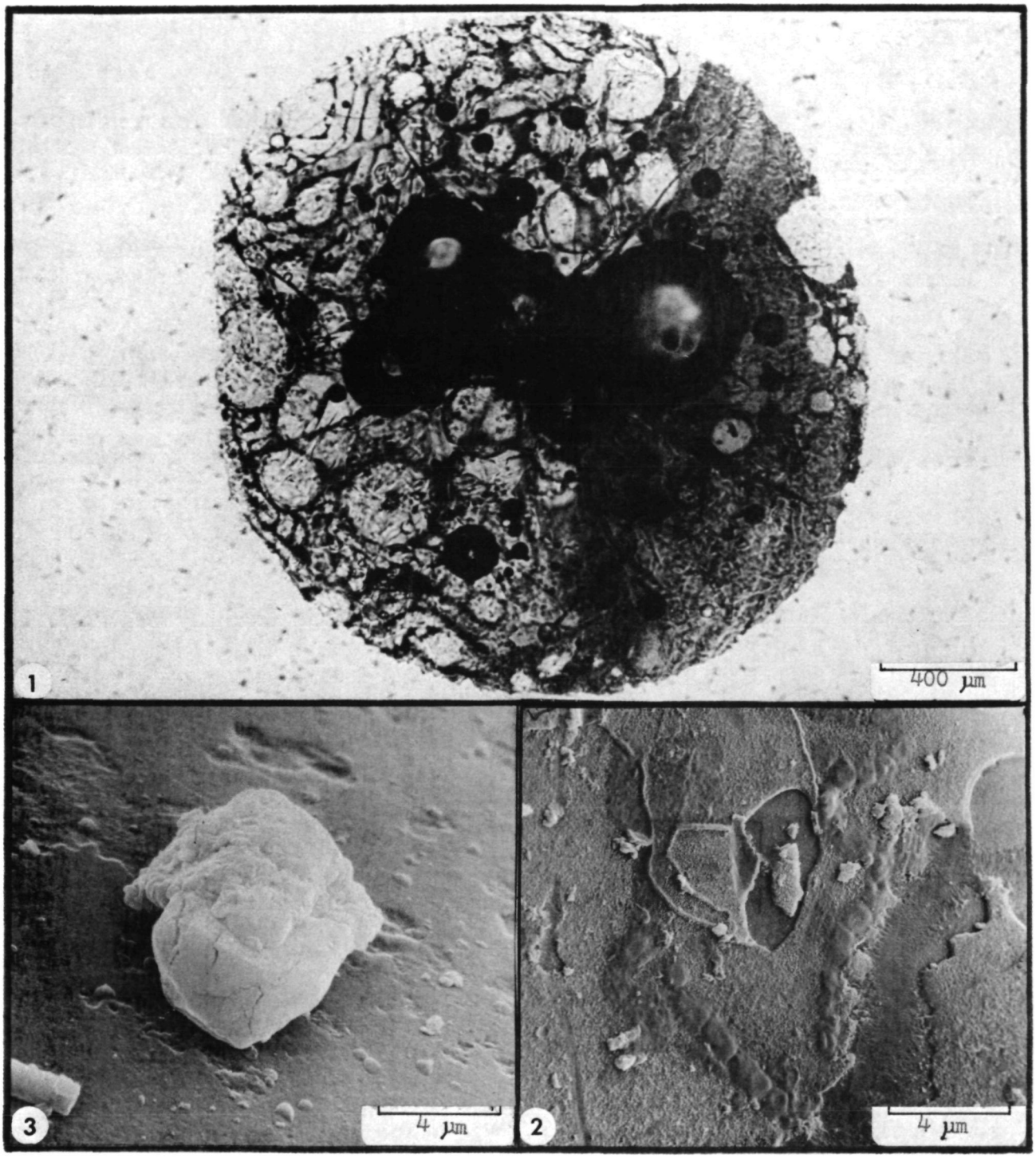
1
400 µm
3
4 µm
2
4 µm

REFERENCES CITED

Agrell, S.O., Agrell, J.E., and Arnold, A.R., 1973, Observations on glass from 15425, 15426, and 15427 (Abst.): In Lunar Science IV, (editor, J. Chamberlain and C. Watkins), Lunar Science Institute, Houston, Texas, p. 12-14.

Akhtar, S., and Cable, M., 1968, Some Effects of atmosphere and minor constituents on the surface tension of glass melts: Glass Techn., v. 9, p. 145-151.

American Society for Testing and Materials, 1965, Standard definations of terms relating to glass products: ASTM C162-56, Pt. 13, p. 145-159.

Barnes, H.L., 1967, Geochemistry of hydrothermal ore deposits: Holt, Rinehart and Winston, New York, 663 p.

Bikerman, J.J., 1958, Surface chemistry, 2nd Edition, Academic Press Inc., New York, 501 p.

Cadle, R.D., and Frank, E.R., 1968, Particles in the fume from the 1967 Kilauea Eruption: J. Geophys. Res., v. 73, p. 4780 4783.

_____, Lazrus, A.L., and Shedlovsky, J.P., 1969, Comparison of particles in the fume from eruptions of Kilauea, Mayon, and Arenal Volcanoes: J. Geophys. Res., v. 74, p. 3372-3378.

_____, Wartburg, A. F., and Grahek, F.E., 1971, The proportion of sulfate to sulfur dioxide in Kilauea Volcano fume: Geochim. et Cosmochim. Acta, v. 35, p. 503-507.

Cameron, N.M., 1968, Glass strength with microscopic dirt bonded to the surface: Glass Techn., v. 9, p. 121.

Carmichael, I.S.E., Turner, F.J., and Verhoogen, J., 1974, Igneous Petrology: McGraw-Hill Book Co., 739 p.

Carter, J.L., 1971, Chemistry and surface morphology of fragments from Apollo 12 soil: Proc. 2nd Lunar Sci. Conf., (Suppl. 2, Geochim. et Cosmochim. Acta), v. 1, p. 873-892.

_____, Padovani, E., and Taylor, H.C., 1973, Morphology and chemistry of particles from Apollo 17 soils 74220, 74241, and 74081 (Abst.): EOS, Trans. Amer. Geophys. Union, v. 54, p. 582-584.

Carusi, A., Cavarretta, G., Cinotti, F., Civitelli, G., Coradini, A., Fukhiquoni, M., Funiciello, R., Taddeucci, A., and Trigila, R., 1972, The source area of Apollo 15 green glass (Abst.): In the Apollo 15 lunar samples, (editor, J. Chamberlain and C. Watkins), p. 5-9.

Chao, E.C.T., 1967, Shock effects in certain rock-forming minerals: Science, v. 156, p. 192-202.

_____, 1973, Apollo 14 glasses of impact origin and their parent rock types: Proc. 3rd Lunar Sci. Conf., (Suppl. 3, Geochim. et Cosmochim. Acta), v. 1. p. 907-925.

Charles, R.J., 1958, Corrosion of soda-lime glass in steam at different temperatures: Jour. Appl. Phys. v. 11, p. 1547.

Chouet, B. A., 1973, Photoballistic analysis of volcanic jet dynamics at Stromboli, Italy: unpub. masters thesis, Massachusetts Institute of Technology, 65 p.

Christiansen, R.L., and Lipman, P.W., 1966, Emplacement and thermal history of a rhyolite lava flow near Forty-mile Canyon, Southern Nevada: Geol. Soc. Amer. Bull., v. 77, p. 671-684.

Clanton, U.S., and Ladle, G.H., 1975, Polyvinyl Acetate-Methyl Alcohol solution as a scanning electron microscope particle mounting medium: Amer. Mineral., v. 60, p. 327.

Coleman, S.M., 1976, Weathering rinds as Quaternary Age-dating technique, Western United States: Prog. Abst. Ann. Mtg., Geol. Soc. Amer., p. 818.

Daly, R.A., 1911, The nature of volcanic action: Amer. Acad. Arts. Sci. Proc., v. 47, p. 47-122.

Duffield. W.A., Gibson, E.K., and Heiken, G.H., 1977, Some characteristics of Pele's Hair: Jour. Res., U.S. Geol. Surv., v. 5, p. 93-101.

Eaton, J.P., and Murata, K.J., 1960, How volcanoes grow; Science, v. 132, p. 925-938.

Fisher, R.V., 1961, Proposed classification of volcaniclastic sediments and rocks: Geol. Soc. Amer. Bull., v. 72, p. 1409-1414.

Fontana, M.G., and Greene, N.D., 1967, Corrosion engineering: 1st edition, McGraw-Hill Book Co., New York, 391 p.

Fontana, M.G., and Staehle, R.W., 1976, Advances in corrosion science and technology: v. 4, Plenum Press, New York, 398 p.

Friedman, I., and Irwin, T., 1967, Water and deuterium in pumice from 1959-60 eruption of Kilauea Volcano, Hawaii: U.S. Geol. Surv. Prof. Paper 575-B, p. 120-127.

Furnes, H., 1974, Volume relations between palagonite and authigenic minerals in hyaloclastics and its bearing on the rate of palagonitization: Bull. Volcan., v. 38, p. 173-186.

Heald, E.F., Naughton, J.J., and Barnes, I.L., Jr., 1963, The chemistry of volcanic gases: 2. Use of equilibrium calculations in the interpretation of volcanic gas samples: J. Geophys. Res., v. 68, p. 545-557.

Heiken, G.H., and Lofgren, G., 1971, Terrestrial glass spheres: Geol. Soc. Amer. Bull. v. 82, p. 1045-1050.

_____, 1972, Morphology and petrography of volcanic ashes: Geol. Soc. Amer. Bull., v. 83, p. 1961-1988.

_____, McKay, D.S., and Brown, R.W., 1974, Lunar deposits of possible pyroclastic origin: Proc. 4th Lunar Sci. Conf., (Geochim. et Cosmochim. Acta), v. 1, p. 1703-1718.

_____, 1974, An atlas of volcanic ash; Smithsonian Inst. Publs. in Earth Sciences, no. 12, 101 p.

Hobbs, P.V., Radke, L.F., and Smith, J.L., 1977, Eruption of the St. Augustine Volcano; Airborne measurements and observations: Science, v. 195, p. 871-873.

Hodge, P.W., and Wright, F.W., 1964, Studies of particles for extraterrestrial origin, 2; A comparison of microscopic spherules of meteorite and volcanic origin: J. Geophys. Res., v. 69, p. 2449-2454.

Holland, L., 1964, The properties of glass surfaces: John Wiley & Sons, Inc., New York, 546 p.

Isard, J.O., 1971, The formation of spherical glass particles on the lunar surface: Proc. 2nd Lunar Sci. Conf., (Suppl. 2, Geochim. et Cosmochim. Acta), v. 3, p. 2003-2008.

Jaggar, T.A., 1917, Volcanological investigations at Kilauea: Amer. J. Sci., 4th Ser., v. 44, p. 161-220.

Jones, G.O., 1971, Glass: 2nd Edition, Northumberland Press Ltd., Gateshead, Great Britian, 124 p.

Kimoto, S., and Russ, J.C., 1969, The characteristics and applications of the scanning electron microscope: Amer. Sci. v. 57, p. 112-113.

Kingery, W.D., Bowen, H.K., and Uhlman, D.R., 1976, Introduction to ceramics: John Wiley & Sons, Inc., New York, 1031 p.

Kofstad, P., 1966, High temperature oxidation of metals: John Wiley & Sons, Inc., New York, 340 p.

Kostov, I., 1968, Mineralogy: Oliver and Boyd, London, 573 p.

Krauskopf, K.B., 1967, Introduction to geochemistry: McGraw-Hill Book Co., New York, 721 p.

Krumbein, W.C., and Petijohn, F.J., 1938, Manual of sedimentary petrography: Appleton-Century-Crofts, 549 p.

Kulp, J.P., and Adler, H.H., 1950, Thermal study of jarosite: Amer. J. Sci., v. 248, p. 475.

Ladle, G.H., and McKay, D.S., 1973, The use of millipore filters in the preparation of scanning electron microscope mounts of particles less than 20 micrometers: Amer. Mineral., v. 58, p. 1982-1083.

Larsen, G., and Chilingar, G.V., 1967, Diagenesis in sediments: Elsevier Publishing Co., New York. 551 p.

Levich, V.G., 1962, Physical hydrodyamics: Prentice-Hall, New York, 305 p.

Lofgren, G., 1974, An experimental study of plagioclase crystal morphology: Amer. J. Sci., v. 274, p. 243-274.

Lucchitta, B.K., 1973, Photogeology of the dark material in the Taurus-Littrow region of the Moon: Proc. 4th Lunar Sci. Conf., (Suppl. 4, Geochim. et Cosmochim. Acta), v. 1, p. 149-162.

Lunar Sample Preliminary Team, 1969, Preliminary examination of lunar samples from Apollo 11: Science, v. 167, p. 1211-1227.

_____, 1970, Preliminary examination of Lunar samples from Apollo 12: Science, v. 167, p. 1325-1339.

Macdonald, G.A., 1972, Volcanoes: Prentice-Hall, Inc., New Jersey, 510 p.

_____, G.A., and Eaton, J.P., 1955, the 1955 eruption of Kilauea Volcano, Volcano Letter, No. 529-530, p. 10.

Margolis, S.V., Barness, V.E., Cloud, P., and Fisher, R.V., 1971, Surface micrography of lunar fines compared with tektites and terrestrial volcanic analogs: Proc. 2nd Lunar Sci. Conf., (Suppl. 2, Geochim. et Cosmochim. Acta), v. 1, p. 909-921.

Marshall, W.R., 1954, Atomization and spraying: Am. Inst. Chem. Engr., New York, 294 p.

McBirney, A.R., and Murase, T., 1971, Factors governing the formation of pyroclastic rocks: Bull. Volcan. v. 34, p. 372-384.

McClaine, L.A., Allen, R.V., and McConnell, R.K., Jr., 1968, Volcanic smoke clouds: J. Geophys. Res., v. 73, p. 5235-5246.

McGetchin, T.R., and Head, J.W., 1973, Lunar cinder cones: Science, v. 180, p. 68-70.

McKay, D.S., 1970, Microcraters in lunar samples: Proc. 28th Ann. Mtg. Elect. Soc. Amer. (editor, C.J. Arceneaux), p. 22-23, Claitor's.

_____, Morrison, D.A., Lindsey, J. and Ladle, G.H., 1971, Apollo 12 soil and breccia: 2nd Lunar Sci. Conf., (Unpublished Proceedings).

_____, Clanton, U.S., Morrison, D.A., Ladle, G.H., 1972, Vapor phase crystallization in Apollo 14 breccia: Proc. 3rd Lunar Sci. Conf., (Suppl. 3, Geochim. et Cosmochim. Acta), v. 1, p. 739-752.

_____, Heiken, G.H., Taylor, R.M., Clanton, J.S., Morrison, D.H., and Ladle, G.H., 1972, Apollo 14 Soils; Size distribution and particle types: Proc. 3rd Lunar Sci. Conf., (Suppl. 3, Geochim. et Cosmochim. Acta), v. 1, p. 983-994.

_____, Clanton, U.S., and Ladle, G.H., 1973, Scanning electron microscope study of Apollo 15 green glass: Proc. 4th Lunar Sci. Conf. (Suppl. 4, Geochim. et Cosmochim, Acta), v. 1, p. 225-238.

_____, and Heiken, G.H., 1973, Petrography and scanning electron microscope study of Apollo 17 orange and black glass: Trans. Amer. Geophys. Union, v. 54, p. 599-600.

Morey, G.W., 1954, The properties of glass: 2nd Edition, Reinhold Publ. Corp., New York, 591 p.

Muenow, D.W., 1973, High temperature mass spectrometirc gas release studies of Hawaiian volcanic glass-pele's tears: Geochim. et Cosmochim. Acta, v. 37, p. 1551-1561.

Murata, K.J., 1966, Chemical analysis of a steam condensate from the pumice cone of Kilauea Iki, 1959-60: U.S. Geol. Surv. Prof. Paper, 537-C, p. 1-6.

_____, and Richter, D.H., 1966, The settling of olivine in Kilanean magma as shown by lavas of the 1959 eruption: Amer. J. Sci., v. 264, p. 194-203.

Naboko, S.I., 1959, Volcanic exhalations and products of their reactions as exemplified by Kamchatka-Kuriles volcanoes: Bull. Volcan., v. 20, p. 121-154.

Naughton, J.J., Lewis, V.A., Hammond, D., and Nishimoto, D., 1974, The chemistry of sublimates collected directly from lava fountains at Kilauea Volcano, Hawaii: Geochim. et Cosmochim. Acta, v. 38, p. 1679-1690.

_____, Hammond, D.A., Margolis, S.V., and Meunou, D.W., 1972, The nature and effect of the volatile cloud produced by volcanic and impact events on the moon as derived from a terrestrial volcanic model: Proc. 3rd Lunar Sci. Conf., (Suppl. 3, Geochim. et Cosmochim. Acta), v. 2, p. 2015-2024.

Nordlie, B.E., 1971, The composition of the magmatic gas of Kilauea and its behavior in the near surface environment: Amer. J. Sci., v. 271, p. 417-463.

Perret, F.A., 1950, Volcanological observations: Carnegie Institution of Washington, 152 p.

Reid, A.M., Lofgren, G.E., Heiken, G.H., Brown, R.B., and Moreland, G., 1973, Apollo 17 orange glass, Apollo 15 green glass and Hawaiian lava fountain glass: Trans. Amer. Geophys. Union, v. 54, p. 606-607.

Richter, D.H., and Moore, J.G., 1966, Petrology of Kilauea Iki lava lakes, Hawaii: U.S. Geol. Surv. Prof. Paper, 537-B, p. 1-26.

Richter, D.H., and Murata, K.J., 1966, Petrography of the lavas of the 1959-60 eruption of Kilauea Volcano, Hawaii: U.S. Geol. Surv. Prof. Paper, 537-D, p. 1-12.

Schaber, G.G., 1973, Lava flows in Mare Imbrium; geologic evaluation from Apollo orbital photography: Lunar Science IV, (ed. Chamberlain and Watkins), Lunar Science Institute, Houston, Texas, p. 653-654.

Schmitt, H.H., Trask, N.J., and Shoemaker, E.M., 1967, Geologic map of the Copernicus Quardrangle of the Moon: U.S. Geol. Surv. Misc. Geol. Inventory Map., I-515.

Sendt, A., 1962, Advances in glass technology: Plenum Press Inc., New York, 307 p.

Shaw, H.R., Peck, D.L., Wright, T.L., and Okamura, R., 1968, The viscosity of basaltic magma; An analysis of field measurements in Makaopuhi lava lake, Hawaii: Amer. J. Sci., v. 266, p. 225-264.

_____, 1969, Rheology of basalt in the melting range: J. Petro., v. 10, p. 510-535.

_____, 1972, Viscosities of magmatic silicate liquids; An empirical method of prediction: Amer. J. Sci., v. 272, p. 870-893.

Smith, R.L., 1960, Ash flows: Bull. Geol. Soc. Amer., v. 71, p. 795-842.

Stoiber, R.E., and Rose, W.E., 1970, The geochemistry of Central American volcanic gas condensates: Bull. Geol. Soc. Amer., v. 81, p. 2891-2912.

_____, and Rose, W.E., 1974, Fumarole encrustations at active Central American volcanoes: Geochim. et Cosmochim. Acta, v. 35, p. 495-516.

Swanson, D.A., Jackson, D.B., Duffiedl, W.A., and Peterson, D.W., 1971, Mauna Ulu eruption, Kilauea Volcano: Geotimes v. 16, p. 12-16.

_____, and Fabbi, B.P., 1973, Loss of volatiles during fountaining and flowage of basaltic lava at Kilauea Volcano, Hawaii: Jour. U.S. Geol. Surv. v. 1, p. 649-658.

Tyrrell, G.W., 1937, Flood basalts and fissure eruption: Bull. Volcan. v. 1, p. 89-111.

Vonnegut, B., McConnell, K., and Allen, R.V., 1966, Evaporation of lava and its condensation form the vapor phase in terrestrial and lunar volcanism: Nature, v. 209 p. 445-448.

Walker, G.P.L., 1971, Grain-size characteristics of pyroclastic deposites: Jour. Geology, v. 79, p. 696-714.

_____, and Croasdale, R., 1972, Characteristics of some basaltic pyroclastics: Bull. Volcan., v. 35, p. 303-317.

Wells, O.C., 1976, Scanning electron microscopy: McGraw-Hill Book Co., 480 p.

Wentworth, C.K., and Williams, H.L., 1932, National res. Council Bull., 89, pp. 49-50: In AGI Glossary of Geology, p. 245, American Geological Institute, 1962.

Wentworth, C.K., 1938, Ash formations of Hawaii: Hawaiian Volcano Observatory, 3rd spec. Rept., 183 p.

White, D.E., and Waring, G.A., 1961, A review of the chemical composition of gases from volcanic fumaroles and igneous rocks: U.S. Geol. Surv. Prof. Paper, 424-C, p. 331-312.

_____, and Waring, G.A., 1963, Volcanic emanations: Data of Geochemistry, Sixth Edition, Chapter K, U.S. Geol. Surv. Prof. Paper, 440-K, 29 p.

☆ U.S. GOVERNMENT PRINTING OFFICE: 1978—771-084/3 19 22